NUMERICAL STUDY OF MICROCHANNEL HEAT TRANSFER WITH NANOFLUID BASED TWO-PHASE SLUG FLOW

S S Geethal Chandima Siriwardana

178262G

Degree of Master of Engineering

Department of Mechanical Engineering

University of Moratuwa

Sri Lanka

March 2022

NUMERICAL STUDY OF MICROCHANNEL HEAT TRANSFER WITH NANOFLUID BASED TWO-PHASE SLUG FLOW

Siriwardana Sitanange Geethal Chandima Siriwardana

178262G

Thesis submitted in partial fulfilment of the requirements for the degree of

Master of Engineering in Mechanical Engineering

Department of Mechanical Engineering

University of Moratuwa

Sri Lanka

March 2022

DECLARATION

I declare that this is my own work, and this thesis/dissertation does not incorporate without acknowledgement any material previously submitted for a degree or diploma in any other University or institute of higher learning and to the best of my knowledge and belief it does not contain any material previously published or written by another person except where the acknowledgement is made in the text.

Also, I hereby grant to University of Moratuwa the non-exclusive right to reproduce and distribute my thesis/dissertation, in whole or in part in print, electronic or other medium. I retain the right to use this content in whole or part in future works (such as articles or books).

S. S. G. C. SIRIWARDANA

Signature Date: 31-03-2022

The above candidate has carried out research for the Masters thesis under my supervision.

Name of the supervisor: **Dr. P.M.T. BANDARA**

Signature of the supervisor: Date: 16/05/2022

Name of the supervisor: **Dr. R.A.C.P. RANASINGHE**

Signature of the supervisor: Date: 16-05-2022

ABSTRACT

Microfluidics has recently gained research attention for its high-end thermal applications, including micro heat exchangers, Lab on a Chip, micro reactors, and MEMS. It has been proven that the addition of suitable nanoparticles to a fluid can enhance the heat transfer efficiency in microchannels, both in single phase and liquid-liquid two-phase flow. In general, slug flow is said to be the most efficient in heat transfer. However, the investigation performed on liquid-liquid slug flow with added nanoparticles was found to be very limited. Hence, this study numerically investigates the heat transfer characteristics in microchannels with liquid-liquid two-phase fluid flow (water and light mineral oil) with added nano particles (Al_2O_3).

The VOF method and phase field equations were solved using ANSYS Fluent and COMSOL Multiphysics to capture two-phase flow interfaces. Adaptive mesh refinement techniques were employed to reduce computational power while maintaining sharp interfaces between fluid phases. The Eulerian mixture model was used to solve the cases containing nanoparticles. Numerical results were validated against published experimental data reported by [1] and [2].

Simulations were conducted for a 3000 micron long microchannel with a diameter of 100 microns for fluid velocity, ranging from 0.1 m/s to 0.5 m/s. First, 1 kW/cm^2 of heat flux is introduced to the channel wall after 1000 microns to mimic the microchip heat generation, also allowing flow to be developed.

Results have shown that using nanoparticles in either phase significantly increases heat transmission. This can be amplified even more when used in the secondary phase, by 58 percent compared with liquid-liquid two phase slug flow. This was accomplished with a nanoparticle fraction of 0.05 v/v in the secondary fluid phase. The addition of nanoparticles to the primary fluid increased heat transfer by 34%. The findings of this study can be used to improve MEMS and micro-to-macro systems that move heat.

THIS PAGE IS INTENTIONALLY LEFT BLANK

DEDICATION

පිදුම

දරුවන්ගේ නිදහස් අධ්‍යාපනය වෙනුවෙන් බදු ගෙවනා

සුවහසක් ශ්‍රී ලාංකික ජනයාට

මෙය පිදුම් දෙමි.

I dedicate this to the

thousands of Sri Lankans who paid and are paying taxes for the free education of the children

Geethal Chandima Siriwardana

ACKNOWLEDGEMENTS

I would like to express my heartiest gratitude to all the lectures of the Department of Mechanical Engineering, University of Moratuwa and the Department of Mechanical Engineering, University of Sri Jayewardenepura for their valuable advice, guidance, and commitment to the MEng in Energy Technology program. Secondly, I would like to express my heartiest appreciation to my supervisors, Dr P M T Bandara and Dr R A C P Ranasinghe, for their advice, patience, and aspiration to complete this report. I would like to express my sincere gratitude to our Course Coordinator of this MEng in Energy Technology program and all group members of MEng in Energy Technology 2018, who gave me the fullest support in my studies in this academic program. Finally, my sincere thanks go to family members who wished, supported, and spared me at their level best for this study.

Geethal, Chandima Siriwardana

2022-02-04

THIS PAGE IS INTENTIONALLY LEFT BLANK

TABLE OF CONTENT

LIST OF FIGURES

LIST OF TABLES

LIST OF ABBREVIATIONS

Roman Symbols

A	Correlation constant for chemical compound
B	regression coefficients for chemical Compound
Ca	Capillary Number.
Co	Confinement number
c_p	Specific heat
C_{ps}	Heat capacity of saturated liquid
D	Diameter of the microchannel
d	Nanoparticle diameter
d_a	Diameter of the aggregate
d_f	Fractal dimension of the aggregates
D_h	Hydraulic Diameter
Di	Internal diameter
Do	Outer diameter
e	Internal energy
e_{Di}	absolute error of the parameter Di
F	Body force
g	Gravitational acceleration
G_z	Graetz number
k	Thermal conductivity of the fluid
K^*	Geometry dependent constants
Kn	Knudsen Number

L	Characteristics channel dimension
L_c	Microchannel length
L_{HT}	Heated length of the microchannel
L_{hyd}	Entry Length of a flow
M	Constant depends on the geometry of the channel
m	The fraction of the cross-sectional area of the tube covered with liquid.
M^*	Dimensionless quantity initiated by the author
n	Constant exponent component
Nu	Nusselt number
p	Pressure
pi	Primary fluid
Pr	Prandtl number
q	Heat flux
Q	Flow rate
r	Distance from the axis
R	Radius of the circular pipe
Re	Reynolds Number
se	Secondary fluid
T	Temperature
$T_{(r)}$	Fluid temperature at a distance of r
T_h	Dimensionless heated perimeter
T_m	Bulk mean fluid temperature
T_w	Wall temperature

u	Flow velocity
$U(r)$	Velocity component in the fully developed laminar flow
U_{avg}	Average velocity
U_B	Bubble Velocity
U_s	Slug Velocity

Greek symbols

ΔP	Pressure drop
μ	Dynamic viscosity
μ_r	Relative Viscosity
λ	Mean free path length
ρ	Local density
ρ_l	density of the liquid
ρ_v	density of the vapor
σ	surface tension
σ_i	interfacial tension between two fluids
τ	Stress tensor
Φ	nanoparticle volume fractions
σ_{l-g}	surface tension between liquid and gas
σ_{s-g}	surface tension between solid and gas
σ_{l-s}	surface tension between solid and liquid
θ_E	Young’s equilibrium contact angle

Acronyms

CFD	Computation Fluid Dynamics
CHF	Critical Heat Flux
CNT	Carbon Nanotubes
EDL	Electric Double Layer
EG-T	Glycol/Water-Toluene
EG-W	Ethylene Glycol and Water
EHF	Extreme High Heat Flux
HHF	High Heat Flux
LoC	Lab On a Chip
LVG	Longitudinal Vortex Generators
MCU	Micro Controller Unit
MEMS	Micro Electromechanical Systems
O/A	Organic to Aqueous Volumetric
PDE	Partial Differential Equations
SF	Stagnant Film
UHF	Ultra High Heat Flux
W-T	Water-Toluene
MWCNT	Multi-Walled Carbon Nanotubes

1 HEAT TRANSFER IN MICROCHANNELS WITH SLUG FLOW OF LIQUID-LIQUID USING NANOPARTICLES

Microfluidic technology has advanced significantly in the last several years. The flow of fluid through microchannels is referred to as microfluidics. A microfluidic device can be identified by its dimensions, at least one of which is less than 1 mm in length. Microchannels are used in heat exchangers, LoCs (Lab on a Chip), MEMS (Micro Electromechanical Systems) and micro reactors. They can also be seen in biomedical applications and molecular biology due to their reagent volume requirements, low cost, and disposability [3], [4].

The overall amount of heat transferred by heat exchangers is mostly influenced by the surface area of the cooling micro heat exchanger or macro channels. Microchannels, as a result of their high surface area to volume ratio, are being used in heat exchangers to boost heat transfer rates [5].

Tuckerman and Pease pioneered the concept of heat removal in electronic cooling through the use of liquid flow in microchannels [6]. When a microchannel was integrated into a heat sink, the heat removal rate recorded in the study was 0.79 kW/cm^2 [7]. Heat sinks with embedded channels in the presence of fluid flow are used to cool electronic devices, and this method of total heat removal has previously been proven and well established as an effective method of total heat removal. Heat sinks with embedded channels in the presence of fluid flow are used to cool electronic devices, and this method of total heat removal has previously been proven and well established as an effective method of total heat removal [8]–[11]. The system's primary disadvantage is the pressure loss across the channel. For the one-square-centimetre chip, the pressure drop was greater than two bars [7].

With the current development rate of microchips, including MCUs (Micro Controller Units) and microprocessors, they produce approximately 1 kW/cm^2 of heat flux [12]. To address this issue, new solutions are needed with better performance.

Due to the ability to increase the thermal conductivity of liquids with added nanoparticles, nanofluids have become the best choice for these instances of cooling requirements. To classify a nanofluid, particles with a low concentration or density (1.0 vol percent) and colloidal dispersion nanoparticles with a single dimension between 1–100 nm must be present in the base fluid. This name was first suggested by Choi in 1995 [13]. These nanofluids have been demonstrated to be capable of being used in heat transfer devices with the potential for improved heat transfer [14]. However, there is a lack of research that makes it hard for them to be used in the field of heat transfer.

Almost every researcher in the field has studied and investigated the heat transfer properties, flow patterns, and properties of numerous nanofluids composed of base fluid materials and various nano substances. Adu-Nada et al. studied the heat transfer capabilities of a nanofluid consisting of CuO, EG, and water in a heated enclosure. Due to the dispersion of the aluminium nanoparticles in water, the dynamic viscosity and friction factor increased. The results of the above study were obtained using the finite-volume method [13].

There are numerous research gaps in this area, particularly with regard to industrial solutions. Thus, the goal of this research is to close the gap and develop an efficient technique for heat removal by the use of liquid-liquid slug flow in microchannels containing nanoparticles, which will help to close the heat transfer gap.

1.1 Numerical investigations of microfluidics and nanofluids

Scientists and researchers are increasingly performing numerical analysis on nanofluids due to the high cost of experimental setups. Additionally, the equipment necessary for conducting nanofluid experiments is frequently excessively expensive. Scientists and researchers are increasingly performing numerical analysis on nanofluids due to the high cost of experimental setups. Additionally, the equipment necessary for conducting nanofluid experiments is frequently prohibitively expensive [15]. Scientists and researchers are increasingly performing numerical analysis on nanofluids due to the high cost of experimental setups. Additionally, the equipment necessary for conducting nanofluid experiments is frequently extremely expensive [16]–[20].

Earlier CFD experiments frequently employed a single-phase approach, which necessitates the use of a stable nanofluid with homogeneous and uniform properties. However, several tests conducted over the last decade indicate that the assumption that "nanofluid is stable and homogeneous" is incorrect in some cases [21]. More precisely, if proper dispersion and stabilization treatments are not used after nanofluid preparation (or production), nanoparticle sedimentation may be detected within a short time period [21]. Because the volume fraction / concentration of the nanoparticle sedimentation layer has increased, the nanofluid characteristics are no longer uniform throughout the fluid region. As a result, numerical models of nanofluid flow and heat transfer qualities may produce results that are in disagreement with one another.

It is possible that contradicting results will be obtained from numerical models of nanofluid flow and heat transfer properties. This study will bridge the divide by conducting numerical simulations to investigate the feasibility of using nanofluid with immiscible liquid-liquid slug flow in the microdomain.

1.2 Aim and significance of this study

Accordingly, the purpose of this research is to evaluate whether or not it is possible to include nanofluid into two-phase slug flow in microchannels by applying relevant CFD techniques such as phase-field modelling, level setting, and volume of fluid modelling. Solvers that are used in the study are based on the Eulerian-Eulerian framework that supports treating nanoparticles as a separate phase. The use of a nanofluid as one of the phases in a two-phase slug flow is also intended to improve the overall heat transfer performance of the system. The following are the primary objectives of this study, which will help to attain the overall goal of the investigation:

- Investigate the influence of flow parameters on the heat transfer coefficient in circular microchannels, including void fraction, slug length, and slug velocity.
- Analyse the flow of liquid-liquid slugs in the presence of nanoparticles and nanofluids.

- Perform CFD analysis to determine the pressure drop compared to liquid slug flow without nanoparticles and liquid-liquid slug flow with nanoparticles.

1.3 Thesis outline

This thesis's primary content can be summarized as follows:

Chapter 01: This chapter discusses the introduction and relevance of the study. Also, the research gap and objectives are presented.

Chapter 02: Literature was looked at to find out what the main research gap was and what the current methods were for doing CFD simulations on nanofluids and two-phase slug flow.

Chapter 03: The purpose of this chapter is to examine the possibilities of improving heat transmission in microchannels by employing two-phase liquid-liquid slug flow. The studies were carried out using CFD simulations combined with conjugate heat transfer using level set and VOF (volume of fluid) methods.

Chapter 04: In this chapter, nanoparticles were introduced to immersible liquid-liquid slug flow to investigate the ability of further enhancement of heat transfer in microchannels. Here, nanoparticles were introduced separately to both the base fluid and the secondary fluid to capture the effect of the nanoparticles.

Chapter 05: A comprehensive analysis of results were done to present and verify the hypothesis of the research. It is discussed in this chapter how different parameters such as contact angle, velocity ratio, volume fraction of two-phase and volume fraction of nanoparticles can have an impact on total heat transfer in microchannels. This chapter is divided into two sections.

Chapter 06: research and illustrate the conclusions that are presented. Also, further developments and recommendations are given.

2 A REVIEW: MICROCHANNEL HEAT TRANSFER AND NANOFLUIDS

2.1 Why microfluidics?

Microfluidics is the study of fluid flow in microchannels. Microfluidics is described as "the science and engineering of systems in which the fluid behaviour dramatically deviates from traditional flow theory due to the system's short length scale. "The relationship between the length and volume scales is depicted in Figure 2.1.

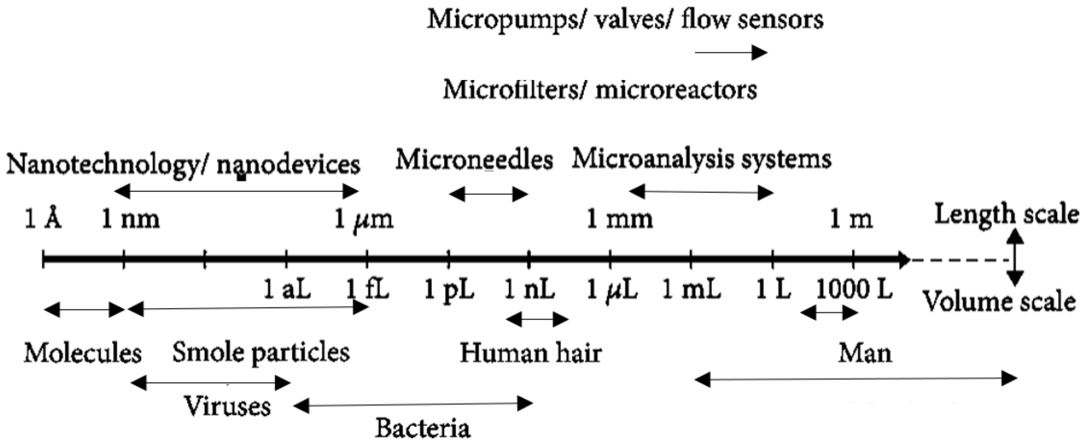

Figure 2-1: Size characteristics of microfluidic devices (Adapted from [22])

The primary advantage of microfluidics is that it takes into account and exploits scaling laws and continuum breakdown to account for newly immersed effects and to achieve higher performance. Additionally, microfluidics theories differ from those of convectional fluid mechanics, as molecular effects such as slip flow become more significant at the small scale. These behaviours are demonstrated through the use of microfluidics devices that manipulate a microscopic amount of fluid [22]. In microfluidics, the critical issue is the microscopic amount of fluid.

Microfluidics is the study of devices with a single dimension on a microscale. Typically, the cross-section diameter is less than 1 mm, which is why they are referred to as microchannels. A microfluidics system is identified by its Knudsen number. The Knudsen number is a scalar quantity that can be calculated using equation 2.1. This equation can be used to determine if a flow is continuous or discontinuous.

$$Kn = \frac{\lambda}{L} \qquad 2.1$$

Where, the mean free path of a molecule is denoted by λ and L are the characteristics channel dimension. According to the theories, if Kn is less than 10^{-3}, the flow is considered to be continuum.

2.1.1 Single phase flow in microchannels

Apart from microscale fluids, conventional and macroscopic fluids are treated as a continuum due to the high molecular density. The Knudsen equation can be used to verify the continuum. Even if the molecules are packed closely together within the fluid in a microchannel, a continuous flow will occur. All physical quantities, including velocity, density, and pressure, are assumed to be defined uniformly throughout the domain space and to vary continuously within the flow [22].

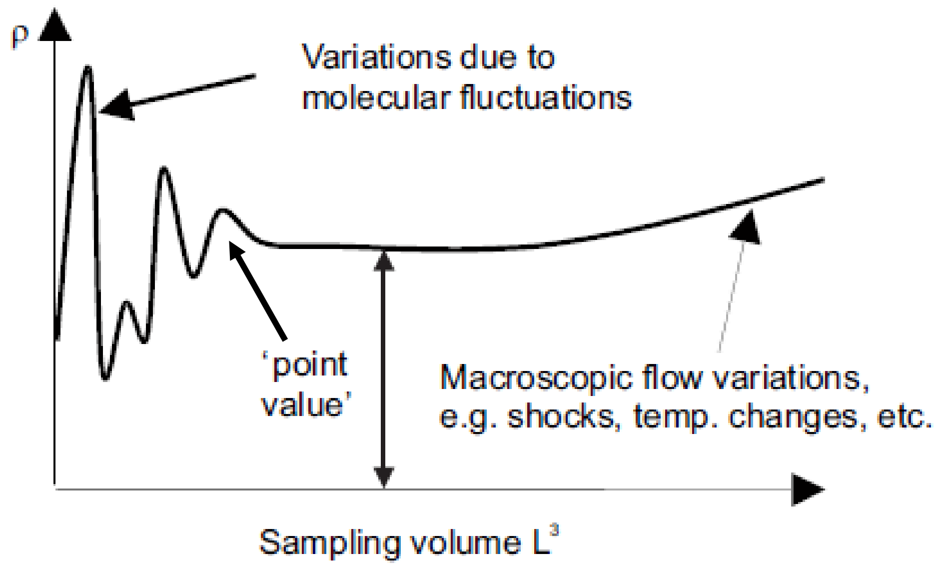

Figure 2-2: Continuum assumption in fluids illustrated by thought experiment for measuring density [23].

As illustrated in Figure 2-2, a fluid can be thought of as a continuum if a constant value for a flow property is obtained at the smallest volume considered. In continuum fluid mechanics, the point value is the smallest continuum volume. As an example, consider a 10 µm diameter channel. It contains nearly 30,000 water molecules with its span (where $\lambda = 0.31\ nm$). This number of molecules is sufficient enough to consider it a continuum since the Knudsen number is less than 10^{-3} [22]. Figure 2-3 shows the molecular packing arrangement of a gas and a liquid.

(a) (b)

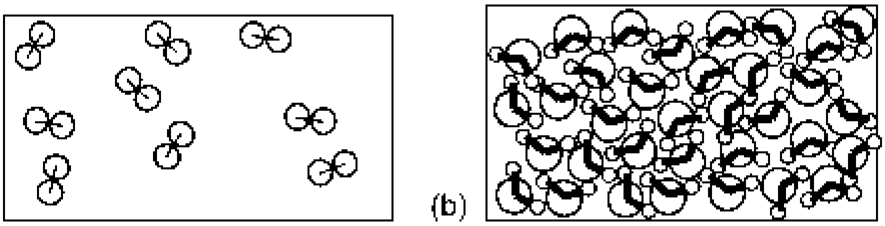

Figure 2-3:Sketches of (a) a gas, such as N_2, at standard conditions, and (b) a liquid, such as H_2O [24].

Because these liquids, such as water, have a continuous behaviour, the three fundamental conservation laws can be used to model thermodynamic fluid problems. It is the three fundamental conservation laws of mass conservation, momentum conservation, and energy conservation that govern our universe. PDEs (Partial Differential Equations) can be used to illustrate the following fundamental laws:

Conservation of Mass

$$\frac{\partial \rho}{\partial t} + \frac{\partial (\rho u_i)}{\partial x_i} = 0 \qquad 2.2$$

Conservation of Momentum

$$\frac{\partial}{\partial t}(\rho u_i) + \frac{\partial}{\partial x_j}\left(\rho u_j u_i\right) = \rho F_i - \frac{\partial p}{\partial x_i} + \frac{\partial}{\partial x_j}\tau_{ji} \qquad 2.3$$

Conservation of Energy

$$\frac{\partial}{\partial t}(\rho e) + \frac{\partial}{\partial x_j}(\rho u_i e) = -p\frac{\partial u_i}{\partial x_i} + \tau_{ji}\frac{\partial u_i}{\partial x_j} + \frac{\partial}{\partial x_i}q_i \qquad 2.4$$

Where repeated indices in a single term denote a summation in accordance with accepted index notation practice (Einstein summation convention). In these equations

ρ is the local density, u_i represents the flow velocity, e is the internal energy, p is the pressure, τ is the stress tensor, F is body force, and q is the heat flux [22].

Microchannel flows exhibit laminar flow characteristics due to their short characteristic length. The following equation 2.5 can be used to determine the entry length of a circular-shaped pipe with laminar flow [3].

$$L_{entry} = 0.05.Re.D \qquad 2.5$$

where D denotes the hydraulic diameter of the circular-shaped pipe and Re denotes the Reynolds number, which is a dimensionless quantity that describes the relative effect of inertial and viscous forces.

Equation 2.6 produces a fully developed velocity profile in a circular pipe with laminar flow.

$$U(r) = \frac{2Q}{\pi R^2}\left(1 - \frac{r^2}{R^2}\right) \qquad 2.6$$

in here, R is the radius of the circular shaped channel, Q is the flow rate, and r is the local radius. The maximum velocity is observed near the channel's centre, where r = 0.

Also, the pressure-drop across the pipe where a laminar flow exists is given in equation 2.7.

$$\Delta P = \frac{32\mu L U_{avg}}{D^2} \qquad 2.7$$

the diameter of a circular channel is denoted by D and

$$U_{avg} = \mathrm{Q/\pi R2} \qquad 2.8$$

U_{avg} is the average fluid flow velocity.

Mathematical expressions are illustrated in figures 2-4. The layer contacting the pipe wall, according to the theories, has zero velocity and obeys Newton's law of viscosity.

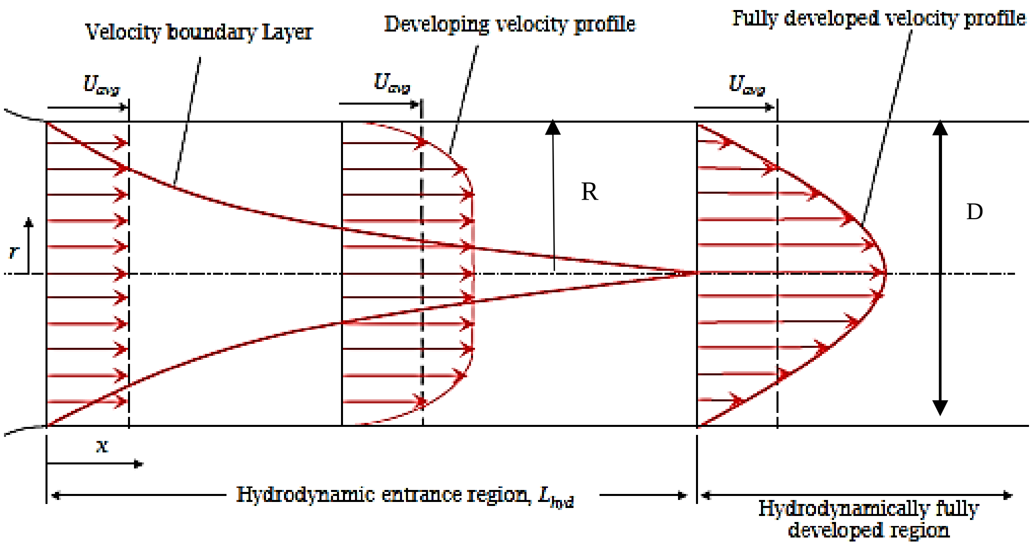

Figure 2-4: In a circular channel with laminar flow, the formation of a velocity boundary layer (Adapted from [5])

2.2 Nanofluids

Nanofluids are a type of fluid (often referred to as liquids) that consists of nanometre (nm) sized solid materials. Nanometre-sized materials are usually based on nanoparticles, nanotubes, nanofibers, nanorods, nanowires, nanosheets, or nanosized droplets [25]. Typically, nanofluids are thought of as two-phase systems, with one phase being a liquid (referred to as the base fluid) and the other being a solid composed of nanoparticles.

In general, metal oxides (such as alumina, zirconia, silica, and titania) are used as nanoparticles, as are oxide ceramics (such as Al_2O_3, CuO), chemically stable metals (such as Au, Cu), various forms of carbon (such as graphite, carbon nanotubes, graphene and fullerene, diamond), and metal carbides such as SiC. Base fluids can be made of oil, carbon-based liquids (such as glycols), water, refrigerants, polymeric solutions, bio fluids, greases, and other communal fluids [15], [25], [26].

2.2.1 Advantages of nanofluids

The most critical parameters in a nanofluid are the particle size and concentration of the nanoparticle. Because of the size of the particles, physical parameters like as viscosity and thermal conductivity are affected. The size of the particles is critical when it comes to clogging. In microchannels, large particles can cause severe problems such as clogging, a short settle time, and a large pressure drop [27]. On the other hand, large particles can be abrasive due to their high momentum and rapid movement.

It has been found that particle size and the concentration of particles directly influence the pH value and viscosity of the nanofluid [28]. Zhao Jia-fei [28] et al. have conducted an experiment based on de-ionized water with different sizes of nanoparticles and changing the concentration of the nanoparticles. It has been demonstrated that the volume fraction of nanoparticles has a considerable impact on the relative viscosity (μ_r). It was evident that relative viscosity also depends on the diameter of the nanoparticle. According to Zhao Jia-fei et al., the experimental data for relative viscosity vs volume fraction presented in Figure 2-5 were collected through a series of experiments. Figure 2-6 depicts the relationship between relative viscosity and particle diameter in a fluid.

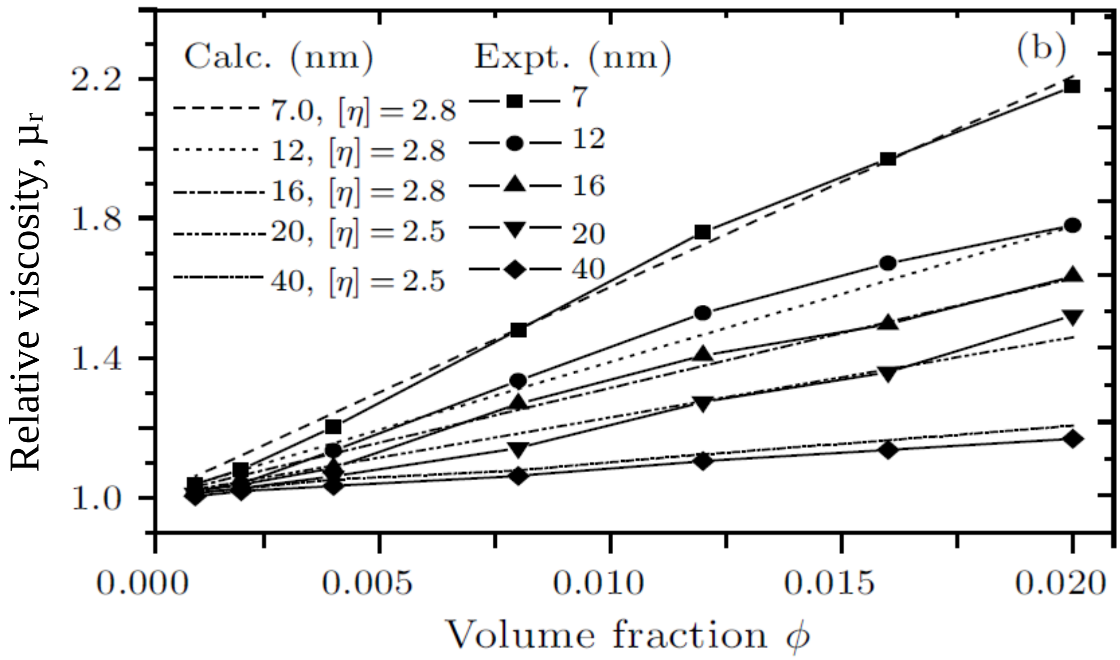

Figure 2-5:Relative viscosity of nanofluids measured experimentally and simulated as a function of volume fraction (Adapted from [28]).

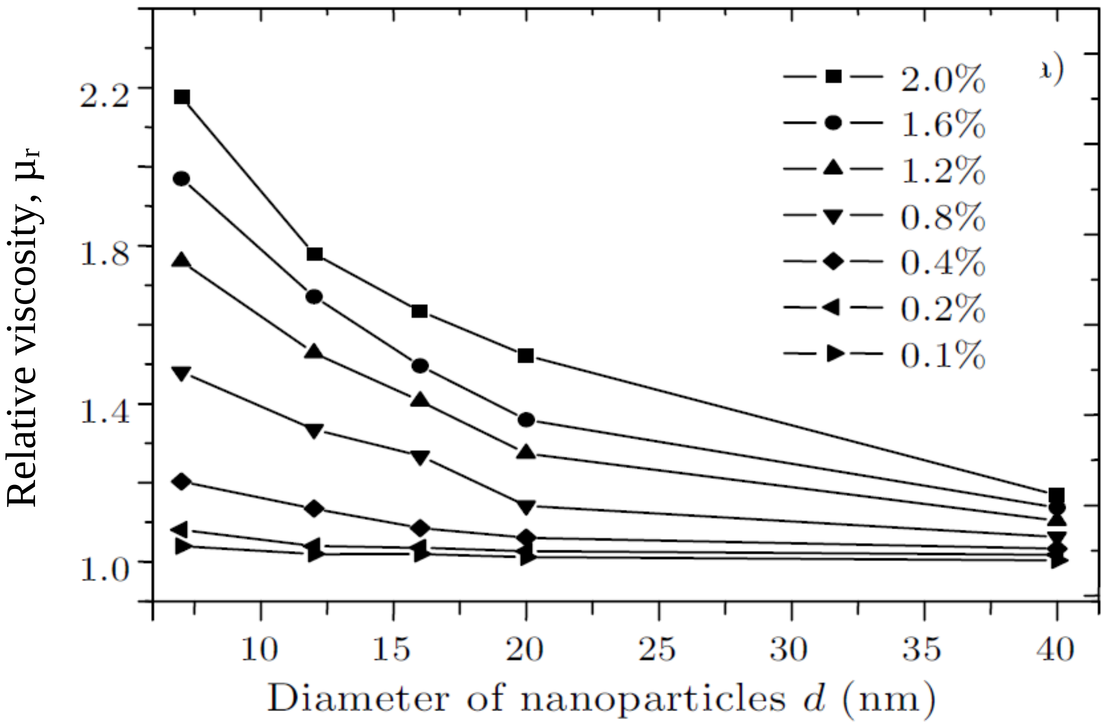

Figure 2-6:The relationship between the relative viscosity of a nanofluid and the diameter of a nanoparticle (adapted from [28])

According to the Figure 2-5, it is noticed that relative viscosity is growing with the increasing volume fraction. The key cause for this result is extent of d_a/ d. Where d means individual nanoparticle diameter and d_a is the diameter of the aggregate [28].

With these results, an equation for relative viscosity according to Krieger equation can be written as:

$$\mu_r = 1 + [\eta](\frac{d_a}{d})^{3-d_f}\Phi \qquad 2.9$$

where, μ_r, η, d_a, d, d_f, and Φ are relative viscosity, intrinsic viscosity, diameter of the aggregate, nanoparticle diameters, fractal dimension of the aggregates and nanoparticle volume fractions, respectively.

On the other hand, due to the dispersion of nanoparticles, small nanoparticles can flow freely through microchannels. The advantages of suspending nanoparticles in a primary or derived fluid are as follows: [15], [26]

- It is conceivable to improve the heat capacity and surface area of a nanofluid.

- The fluid's effective thermal conductivity can be increased.
- The surface of the flow passage, the base fluids, and the collisions and interactions of the particles can all be enhanced.
- Particle clogging is minimized

Due to the aforementioned reasons, nanofluids are far superior to conventional heat transfer fluids when designing heat transfer fluids.

2.3 Heat transfer in microchannels

Over the last few decades, there have been many studies on heat transfer within microchannels. There are several reasons for this, including the growth of electronic technology and its industry mentioned previously [15]. Heat transfer is a term that refers to the quantity of energy that can be transported in the form of heat from one system to another or between surrounding. This is primarily owing to the temperature difference between the two systems, as well as the outside temperature environment. Heat transmission occurs in three primary modes: conduction, convection, and radiation [29].

When heat is transferred through a circular microchannel, a thermal entry length is developed as the heat enters as a result of the formation of a thermal boundary layer. This occurs when a cold fluid is introduced into a relatively warm microchannel, or vice versa [30]. This thermal entrance length (L_{th}) can be expressed as follows (2.10):

$$L_{th} = 0.05RePrD \tag{2.10}$$

Pr denotes the Prandtl number, a two-dimensional variable that quantifies the relative effect of momentum diffusivity. The Prandtl number can be expressed as follows:

$$Pr = \frac{\mu c_p}{k} \tag{2.11}$$

Where, μ, c_p and k denote the viscosity, specific heat capacity, and thermal conductivity of the fluid. To identify a thermally fully developed flow, non-dimensional temperatures must remain constant. It can be shown as below:

$$\frac{T_{\hat{w}} - T_{(r)}}{T_{\hat{w}} - T_m} = constant \quad 2.12$$

here, $T_{\hat{w}}$, $T_{(r)}$, and T_m denote the wall temperature, fluid temperature at r, and aggregate average temperature of the fluid, respectively. The evolution of a thermal boundary layer along a microchannel is depicted in Figure 2-7.

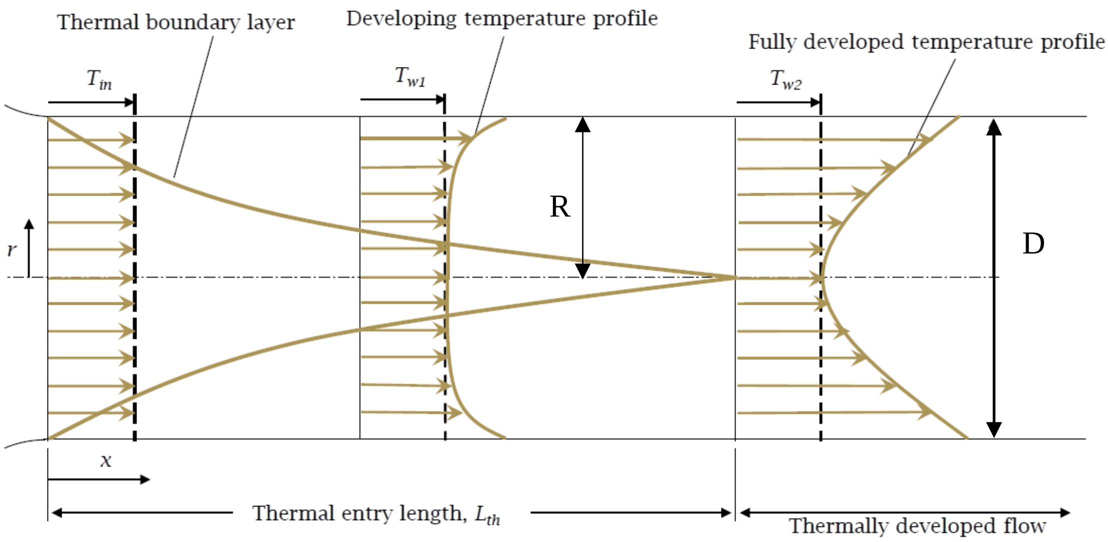

Figure 2-7:The formation of a thermal boundary layer in a circular duct (Adapted from [5])

The conventional fluids used for heat transfer have poor heat conduction compared with metals, except liquid metals [30]. As an example, water conducts heat approximately three orders of magnitude slower than copper. As a result, the world requires a new, improved method of conducting heat from fluid-based systems. Today, the best option, given current technology, will be to transfer heat between systems via nanofluids.

2.3.1 Heat capacity of liquids

Liquid-phase heat capacity is an essential parameter for heat exchangers. Considering the heat capacity of the working fluid is essential when sizing and rating heat exchangers in general, as well as when completing energy equilibrium design calculations, is essential [31]. The achieved relationship for the heat capacity of a liquid can be articulated in a polynomial of the form which is shown in equation (2.13).

$$C_{ps} = A_1 + A_2T + A_3T^2 + A_4T^3 \quad 2.13$$

here, C_{ps} is heat capacity of saturated liquid. Where, A_1, A_2, A_3 and A_4 are the correlation constants for a specific chemical compound and T is the temperature. Figure 2-8 shows the heat capacity variation with its temperature [31]. This plot shape might be different with different liquids due to the chemical composition.

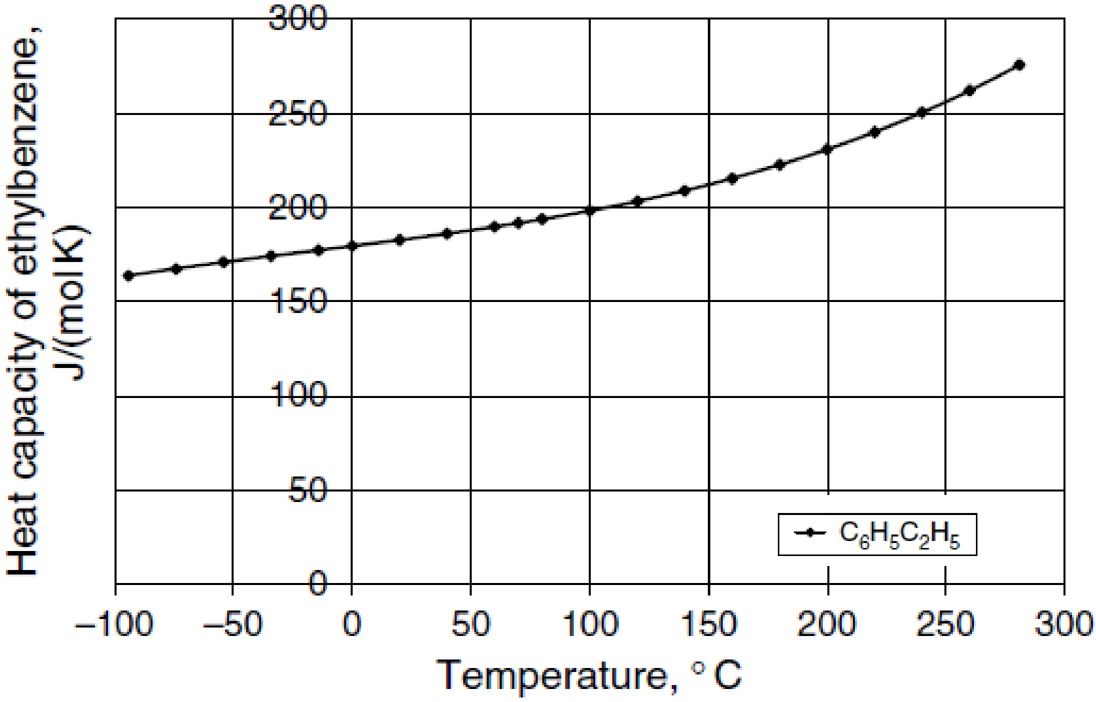

Figure 2-8: Ethylbenzene's ($C_6H_5C_2H_5$) heat capacity against temperature (Adapted from [31])

2.3.2 Thermal conductivity of liquids

Organic substances' thermal conductivity and temperature can be correlated mathematically. [31], [32]. This can be expressed as follows:

$$log_{10}k_{liq} = B_1 + B_2\left(1 - \frac{T}{B_3}\right)^{2/7} \quad 2.14$$

where, k_{liq}, B_1, B_2, B_3 and T are thermal conductivity of liquid, the regression coefficients for chemical compound and temperature. Figure 2-9 and figure 2-10 show the thermal conductivity of liquid benzene and water changes with temperatures, respectively.

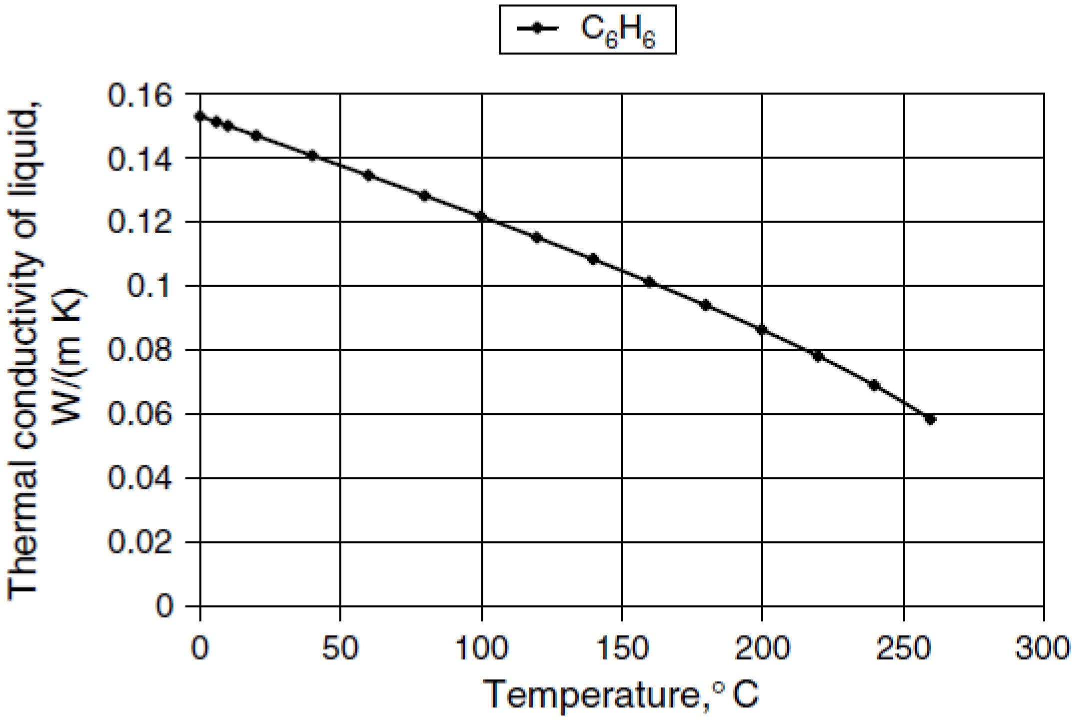

Figure 2-9:Thermal conductivity of benzene (C_6H_6) (Adapted from [31])

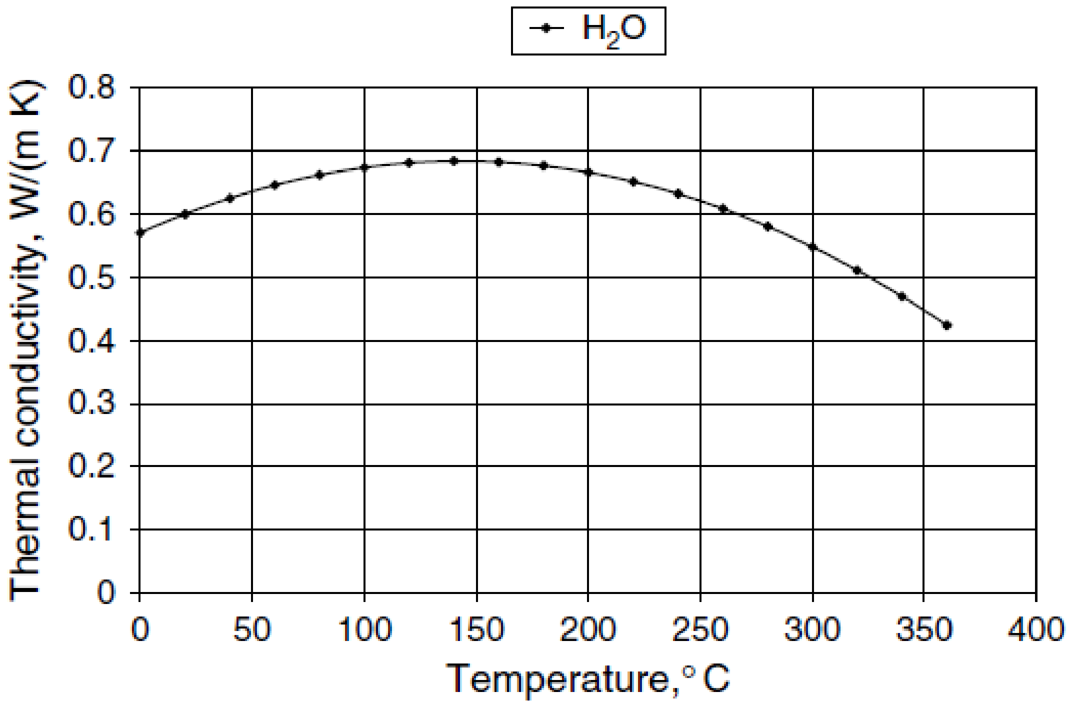

Figure 2-10: Thermal conductivity of water (H_2O) (Adapted from [31])

2.3.3 Thermal conductivity of nanofluids

Nanofluids have significantly improved thermal conductivity when compared to conventional liquids. Nanofluids have a thermal conductivity that is significantly greater than that of their underlying liquid. Based on the nanoparticles which are used in the nanofluid, it can be categorized into three main groups [26].

- Nanofluid with ceramic particles
- Nanofluid with pure metallic particles
- Nanofluid with CNTs (Carbon nanotubes)

With different proportions of these nanoparticles, different types of nanofluids can be formed with different properties. More details will be discussed in the latter part of this chapter.

2.4 Heat transfer in a single-phase flow

Heat transfer in a single-phase channel has generated considerable interest. As a result, research is conducted utilizing methodologies that have been established in the literature. Single-phase research is also being undertaken on microfluidic channels, as previously stated, owing to the high surface area to volume ratio of these channels. Hetsroni et al. [33] conducted a numerical and experimental study to compare total heat transfer in microchannels in 2005. As a result of the strong principle of superposition of hydrodynamic and thermal effects, heat transfer occurs in microchannels. Theoretical models were used to correct several hypotheses related to heat transfer mechanisms in this study. As a matter of fact, the effect of Reynolds number, axial conduction, energy dissipation, and heat loss on the surrounding environment has been determined. The two models were built on the traditional Navier-Stokes equation and the full Navier-Stokes equation with energy equation. In 2011, Ebadian [34] published a review of excessive heat removal technologies. Results has divided heat flux into three sections according to the review. Heat flux in the range of 100 - 1000 W/cm^2 has classified as High Heat Flux (HHF), range of 10^3 - 10^4 W/cm^2 as Ultra high heat flux (UHF) and heat flux which is more than 10^4 W/cm^2 as Extreme high heat flux (EHF). Based on his review, the most successful HHF removal technology is heat pipe. The effect of heat removal in HHF removal using microchannels, spray, jet impingement, piezoelectric effect, and enhanced surfaces was examined. Maximum heat flux removal achieved in the last few decades was found during the survey. Outcomes of the survey has demonstrated in Figure 2-11.

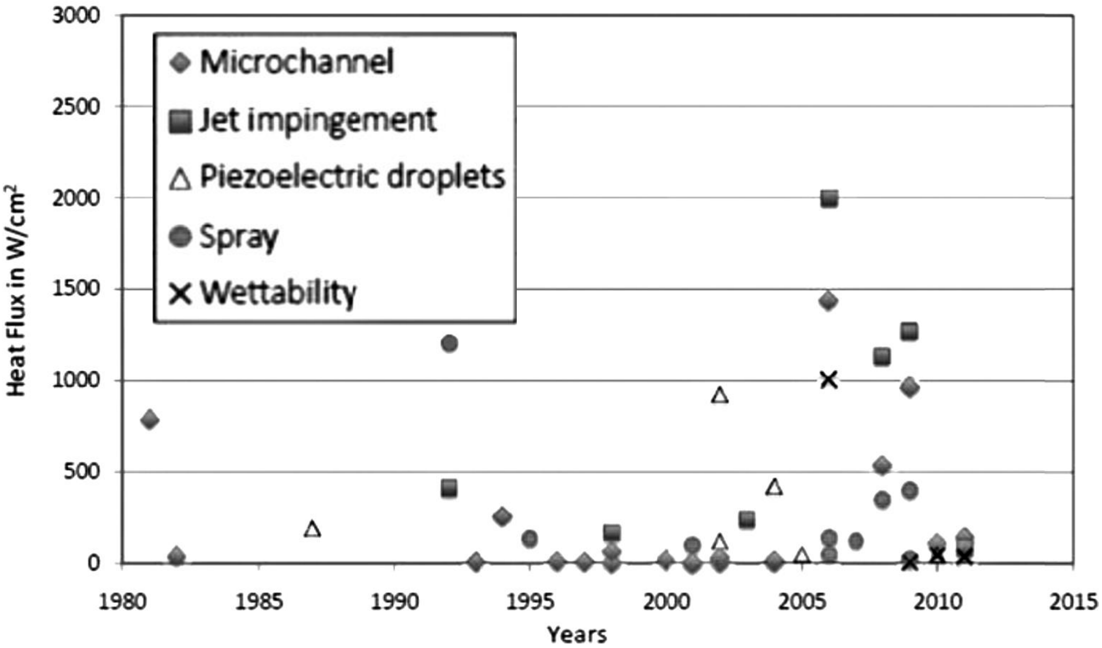

Figure 2-11: Maximum heat fluxes reported over the years (adapted from [34])

Edabian has also made reference to the Bond number's significance (Bo_d). The bond number is used to study the surface tension-gravitational effect ratio. This is critical when dealing with phase changing situations in heat transfer. The Bond number has the following correlation, as shown in equation (2.15).

$$Bo_d = \frac{g(\rho_l - \rho_v)D_h^2}{\sigma} = \frac{1}{Co^2} \qquad 2.15$$

here, g, ρ_l, ρ_v, D_h^2, σ and Co represent gravitational acceleration, liquid density, vapor density, hydraulic diameter, surface tension, and confinement number, respectively. In 1997, Kew and Cornwell [35] established the confinement number. Confinement number is critical when liquids are boiling in narrow passages. Capillary flow, flooding in vertical up flow, and heat transfer in restricted areas all require consideration of a variety of conditions. The following equation (2.16) expresses the concept of confinement number.

$$Co = \frac{\left[\sigma/\left(g(\rho_l - \rho_v)\right)\right]^{\frac{1}{2}}}{D_h} \qquad 2.16$$

Heat exchangers are critical to developing scaling when working in extreme temperatures. Scaling occurs when a minimal film coats the entire surface of a heat exchanger [36], [37]. In 2002, Karabelas [36] did an experiment to identify key issues regarding scale formation in tubular heat exchangers. Karabelas discussed the propagation flow chart in his study to help understand the scale formation based on the formation's physics.

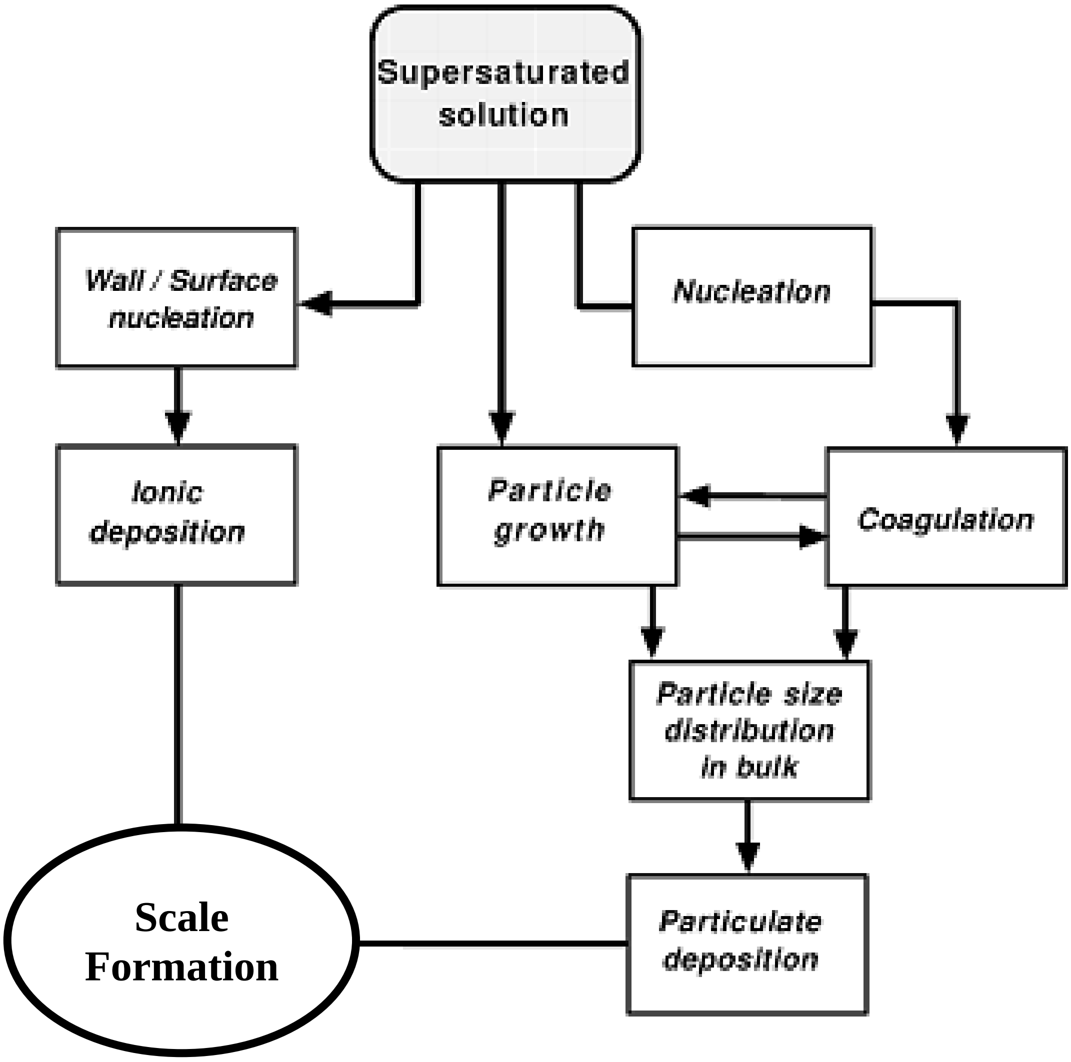

Figure 2-12: Physical processes occurring in the pipe flow of supersaturated (adapted from [38])

For scaling, several physical factors are involved. In Karabelas study, the effect of supersaturation, the effect of flow velocity, the effect of temperature, and the effect of particles on scale formation are included in his modelling, shown in figure 2-12. In 2006, Morini [37], did a study to model scaling in adiabatic and diabatic microchannels. Adiabatic means there is no heat transfer through the microchannel wall [38], [39] whereas diabatic indicates that heat is transferred through the microchannel wall. With respect to convection studies, the Nusselt number is an important parameter with respect to convective heat transfer studies. Morini argued that the Nusselt number is dependent on the Reynolds number even when the flow is laminar, and the entrance effect is paired with viscous dissipation. When applied to a single fluid layer, the Nusselt number represents the ratio of convectional to conductional heat transmission [29]. The Nusselt number can be represented by Equation (2.17).

$$Nu = M Re_L^{n_1} Pr^{n_2} \qquad [29] \qquad 2.17$$

where, M, $n_1$and n_2 are constant depends on the geometry of the channel, constant exponent component and Pr is Prandtl number. Morini, has obtained a Nusselt number equation based on his experimental results which is shown in equation (2.18)

$$Nu = \frac{q}{k T_h^* (\bar{T}_w - \bar{T}_b) \mathrm{L}_c} \qquad 2.18$$

where, the heat removed by the working fluid is denoted by q, T_h^* is the non-dimensional heated perimeter of the microchannel, L_c is the length of the microchannel and k denotes the fluid's thermal conductivity.

In 2006, Celata et al. [40] mentioned in the study investigational results for scaling in single-phase laminar flow at a microscale under uniform heat flux. The experiment was conducted with four different diameters: 528 µm, 325 µm, 259 µm, and 120 µm. The largest of the above clearly demonstrated the best heat transfer performance of thermally rising flow where the Nusselt number increased in comparison to the fully developed point marked closer to the inlet. Table 2-1 details the experimental parameters and conditions.

Table 2-1: Celata's Experimental conditions [40]

D_i (μm)	D_o(μm)	e_{Di}(μm)	L_c(mm)	L_{HT}(mm)	Re	G_z	M*x10^6	K^*(%)
528	859	3.9	79.0	36.8	50-2775	9-233	3-70	0.001-0.1
325	909	4.7	79.5	37.6	274-2304	10-117	8-95	0.03-1.2
259	951	4.4	82.1	36.4	105-2576	3.5-103	12-330	0.06-1.4
120	804	2.4	65.4	35.4	279-3138	6-58	17-170	0.1-10
50	363	1.3	66.0	34.2	114-1450	1-13	32-428	0.6-35

where, K^* is geometry dependent constants and D_i and D_o are internal diameter and outer diameter, respectively. e_{Di} is absolute error of the parameter D_i, L_c is the microchannel's length, L_{HT} is heated length of the microchannel while G_z denotes Graetz number and M is a dimensionless quantity initiated by the author.

Rosa [41] et al. summarized the overall relationships between fluid dynamics models in 2009. The results of his study are depicted in Figure 2-13.

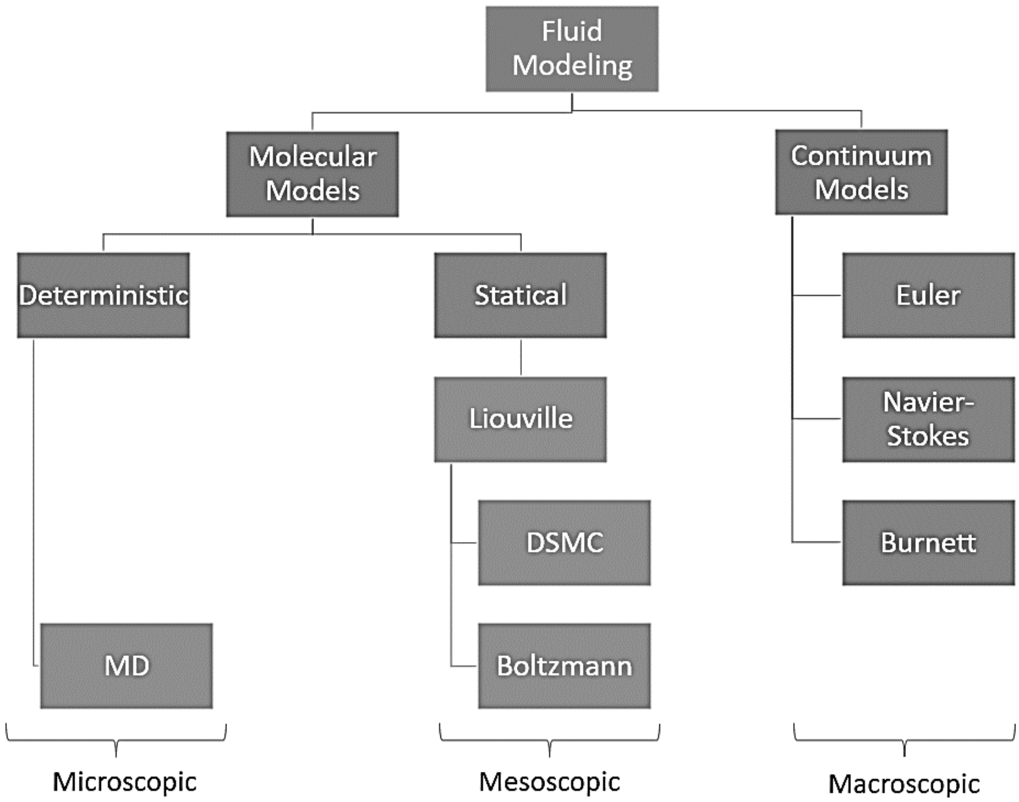

Figure 2-13:General relationships of models in fluid dynamics (adapted from [41])

Rosa concluded his study by providing detailed conclusions on the entrance effect, temperatures dependent on rarefaction (reduction in density), properties, compressibility effect, coupled heat effect between solids and fluids, viscous heating of fluids, surface roughness, and EDL (Electric Double Layer) effect.

Rosa asserts that the entry effect on heat transport is proportional to the Nusselt number. This is due to the thermal entry length, which typically accounts for a significant portion of the microchannel's total length. Temperature-dependent properties such as viscosity must be considered due to the microchannel's two different temperatures at the inlet and outlet. Rarefaction (reduction in density) occurs in conjunction with the compressible effect only in gas flow. In the case of commercial micro heat sinks, conductive heat transfer must be considered in addition to the solid channel to account for the three-dimensional effect. Viscous heating has an effect on the flow's Nusselt number. With a constant wall temperature in a heated microchannel, the Nusselt number tends to increase in the flow and tends to decrease with a constant wall heat flux. Surface roughness has an effect on the Nusselt number depending on the cross-sectional geometry, increasing or decreasing it within the limits of experimental uncertainty. EDL effects can be applied to a segment of the microchannel's hydraulic diameter.

In 2017, Zhai et al. [42] used single and laminar convection to explore convective heat transfer in micro-channel heat sinks. To begin, this research developed a fabricated model to estimate the flow and heat transfer rates in microchannel heat sinks using a computer simulation. Following that, experimental and numerical studies were conducted to verify the theoretical analysis's accuracy. The findings indicate that convective thermal resistance plays a significant role in microchannel heat sink efficiency and performance. Thus, to improve heat transfer, convection thermal resistance should be reduced. The lowermost wall of the microchannel heat sink has a uniform temperature field due to the uniform flow distribution.

2.5 Nanofluids in microchannels

As previously stated, nanofluids are fluids that contain nanoparticles within their base fluid. Due to the high conductivity of the particles in a nanofluid, the bulk fluid's thermal conductivity has increased [43]. The Maxwell and Hamilton-Crosser findings appear to appropriately describe the thermal conductivity behaviour. By introducing nanoparticles to the system, it experienced an increment in the overall thermal conductivity with its Reynolds number. Jung et al. [44] conducted an experiment in 2009 on Al_2O_3 nanofluid with a 170 nm microchannel diameter and determined that the Nusselt number rises with respect to Reynolds number. These findings deviate from conventional analysis, while also providing a new avenue for future research. Bowers et al. [43] observed that as the temperature of the nanofluid, silica and alumina, decreases, the viscosity of the nanofluid increases. Additionally, nanofluids exhibited nearly Newtonian rheological behaviour over a broad shear rate range. In 2016, Manay and Sahin [45] conducted a study in 2016 on the heat transmission and pressure loss of nanofluids in a microchannel. They did their study with titanium oxide (TiO_2) within the range of volume fraction from 0.25 % to 2.0 % with a microchannel whose diameter is equal to 200 µm. The insights of his study are that the nanosized TiO_2

nanoparticles provide a lower surface temperature than the based fluid (water). Due to the increasing thermal resistance caused by particle deposition, the surface temperature decreased as the particle volume fraction increased up to 0.015 percent but increased after reaching 1.50 percent. The second observation was that all nanofluids had a higher Nusselt number value than the based fluid. As the solid fraction increased, the thermal conductivity of the fluid increased, resulting in an increase in heat transfer. When volume concentrations exceed 1.5 percent (v/v), the improvement in heat transfer ceases and the volume concentration begins to decrease. When the particle concentration is 1.5 percent (v/v), the Nusselt number is always greater than when the particle concentration is 2.0 percent (v/v). The increment of the viscosity effect was dominant when volume concentration was higher than 1.5% (v/v), where viscosity had dominated the thermal conductivity. When nanofluid was used as the coolant instead of pure water, the thermal resistance of the fluid was reduced. The surface temperature significantly decreased up to a mass flow rate of 10 kg/h with a Reynolds number of 200 for both pure water and nanofluids. Thermal resistance decreased significantly at the same mass flow rate.

The heat transfer characteristics of a laminar nanofluid developing in a circular tube were investigated quantitatively by Tahir and Mital [46], who carried out their research in 2012. Using it as a response variable, they evaluated the influence of the heat transfer coefficient along the duct axis on particle diameter, Reynolds number, and volume percent. Using three separate factorial methodologies, they ran 27 simulations and conducted multiple regression analyses in order to develop a forecast equation that can account for the effect of these tri-variables on the mean heat transfer coefficient. Changes in the tri-independent variables, according to their numerical analysis, appeared to account for nearly all of the variation in the heat transfer coefficient. The Reynolds number was the most important variable, exerting the greatest influence on the average heat transfer coefficient, whereas the volume fraction had the least significant influence. According to the findings of the study, the coefficient of heat transfer rises linearly with the fluid's volume proportion and Reynolds number. However, when particle size grows, it eventually exhibits a non-linear parabolic fall, which is not as dramatic as it appears. Furthermore, there is only a weak association between the three self-governing variables and their effect on the average heat transfer coefficient (see Figure 2-14). Figure 2-14 depicts the percentage increase in the lengthwise heat transfer coefficient down the axis of the channel for various size and volume fraction combinations when the Reynolds number is equal to 750. For example, Figure 2-15 illustrates the proportional decrease in surface temperature along the channel axis for various diameter and volume fraction combinations at 750 Reynolds number, whereas Figure 2-16 represents the increase in nanofluid heat transfer coefficient along the channel axis for several Reynolds numbers, with the largest increase occurring for 100 nm particle diameter and 4 percent volume fraction at 750 Reynolds number, respectively.

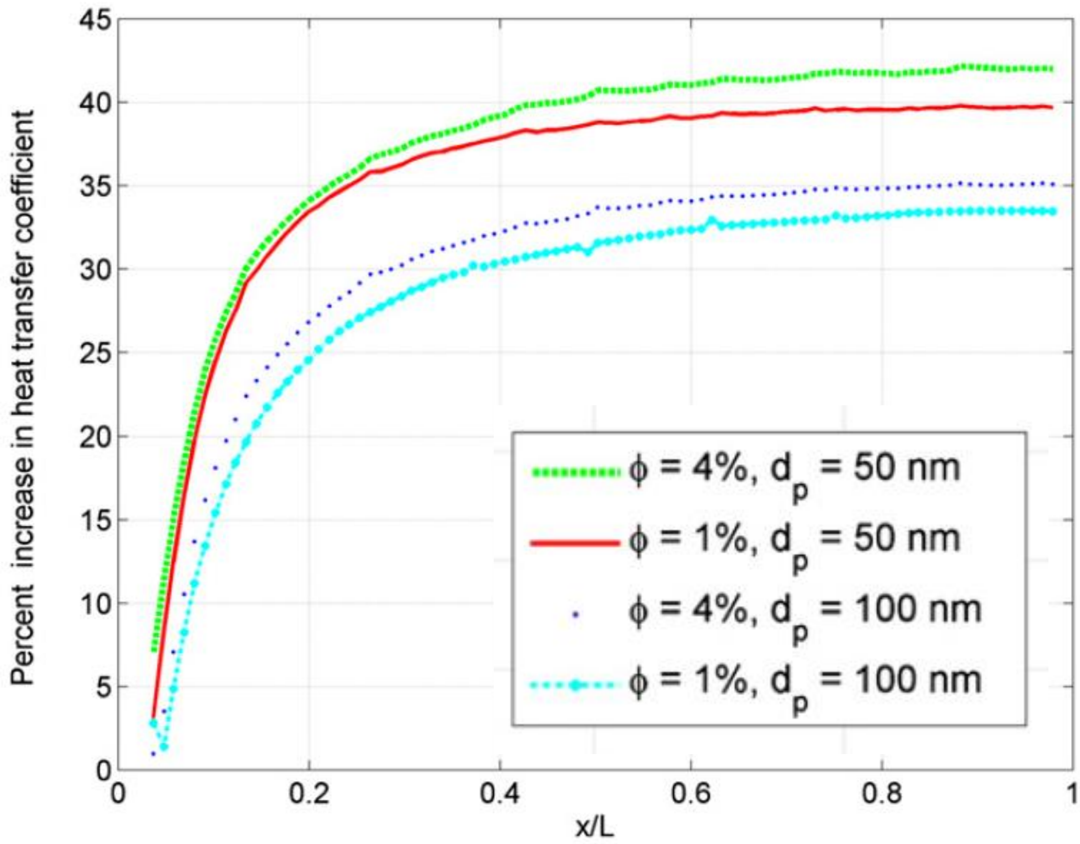

Figure 2-14:Increase in heat transfer coefficient along tube axis as a function of diameter and volume fraction at 750 Reynolds number [46].

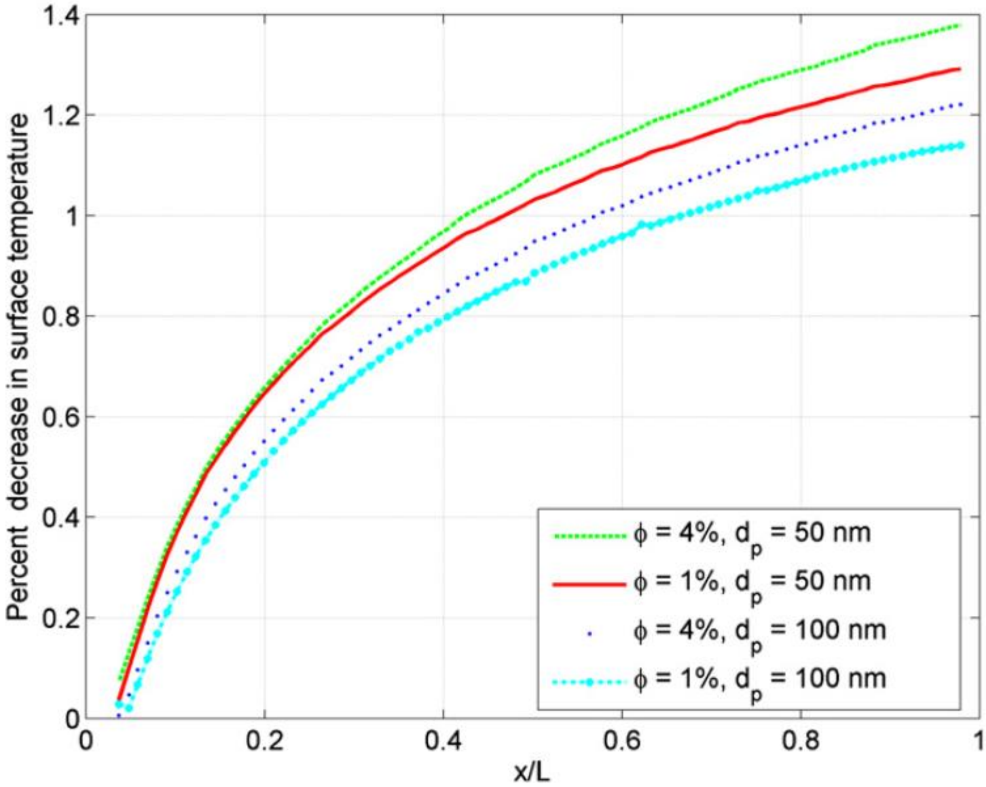

Figure 2-15: At 750 Reynolds number, reduced surface temperature along the tube axis by a percentage [46].

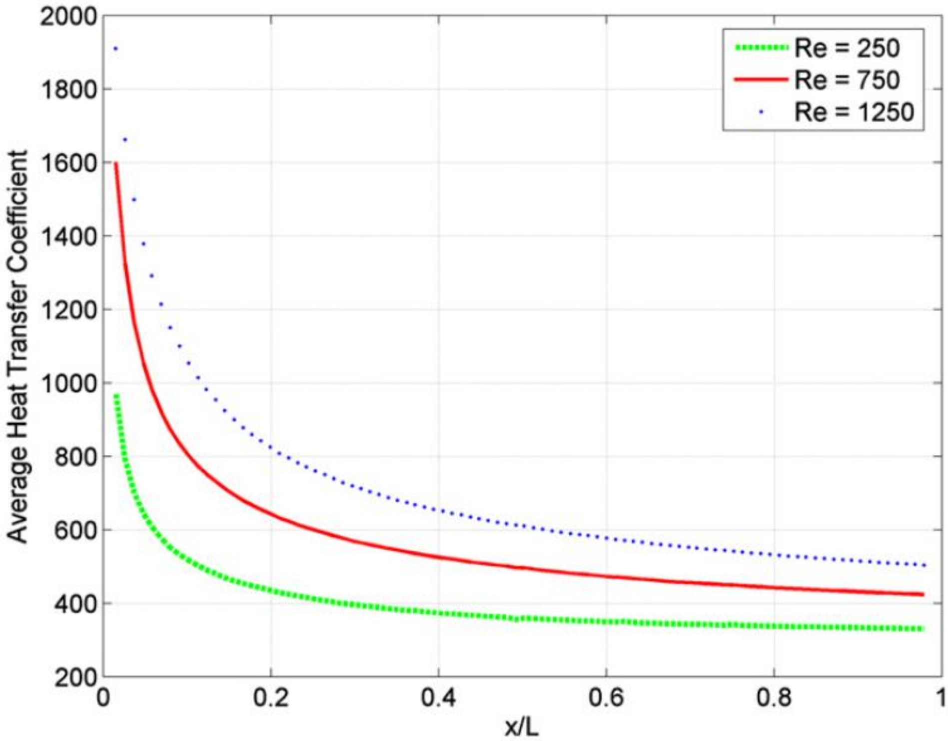

Figure 2-16: Increase in heat transfer coefficient of nanofluid down tube axis for several Reynolds numbers and 100 nm particles with 4 percent volume fraction [46].

2.6 Wall temperature

Heat transport in microchannels is also temperature dependent. There are two types of wall temperatures described in the literature. Combined with the constant wall heat flux, the bulk mean temperature of the fluid and channel wall temperatures rise linearly in the entirely formed region of the channel under the persistent heat flow. The boundary conditions for a constant wall heat flux are depicted in Figure 2-17. T_{in}, T_{out}, T_{wi}, T_{wo}, T_m, ΔT are the inlet and outlet temperatures, the temperature of the inside and outside channel walls, the temperature of the bulk fluid, and the temperature difference between the inner and outside channel walls. [5].

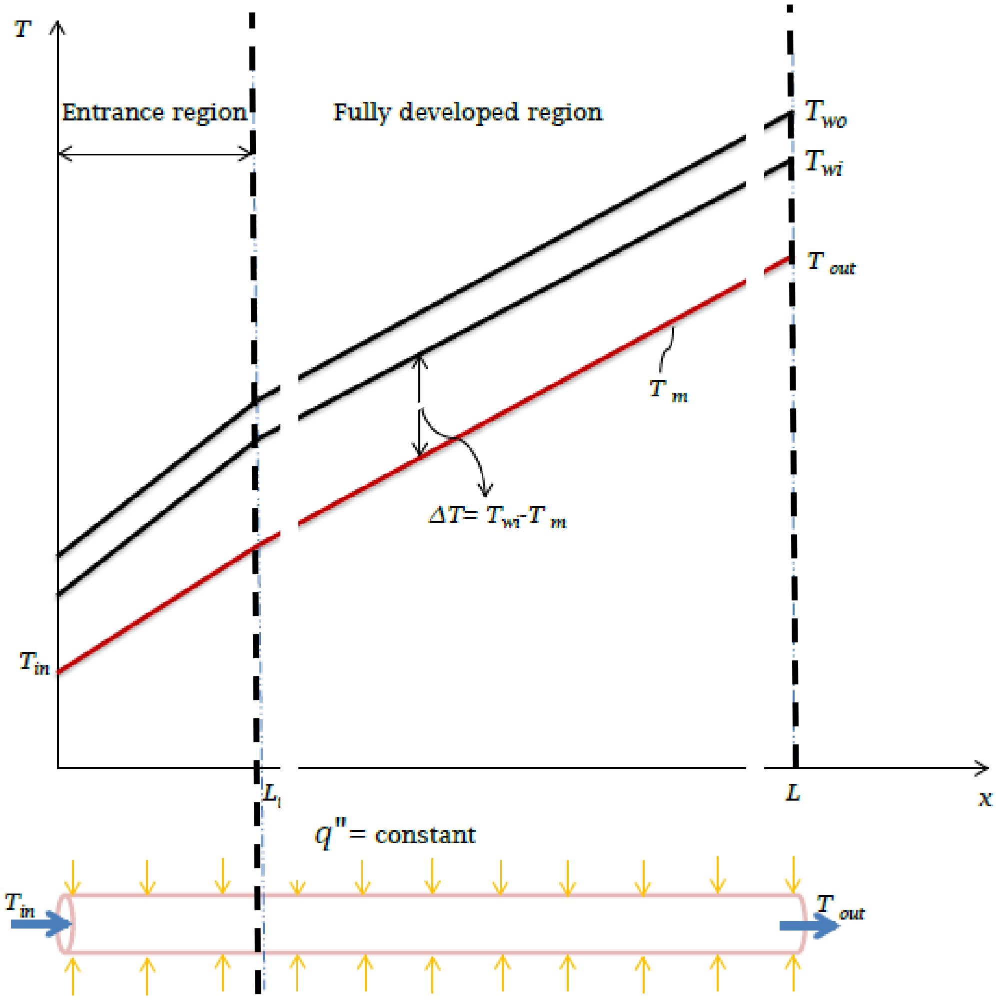

Figure 2-17:Variation in the temperature of the channel wall and the bulk fluid in channels with a constant wall heat flux boundary condition (adapted from [5])

The second type of wall temperature is constant wall surface temperature, which indicates that under constant wall temperature heating, the difference between the inside wall temperature (T_{wi}) of the channel and the fluid's bulk temperature (T_m) diminishes exponentially. This behaviour is illustrated in figure 2-18 [5].

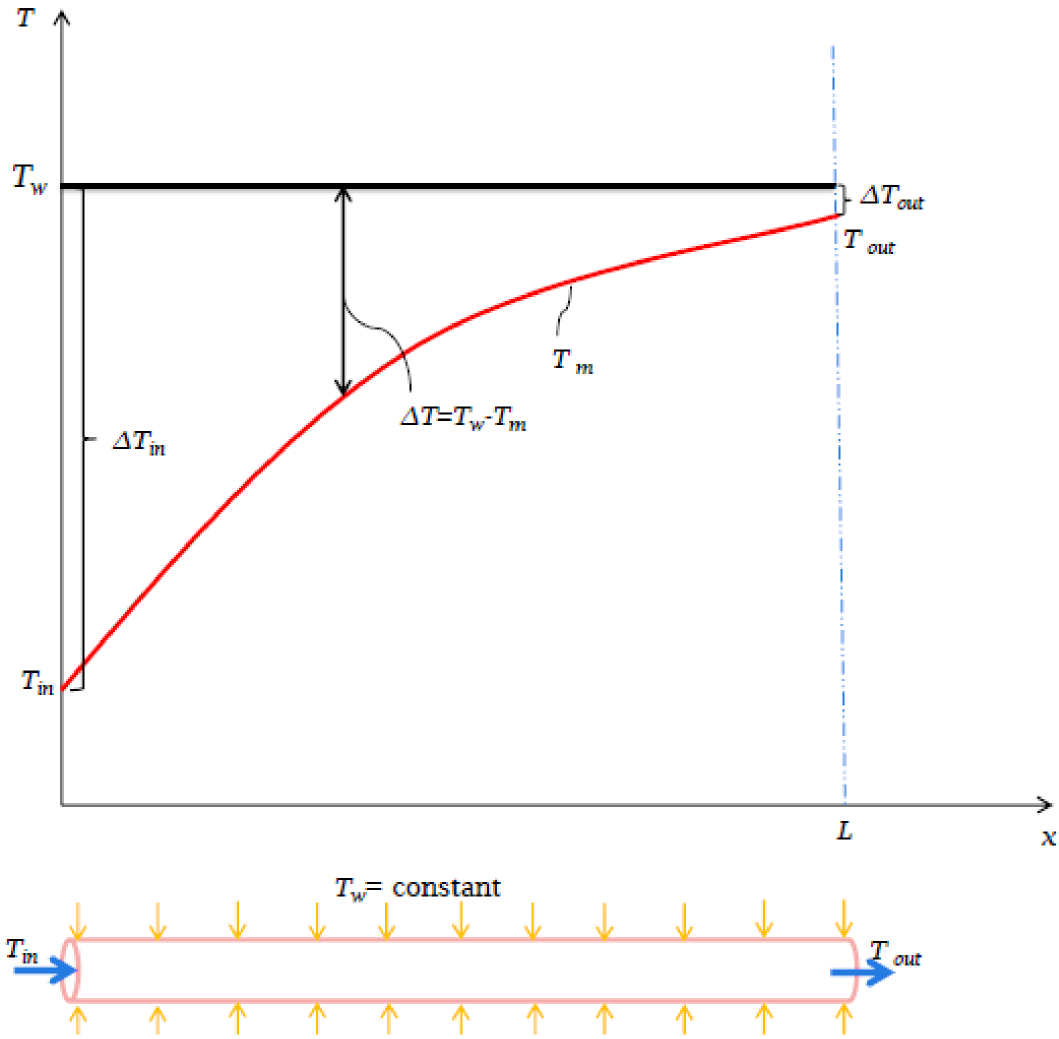

Figure 2-18: Variation of the temperature of the channel walls and the bulk mean fluid temperature at constant temperature condition of the wall's boundary [5].

Khan et al. [47] simulated the flow and temperature fields, as well as heat transfer, in a microchannel heat exchanger using a computer. They investigated the movement of flow and fields of temperature, along with the movement of heat through a microchannel heat exchanger. Hydrogen was the most efficient fluid in every way. It required less pumping work, had a more homogeneous flow distribution, and had low channel temperature rises.

In 2006, Renksizbulut et al. [48], examined slip-flow and heat transmission in rectangular microchannels with constant wall temperature. As a result, the effect of rarefaction (reduction in density) has been observed to develop three-dimensional laminar flow where it has constant property in rectangular microchannels where the Knudsen number is less than 0.1. Due to the existence of strong gradients close to the entrance of the channel, the region's slip velocity and temperature jump are significant. However, slip velocities in the corner regions were rationalized because the flow develops across the channel axis due to the low velocity gradient. While rarefaction (reduction in density) features have a small effect on entry lengths, they demonstrate an extraordinarily nonlinear relationship with channel aspect ratios throughout a large range of Reynolds numbers.

Recreation (reduction in density) of thermal micro-flow using the lattice Boltzmann technique with a Langmuir slip model has conducted by Chen and Tian [49] in 2010 to investigate the physical picture and the application of Langmuir slip model. Implementing the Langmuir slip model for the lattice Boltzmann method to detect velocity slip and temperature increment in micro-flows with a temperature change has been discussed in this study.

2.7 Flows with two phases and heat transfer

Two-phase heat transmission can be broadly divided into two types: latent (boiling) and sensible (non-boiling) two-phase heat transfer. Latent two-phase heat transfer is the most common type. Pool boiling, which occurs when a heating surface is immersed in a pool of initially relatively stable liquid, and flow boiling, which occurs when a heating surface is immersed in a flowing stream of fluid, with the heating surface possibly being a channel wall that confines the flow, are the two categories of heat transfer during boiling. Pool boiling is the most prevalent form of heat transmission in boiling [50].

Non-boiling two-phase heat transfer occurs when two phases of matter exist within the channel; generally, one phase is a based liquid, most commonly water. The secondary phase can be a stable gas or another liquid that does not mix with the primary phase. The focus of this review is on non-boiling two-phase heat transfer.

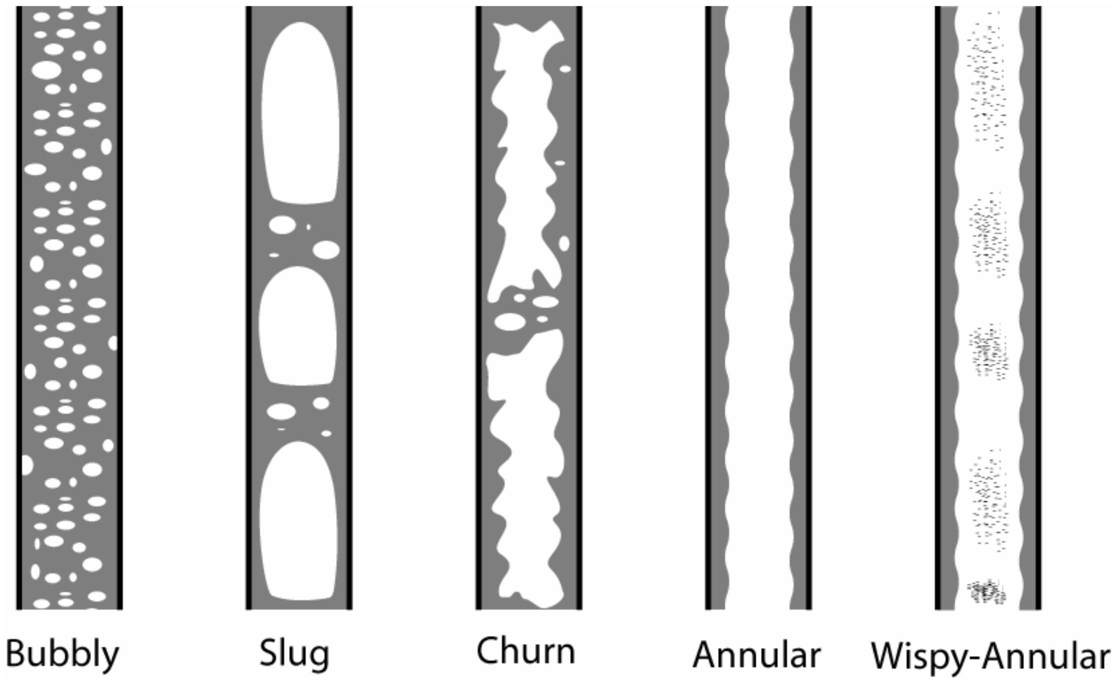

Figure 2-19: Vertical rising flow patterns in a tube

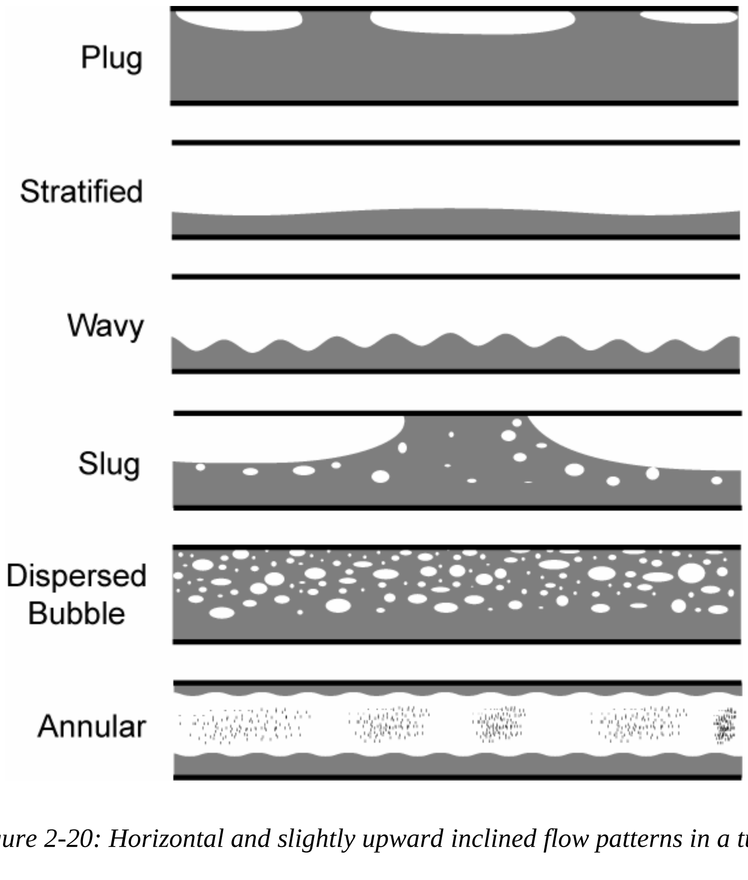

Figure 2-20: Horizontal and slightly upward inclined flow patterns in a tube

In 2010, Ghajar and Tang [51] have done a study on the importance of non-boiling two-phase flow for industrial applications involving heat transfer through pipes. According to their study, a low velocity is required to achieve the required high heat transfer rate. Vertical pipes were used to investigate turbulent gas-liquid flow using a variety of different flow patterns and fluid combinations. During the investigation of non-boiling two-phase flow heat transfer in pipes, the vacancy percentage has received substantial consideration. Same author Ghajar [52] explained the distinction between vertical upward two phase flow and horizontal two phase flow in 2005.

2.7.1 Heat transfer via two-phase liquid-liquid flow

In microchannels, liquid-liquid two-phase flows give much superior fluid flow and heat transfer properties than single phase fluid flows. There are a number of heat transfer and pressure drop relationships for two-phase gas-liquid flow, but few for two-phase liquid-liquid flow.

In 2010, Janes et al. [53] has done a study on liquid-liquid two-phase and heat transfer in gas-liquid plug flow system. The study experimented with water-air, oil-air, and oil-water mixtures and obtained single-phase oil and single-phase water as a benchmark. They discovered that the flows behave almost identically to Taylor flows.

To measure the influence of friction on two-phase liquid-liquid flow, the experiment that is most applicable is employed. To enable visualization of the flow Lim et al. [54] conducted a research on the heat transfer characteristics and flow visualisation of gas–liquid two-phase flow in a microchannel subjected to a continuous heat flux at the wall in 2013. A link between the Nusselt number and the axial position, as well as a correlation between the Nusselt number and the void %, have been established as a result of these studies.

2.7.2 Pressure-drop in two-phase liquid-liquid flow

Pressure-drop across a microchannel is critical in determining the amount of energy required for pumping, parasitic energy loss, and flow stability. Most of all the heat transfer within the channel is affected by the pressure drop. This variable should be explored using a variety of methodologies, including experimental, empirical, and semi-analytical.

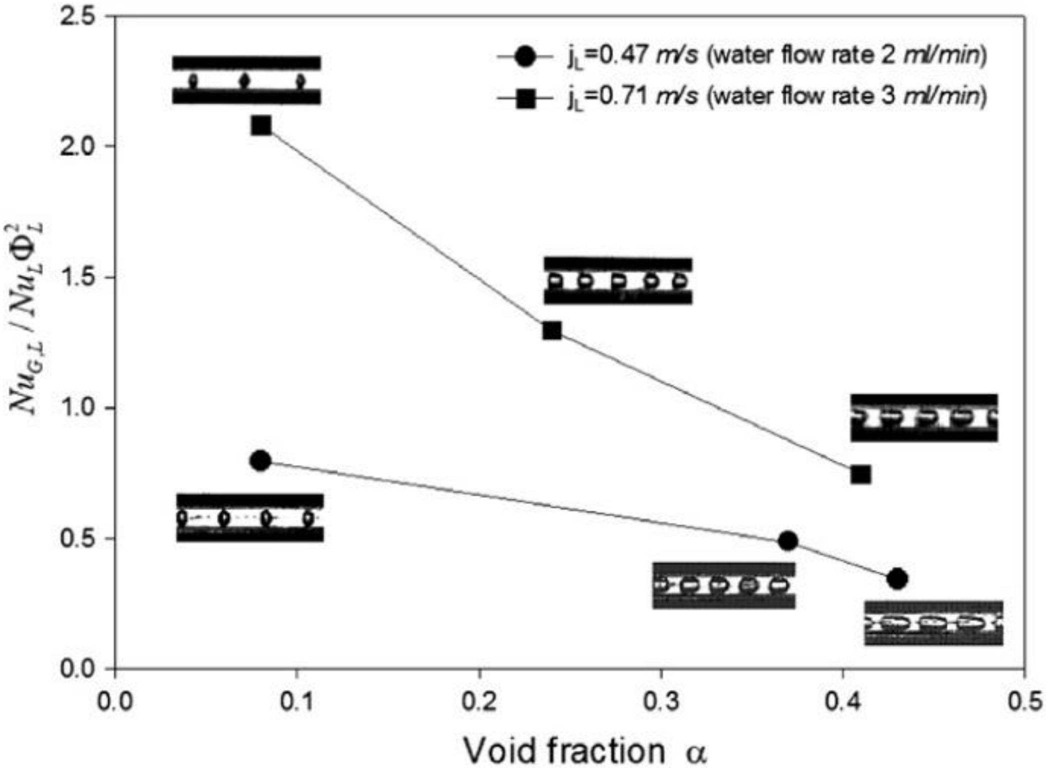

Figure 2-21: Enhancement of two-phase heat transfer at various void fractions [54]

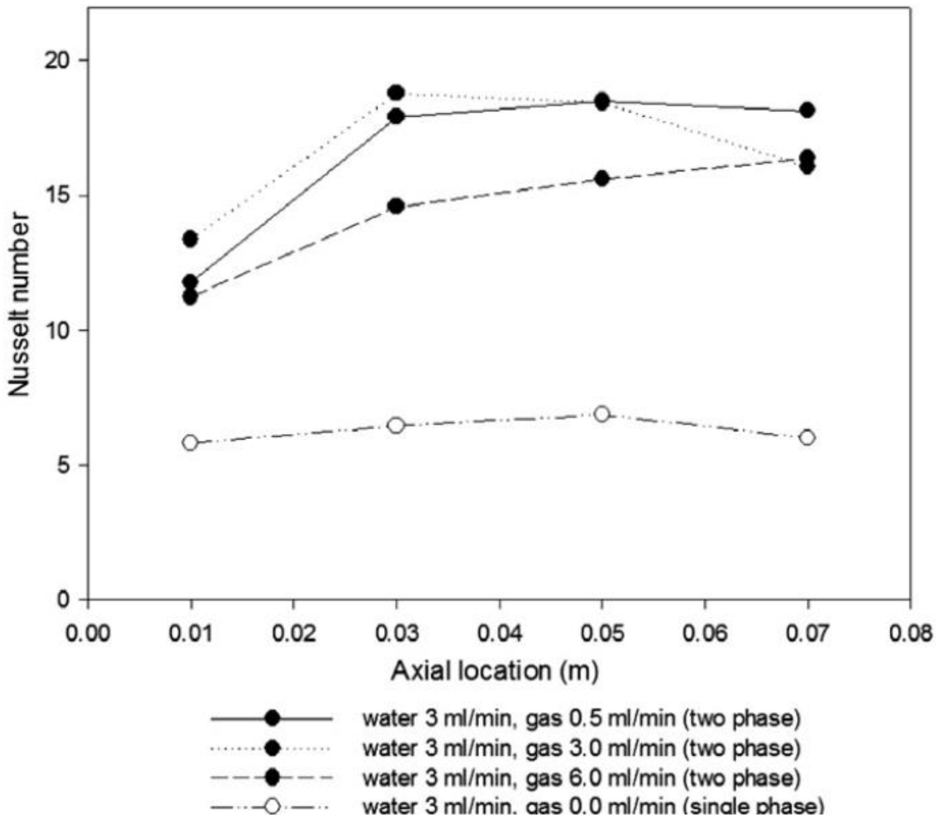

Figure 2-22: Nusselt number comparison between single-phase and two-phase flow in a 300 µm diameter duct with varying water flow rates [54]

Numerous methods for estimating the pressure drop in a Taylor flow have been devised. Syringe pumps are frequently used in microchannel networks due to their simplicity.

Pressure-drop in a circular channel basically occurred because of the fluid friction. According to Ladosz and Rohr [55], microchannel fluid friction can be used to operate small volume droplets such as amalgamation, splitting, and phase separation. In 1949, Lockhart and Martinelli [56] devised a model to examine pressure drop efficiency in gas liquid two-phase flow. have developed a model to investigate efficient pressure drop in two-phase gas liquid flow. The non-dimensional pressure drops and frictional pressure gradients between the liquid and gas phases as they travel through the pipe ratio are the essential aspects to this relationship. The disadvantage of this correlation was that it was based heavily on investigational data and only sporadically on physical modelling. In 1975, Taitel and Dukler [57] demonstrated in 1975 that the hold up and non-dimensional pressure drop for stratified flow are only functions of the ratio of the liquid's frictional pressure gradient to that of the gas when they each phase flow through the pipe at constant friction ratio.

Ladosz and Rohr [55] researched and developed a pressure drop model for liquid-liquid slug flow in rectangular microchannels. They mentioned that in microchannels, laminar flows govern and are classified by its parabolic velocity profiles. Additionally, multiphase flow interfaces disrupt this velocity profile, resulting in additional pressure losses due to the pressure drop across the interface. The resulting regime's velocity profile is depicted in Figure 2-23.

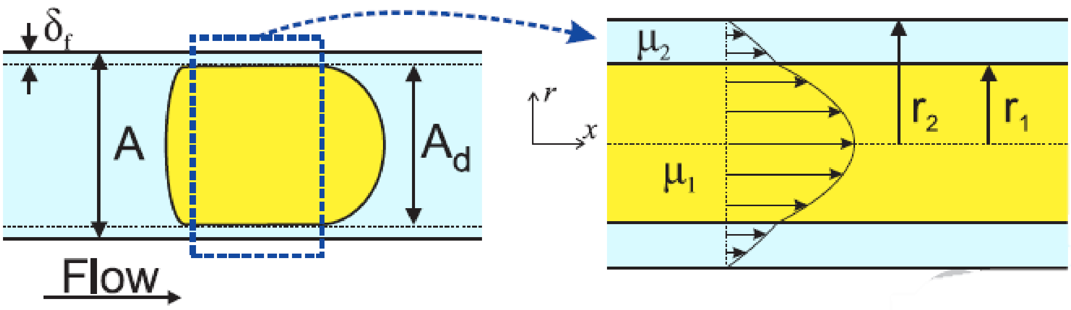

Figure 2-23: A circular channel with a radius of r_2 and a droplet with a radius of r_1.

The pressure-drop in a microchannel due to volume changes can be written as follows:

$$\Delta P = \Delta P_{frictional} + \Delta P_{interfacial} \qquad 2.19$$

Pressure drop is made of three separate components in liquid–liquid slug flows: frictional losses in the continuous phase, dispersed phase, and interfacial. This can be expressed in the following manner:

$$\Delta P = \Delta P_{frictional,continuous} + \Delta P_{frictional,dispersed} + \Delta P_{interfacial} \qquad 2.20$$

In 2009, Walsh et al. [58] mentioned a mathematical expression to find the pressure drop due to the bulb or the slug which is shown in equation (2.21)

$$\Delta P_{bulb} = 7.16(3Ca)^{2/3}\frac{\sigma_i}{D} \qquad 2.21$$

where, σ_i denotes the interfacial tension between two given fluids, D denotes the diameter, and Ca denotes the Capillary Number. This study established the scaling in a model aimed at predicting the pressure drop in a droplet or slug segmented flow as a function of the ratio of the single-phase length to the channel diameter and the ratio of the Capillary number to the Reynolds number, thereby demonstrating the deficiencies of Bretherton's theory.

Jovanovic et al. [59] demonstrated the results of drop in pressure for various two-phase fluid flows and compared them to theoretical and experimental variances in 2011.The sizes of the discrete phase particles were determined to be dependent on the organic to aqueous flow ratio, viscosity, velocity, and slug capillary diameter.

Figure 2-24 shows the theoretical model pressure drop with respect to slug velocity. Illustrated models are moving film (MF) and stagnant film (SF), Kashid et al. [60] model and Salim et al. [61] model in the instance of the Water - Toluene (W-T) flow in a 248 μm channel diameter. The aids of the discrete and continuous phase frictional pressure-drop and the boundary pressure drop to the total slug flow, pressure drop at an organic to aqueous volumetric fraction (O/A) fraction in the case of a Water - Toluene (W-T) flow in a capillary with a diameter of 248 3μm are shown in Figure 2-25. The pressure-drop as a function of slug velocity is illustrated in Figure 2-26 for water-toluene (W-T) and ethylene glycol/water-toluene (EG-T) slug flows in 248 μm and 498 μm passageways, respectively, using the stationary film model (solid line).

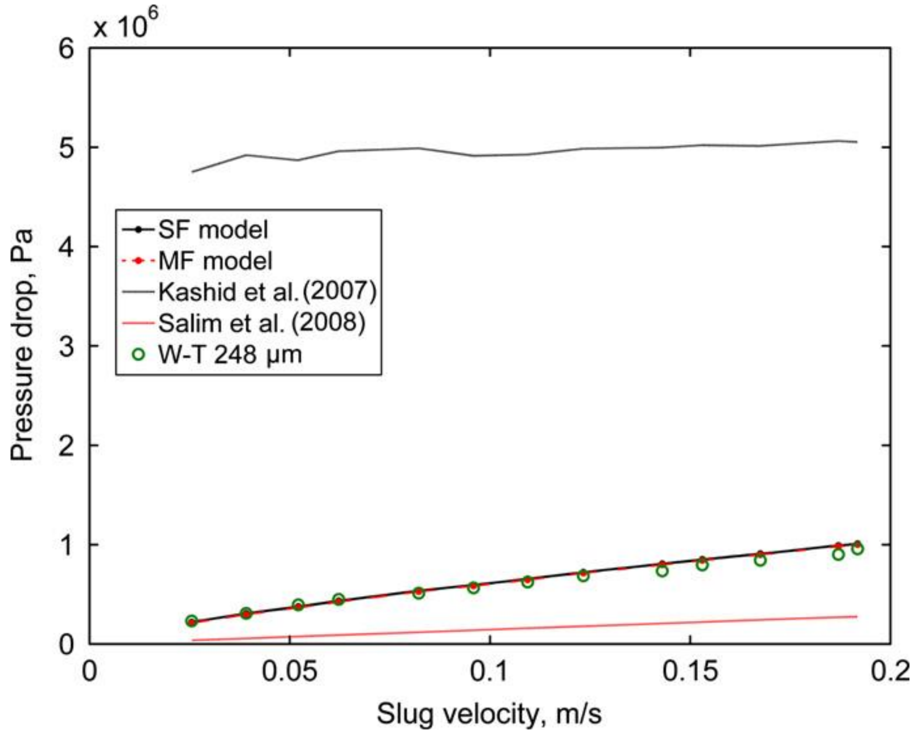

Figure 2-24: Shows the theoretical model pressure drop with respect to slug velocity. Illustrated models are stagnant film, moving film, Kashid el at. [60] model and Salim et al. [61] model on the case of the water-toluene (W-T) flow in a 248 µm capillary [59].

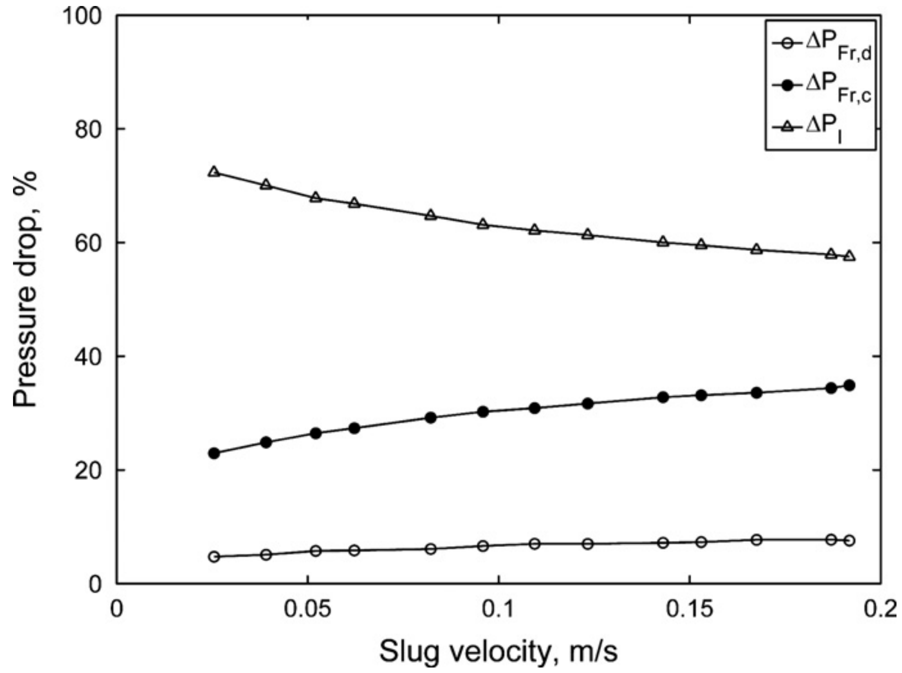

Figure 2-25: Contributions of the dispersed and continuous phase frictional pressure drops, as well as the interface pressure drop, to the total slug flow pressure drop when the organic to aqueous volumetric ratio (O/A) in an instance of water-toluene (W-T) flow in the 248 µm capillary[59].

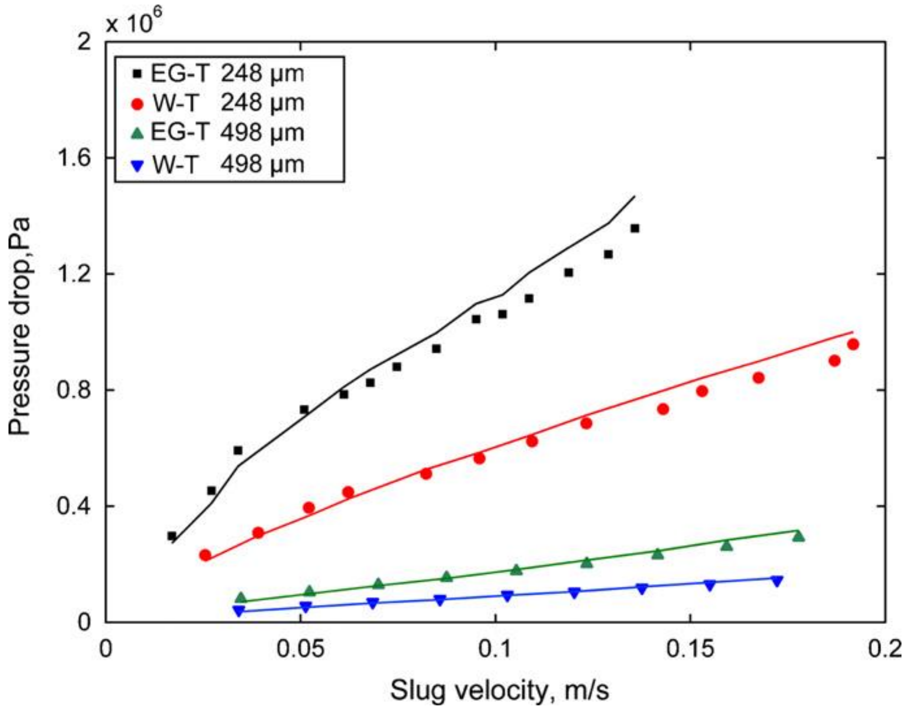

Figure 2-26: The stagnant film model was used to calculate the water-toluene (W-T) and ethylene glycol/water-toluene (EG-T) slug flow pressure drop in the 248 µm and 498 µm capillaries as a function of slug velocity at an O/A ratio of 1 (solid line)[59]

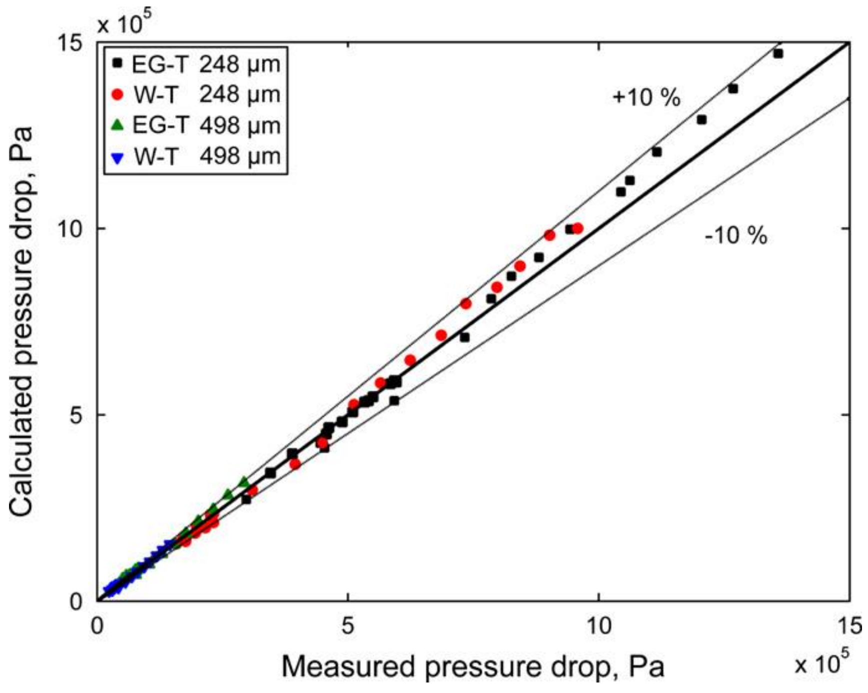

Figure 2-27: The water-toluene (W-T) and ethylene glycol/water-toluene (EG-T) slug flow pressure drop in the 248 µm and 498 µm capillaries was compared to the measured slug flow pressure drop using the stagnant film (SF) model [59].

The figure 2-27 compares the water-toluene (W-T) and ethylene glycol/water-toluene (EG-T) slug flow pressure drop in capillaries with diameters of 248 μm and 498 μm, respectively, as predicted by the stationary film model and as measured.

2.8 Bubble velocity and film thickness

In two-phase flow in a microchannel, as previously mentioned, several research gaps must be filled. In addition, the heat transfer processes related with the transition from sliding slug to Taylor flow are understudied and under experimented. Even the experiments are based on the two-phase movement of gas and liquid. Fairbrother and Stubbs published The Hydrodynamics of Slug Flow in 1935 [30]. Numerical analysis of the two-phase slug flow was performed using the parameters included in this research. Salim et al. [61] performed an experiment on the pressure drop, flow patterns, and wall wetting abilities of oil-water flow in microchannels. As a result of the experiment, distinct flow patterns were observed in different microchannels that were initially saturated with water. They began by dipping the quartz and glass microchannels in oil. The thickness of the coating has a noticeable effect on the slug and bubble velocities. The following equation creates a link between the thickness of the film and the velocities of the slug and bubble.

$$\frac{U_s}{U_B} = 1 - m \qquad 2.22$$

The overall heat transmission in the two-phase slug flow is controlled by this slug length. He et al. [62] discovered the total heat transfer is mainly controlled by the slug length and the fraction of the wall taken by the slug by using a numerical investigation. In 2007, Urbant et al. [63] numerically examined how the size of a water droplet in a microchannel can affect enhancement of heat transfer in mineral oil. This resulted in improved heat transfer efficiency and a higher Nusselt Number value.

2.9 Two-phase nanofluidic heat transfer in microchannels (slug flow)

Two-phase nanofluidic heat transfer entails the formation of a two-phase flow by two non-mixing liquids, one or both of which contain nanoparticles. The use of nanofluid in a two-phase system is believed to improve the system's total heat transfer. However, it has been demonstrated that the use of nanoparticles in conventional fluids and single-phase flow systems significantly improves overall heat transfer in the system, as discussed in this chapter. Adham et al. [64] discussed a variety of microchannel heat sink-related topics. They noted that additional research is necessary to examine various aspects of these heat sinks, including nanofluids and microchannel shapes.

Cheng and Xia [65] stated in 2018 that two-phase flow utilizing nanofluids significantly improves heat transfer. However, the fundamentals of boiling heat transfer and critical heat transfer (CHF) singularities in nanofluids remain unknown. Cheng and Xia concluded by stating that physical properties should be investigated in order to create a consistent database and general prediction approaches along with models. The effect of heat transfer parameters such as size and type on the development of nucleate heat transfer should also be investigated. Additionally, the underlying theories for these shifts should be identified. To assess the potential benefits of nanofluids, macroscale channel studies on their two-phase flow, heat transfer, and CHF should be conducted.

Sabaghan et al. [66] conducted a study on the effect of longitudinal vortex generators on nanofluid flow and heat transfer in a microchannel: Two-phase numerical recreation and developed an inclusive simulation process capable of estimating the effect of longitudinal vortex generators (LVGs) within a microchannel (rectangular shaped) on various nanofluids including TiO_2/water, TiO_2/transformer oil, and TiO_2/EG-W. (Ethylene Glycol and Water). When compared to ordinary microchannels, these LVGs have a considerable impact on heat transport. In Figure 2-28, results of the experiment are illustrated. The temperature and velocity effects on LVG enhanced microchannels subjected to increased heat transfer are shown in Figure 2-29.

Numerous researchers have conducted studies on boiling heat transfer with the use of nanofluid to increase the heat transfer capacity. Kamel et al. [67] says the valuation of the point heat transfer coefficient (HTC) with the existence of nanofluids is compulsory for understanding the three-dimensional differences of the temperature along the channel flow.

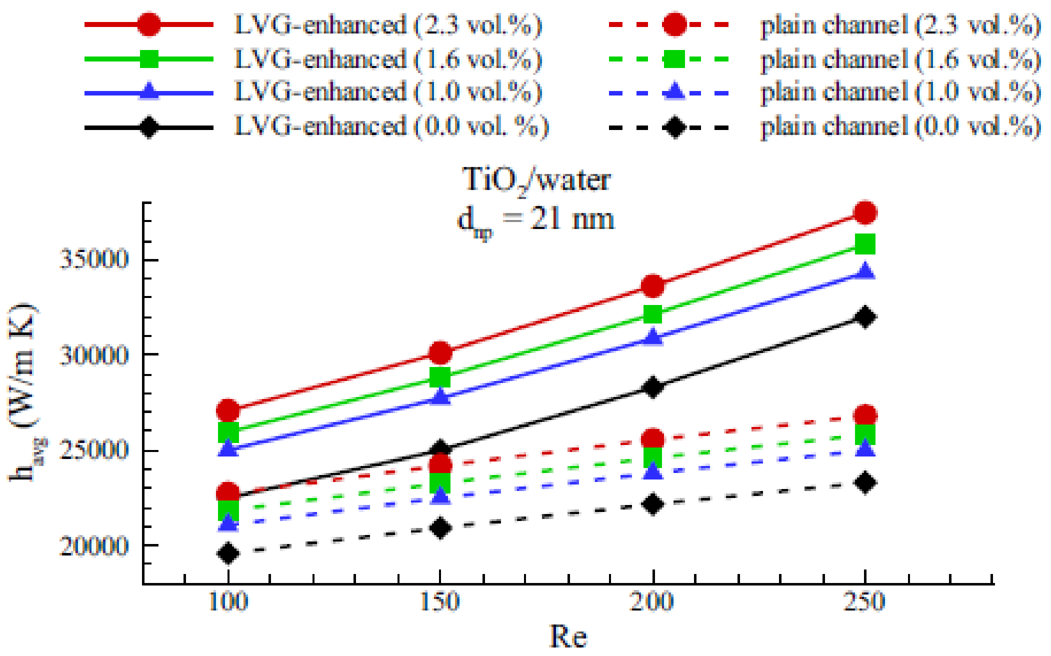

Figure 2-28: Comparison of convective heat transfer coefficient friction factor between the LVG-enhanced microchannel and the plain channel [66].

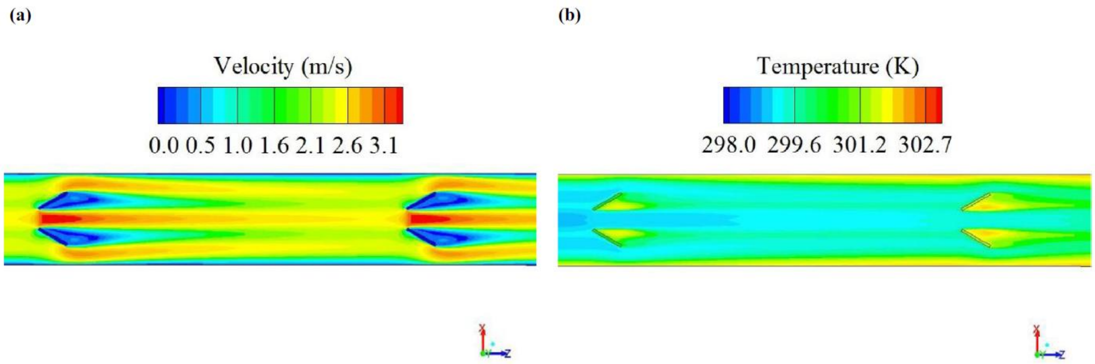

Figure 2-29: The LVG-enhanced microchannel's velocity (a) and temperature (b) contours [66].

Nanofluids have the potential to improve or deteriorate pool boiling temperatures (HT and CHF), depending on the material, size, and concentration of the nanofluids. Additionally, the material, shape, alignment, and coarseness (roughness) of the heated surface, the wetting agent, base fluid, process pressure, and heat flux are all considered. It is convinced that nanofluids can significantly improve pool boiling, HT, and CHF when a proper balance of these influences is engineered to meet specific requirements [68].

2.10 Summary

Experimental and computational studies of two-phase flow in microchannels, including their hydrodynamics, hydrokinetics, and heat transfer characteristics, are reviewed in this chapter. It was demonstrated that two-phase flow has a significantly greater capacity for heat transfer than conventional single-phase flow. Two-phase flow, on the other hand, has a much higher Nusselt number than single phase flow. When it comes to two-phase flows, the literature indicates that non-mixing two-phase slug flows have a significant heat transfer advantage over gas-liquid two-phase flows. The primary disadvantage of two-phase slug flow is the significant pressure drop. This requires a significant amount of pumping power to achieve the desired slug flow. Therefore, the analysis of pressure drop in two-phase liquid-liquid flow will attract a great deal of interest from scientists whose connections are necessary for the creation of microfluidic schemes. It has been experimentally established that the pressure drop in a slug flow rises as slug velocity increases, hence enhancing heat transfer inside the channel [5], [30].

Despite the fact that a few theoretical models have been developed to account for the link between heat transmission and hydrodynamic constraints, there are significant differences of over 500 percent between the Nusselt number relationship and the findings. To better comprehend the interaction between heat transport and other characteristics, it is essential to build novel theoretical representations.

Another way to improve heat transfer is to use nanofluids. Comprehensive reviews on the use of nanofluids in heat transfer applications are included in this chapter. A nanofluid's relative viscosity increases with volume fraction and heat transfer. While researchers frequently use nanofluid in a microchannel as a single phase, very few studies on two-phase liquid-liquid slug flow are available in the literature.

It is clear that, more research needs to be conducted to find the actual behaviour of a nanofluid in a liquid- liquid two-phase system. This research gap needs to address due to its efficiency in heat transfer.

3 NUMERICAL ANALYSIS ON CIRCULAR MICROCHANNEL

Methods for conducting numerical fluid flow assessments in microchannels are described in this chapter. It discusses the study's simulation procedure.

3.1 Problem Formulation and solution procedure

In this study, two-dimensional axisymmetric approximations were employed, to model circular cross-sectional channels leading to reduce the computational power requirement. Because the circular cross section of the microchannels is geometrically similar, it is even more convenient to use two-dimensional space rather than the computationally expensive three-dimensional space.

3.1.1 Interface tracking in two – phase liquid – liquid Flow

Numerous methods exist for tracking interfaces, one of which makes use of the Eulerian interface framework. When implemented, each of these methods has a number of advantages and disadvantages. Volume of fluid, forward-facing tracking, phase field, and level set approaches are the most used and reliable today.

In 1981, Hirt and Nichols [69] pioneered the volume of fluid method for implicitly tracking interfaces via a volume fraction function. Using a volume percentage between zero and one, the average amount of one of the fluids in each cell is calculated. A cell with a transitional volume fraction, on the other hand, will have a value in the middle. The primary advantage of this method is that it allows for fully mass conserved calculations, whereas it requires a special method to study convection in a discontinuous volume fraction field.

The level set algorithm was introduced in 1987 by Osher and Sethian [70]. This method is applicable to image processing, inverse problems, crystal growth, and modelling multi-phase flows. This method is novel in that it allows for the embedding of the interface in a higher dimensional function.

The phase field method is the next method that can be used for interface tacking. This has a wide range of engineering applications. For instance, environmental engineering, petroleum engineering, and chemical engineering all employ the phase field method when dealing with multiphase flows. The primary advantage of this method is that it does not require any prior assumptions about the interface's shape [71]. Phase Field method use Navier Stokes, continuity and Cahn Hilliard equations which were solved together to determine the phase interface [72].

In this present work, two methods were used to track the interface of two phases. First, the Phase Field method was used to visualize the two-phase slug flow. Then the Volume of Fluid method was used to obtain a refined edge between the two interfaces.

3.1.2 Governing Equations

By solving the governing equations, the mass-momentum-energy conservation rules were derived. Different solving models have different representations of these governing equations according to their method of solving the model. Governing equations are expressed in different formats based on the method used for interface tracking.

- **Phase Field Method**

Mass Conservation [73]:

$$\frac{\partial}{\partial t}\left(\epsilon_{pr}\rho_r\right) + \nabla.\left(\rho_r v_r\right) = q_r - \rho_r \alpha_r \frac{\partial \epsilon_{vol}}{\partial t} \qquad 3.1$$

where $\rho_r, q_r, \epsilon_{pr}$ and α_r are the density of the fluid, source term, porosity, and Biot Coefficient in the reservoir domain, respectively.

Darcy's Velocity in $\Omega_r(t)$ [73]:

$$v_r = -\frac{K_r}{\mu_r}\left(\nabla p + \rho_r g\right) \qquad 3.2$$

where K_r and μ_r are the permeability and fluid viscosity of $\Omega_r(t)$ respectively.

Pressure Equation p [73]:

$$\rho S \frac{\partial p}{\partial t} - \nabla . \frac{\rho K}{\mu} (\nabla p + \rho g) = q_m - \rho \alpha X_r \frac{\partial \epsilon_{vol}}{\partial t} \qquad 3.3$$

- **Volume of Fluid method**

Continuity Equation: [74]

$$\frac{\partial \rho}{\partial t} + \nabla . U = 0 \qquad 3.4$$

Momentum Equation: [74]

$$\rho \left(\frac{\partial U}{\partial t} + (U . \nabla) U \right) = -\nabla p + \nabla . \left(\mu (\nabla U + \nabla U^T) \right) + F \qquad 3.5$$

Energy Equation: [74]

$$\frac{\partial (\rho E)}{\partial t} + \nabla . \left(U(\rho E + p) \right) = \nabla . (k \nabla T) \qquad 3.6$$

Volume Fraction Equation: [74]

$$\frac{\partial (\emptyset)}{\partial t} + \nabla . (\emptyset U_s) = 0 \qquad 3.7$$

**Note: Definitions of the notations are mentioned in the list of abbreviations.*

The velocity U is treated as mass averaged variable, according to $U = \left[\emptyset \rho_s U_s + (1 - \emptyset) \rho_p U_p \right] / \rho_p$. The subscript s and p denote secondary and primary phase and ρ_p is the density of mixture.

3.2 Methodology

Initially, fluid flow and heat transport were numerically modelled in COMSOL Multiphysics using the solver. To capture the interface in these simulations, level set equations are solved. The model was then simulated using ANSYS Fluent in chapter 04. In ANSYS, the interface was captured using the VOF method. Unlike COMSOL Multiphysics, ANSYS Fluent enables users to create multiphase domains with more than two phases. This enables the numerical model to treat nanoparticles as a distinct phase.

3.2.1 Problem Setup

A two-phase slug flow with different hydrodynamic characteristics was used to investigate flow growth and early heat transfer. After selecting the numerical model, the geometry was approximated using an axisymmetric approximation.

COMSOL Multiphysics was used to investigate the shape of the droplet by varying the contact angle of the microchannel's wetted wall. This technique was also used to investigate droplet shape and formation, as well as slug length, by varying the velocities of the two phases at the cross junction. Boundary conditions and numerical model is presented in figure 3-1.

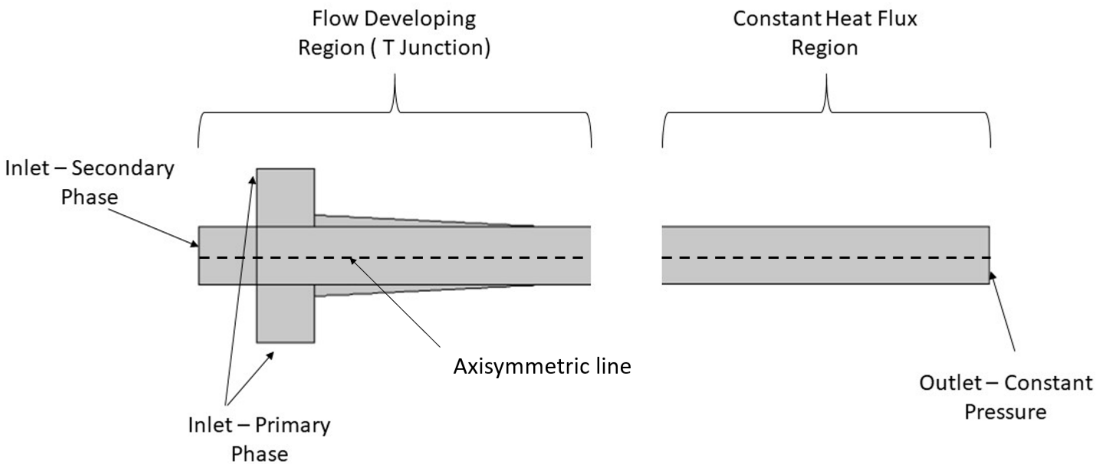

Figure 3-1:Schematic diagram of two-phase flow model with Cross-Junction (One half has mirrored via axisymmetric line)

An interior diameter of 100 micrometres and a length of 3600 micrometres comprise the geometrical model. This model is composed of two major sections. The first is a cross-shaped junction that was used to investigate the effect of inlet velocity on slug length. With a 3600-micrometer length microchannel, as shown in Figure 3-1, the heated segment can have a hydrodynamically produced flow. To improve representation in Figure 3-1, the geometry was mirrored along the axisymmetric line. The primary and secondary fluids were water and light mineral oil, respectively, and the microchannel wall was believed to be built of aluminium. Table 3.1 lists the properties of the materials.

Table 3-1: Properties of materials

Material	Density [kg/m³]	Specific Heat [J/Kg.K]	Thermal Conductivity [W/m.K]	Viscosity [Pa.s]
Water	998	4182	0.6	0.001002
Light mineral oil	838	1670	0.17	0.023
Aluminium	2690	917	239	N/A

Typically, the development length is less than ten times the diameter of the microchannel. This allows for complete development of the slug flow prior to entering the heated zone. This study makes use of a uniform heat flux of 1 kW/cm^2, which approximates the rate of heat generation in a microchip [75]. Using varied velocities for different scenarios, the inlets are set up to have a uniform velocity boundary condition while the exit is set up to have a zero-gauge pressure. The specifics of each study, along with their associated approaches, are listed in Table 3.2. The capillary number was determined using the equation below for table 3.2.

$$Ca = \frac{\mu_l U_s}{\sigma} \qquad 3.8$$

where, $Ca, \mu_l, U_s and\ \sigma$ are the Capillary number, dynamic viscosity of the liquid, superficial velocity, and surface tension, respectively. The Reynolds number was calculated using equation 3.14.

$$Re = \frac{\rho U_m D}{\mu_l} \qquad 3.9$$

where, Re, ρ, U_m, D & μ are the Reynolds number, density of the fluid, mean velocity, pipe diameter and dynamic viscosity of the liquid, respectively.

The velocities within each phase determine two-phase flow patterns. This velocity determines the flow type: bubbly, slug, churn, slug annular, or annular slug annular. A velocity map was done by Triplett et al. [76] in 1999 for a 1.45 mm circular test section. The results are shown in Figure 3-2.

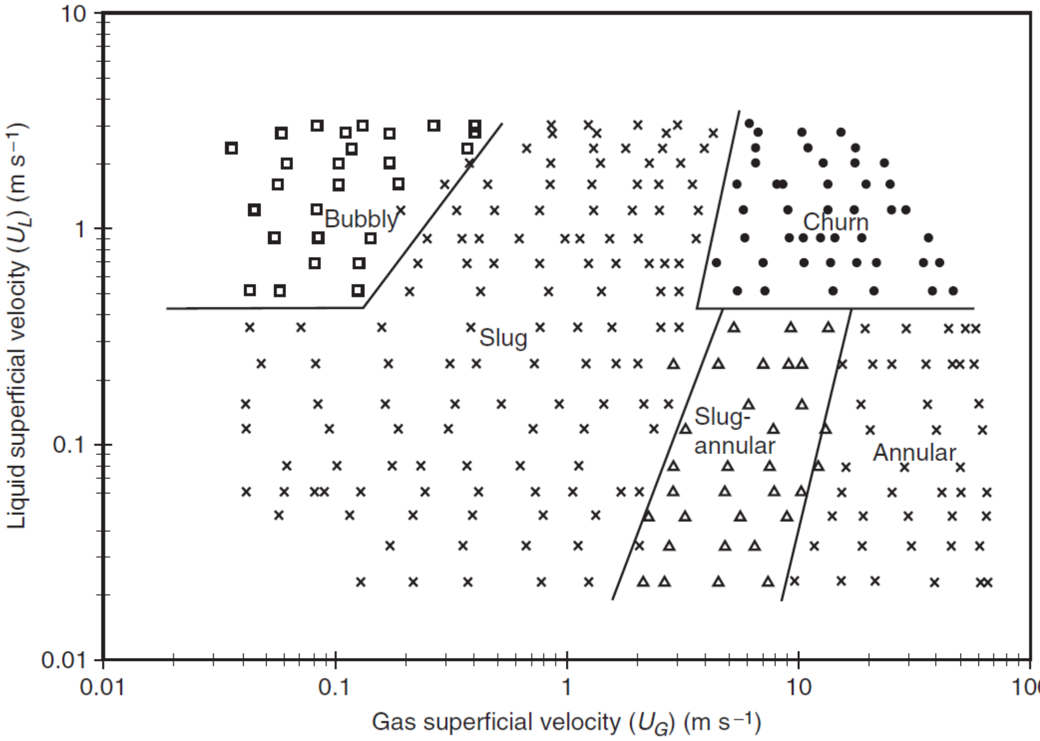

Figure 3-2: Flow shape map as detected by [76] circular test section where diameter is 1.45 mm. Transition lines are not from the Triplett et al. but are indicatives.

However, there are no conclusive studies on the velocity interaction at the inlet for liquid–liquid two-phase flows.

Table 3-2: Different test cases considered for the study

Propose of the case	Case no	Inlet Velocity Light mineral oil[m/s]	Inlet Velocity Water [m/s]	Contact angle [degree]	Capillary number	Reynold Number
Effect of inlet velocities [Water]	1	0.1	0.1	170	0.00206	19.92
	2	0.1	0.2	170	0.00305	29.88
	3	0.1	0.3	170	0.00407	39.84
	4	0.5	0.5	170	0.01017	99.60
Effect of inlet velocities [Light mineral oil]	1	0.2	0.1	170	0.00305	29.88
	2	0.2	0.2	170	0.00407	39.84
	3	0.2	0.3	170	0.00509	49.80
Effect of Contact Angle	1	0.2	0.2	90	0.00407	39.84
	2	0.2	0.2	135	0.00407	39.84
	3	0.2	0.2	170	0.00407	39.84

3.2.2 Mesh generation for the numerical analysis

Mesh generation and mesh sizing is an important step in numerical simulations since the accuracy of the results is highly dependent on the size of the mesh elements. Therefore, mesh generation needs to be given special consideration to capture the accurate physics of the fluid flow and heat transfer. The flow in a microchannel can be accurately studied using a mesh with a D/100 or lower element size. The thin liquid layer that forms between the microchannel and the bubble can be detected using an element of this size [77].

COMSOL Multiphysics makes use of the adaptive mesh refinement approach, one of several available mesh refinement methods. Local adaptive mesh refinement will reduce the computational power while preserving the precision. Here, mesh adaptation happens while the solution is running, and the mesh will change continuously. The refinement is happening by estimating the error indicator on the initial coarse mesh by identifying the high gradient areas. The generated mesh is shown in Figure 3-3.

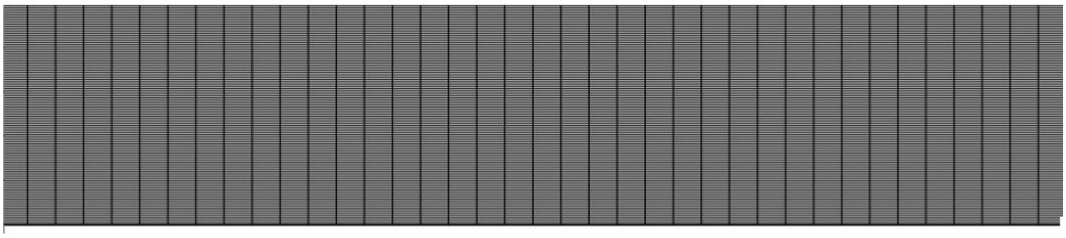

Figure 3-3: The simulations' mesh elements

In these studies, mainly rectangle mesh has been used with a mesh quality of around 0.98. This has ensured a reliable solution for point functions once the numerical study was conducted. The details of the mesh which was used in this study are mentioned in table 3-3. To increase the mesh accuracy, triangles and quadrangle-type mesh elements were used here. However, the effect of the mesh refinement has no significant effect on the results, according to [78]. As a result, for simulations, a mesh with over 0.5 million elements was chosen.

Table 3-3: Mesh Details

Mesh Vertices	**561317**
Triangles	**4**
Quads	**558892**
Edge elements	**6126**
Vertex elements	**16**
Domain element statistics	
Number of elements	**558896**
Minimum element quality	**0.5392**
Average element quality	**0.9889**
Element area ratio	**0.05311**
Mesh area	**348000 µm²**

Validation of the numerical procedure can be done by comparing the film thickness obtained by the present study with different correlations available in the literature. The number of mesh elements within the film in the fluid flow was used to compute the film thickness in this investigation. Figure 3-4 shows the obtained film thickness from the study by overlaying the mesh on the volume fraction of water. Figure 3-5 illustrates the film created around a droplet and its thickness. This film is created due to the separation of Taylor bubbles or droplets from the channel wall. As a result, the bubbles' shear stress is substantially lower than the shear stress on the wall from liquid layer. Due to this, bubbles or droplets tend to move faster than the rest of the fluid. Heat transfer and mass transfer are dependent on the film thickness created between the channel wall and droplets. Due to the fact that the majority of studies in the literature have used this method to determine film thickness, this is the correct procedure to follow.

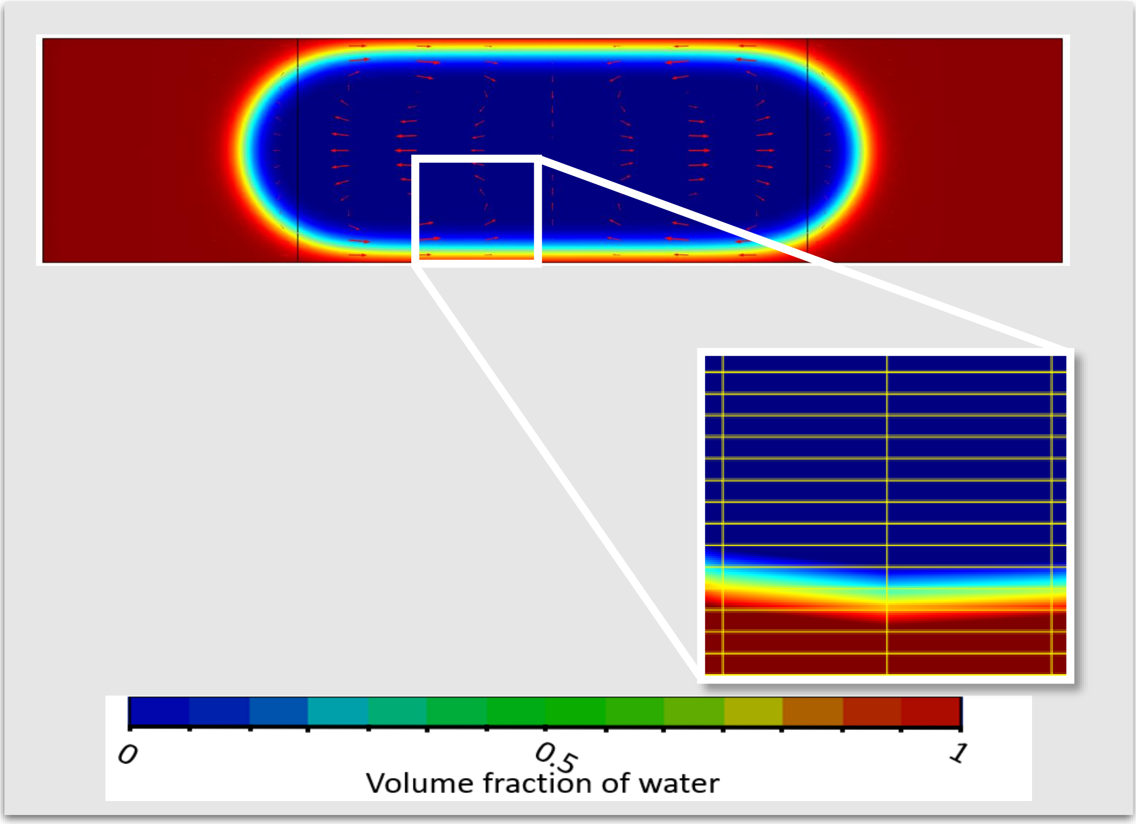

Figure 3-4: Generated mesh overlay with the volume fraction of water

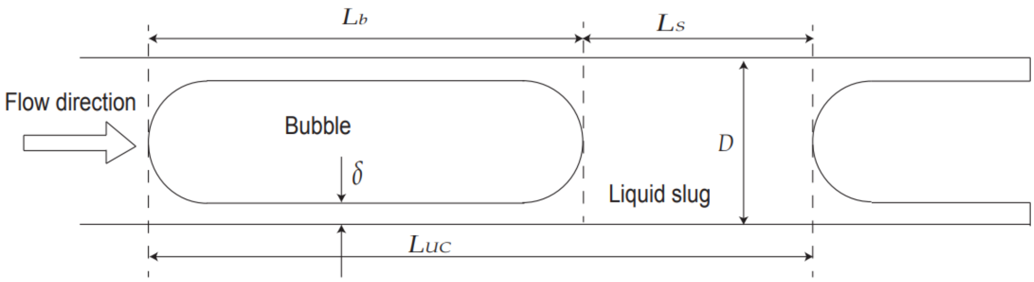

Figure 3-5: Schematic of a slug and bubble two-phase flow unit cell [5]

From the literature, different film thickness correlations can be obtained. Table 3-4 states the different correlations that have been obtained from the literature.

Table 3-4: Capillary Number

Calculation method		**Capillary Number (Ca)**	
		0.0044	**0.0038**
$\boldsymbol{\delta = 1.34 * R * Ca^{\frac{2}{3}}, 10^{-3} < Ca < 10^{-2}}$ **[79]**	(3.10)	1.82	1.61
$\boldsymbol{\delta = \frac{D}{2}\left(\frac{1.34 * Ca^{\frac{2}{3}}}{1+3.35 * Ca^{\frac{2}{3}}}\right), 10^{-3} < Ca < 1.4}$ **[80]**	(3.11)	1.67	1.49
$\boldsymbol{\delta = \frac{0.670D * Ca^{2/3}}{1+3.13Ca^{2/3}+0.504Ca^{0.672}Re^{0.589}-0.352We^{0.629}}, Ca < 0.3}$ **[81]**	(3.12)	1.68	1.50
Present Study		1.5 ± 0.5	1.5 ± 0.5

Different correlations for capillary number were investigated using the literature, and minimum and maximum values with a maximum error of 8% were used in the study.

3.2.3 Void Fraction

Void fraction is the ratio of the flow field employed by the secondary phase to its primary fluid domain. In this case, droplets act as the secondary phase flow. In a two-phase flow, the void fraction has an impact on many slug flow parameters, such as pressure drop, heat transfer, and flow pattern change. The void fraction can be determined using the equation 3.13. But finding the void fraction using inlet flow conditions is not a promising method due to the two-phase is tends to slip at the inlet because of the flow development.

$$\beta = \frac{U_s}{U_s + U_p} \tag{3.13}$$

Table 3-5: Calculation models for different parameters

Parameter	Calculation method
Water flow rates	1206 - 2413 μl/min
Silicon oil flow rate	302 - 2715 μl/min
Mixture velocity	$U_{TP} = U_p + U_s$
Homogeneous void fraction	$\beta = \frac{U_s}{U_p+U_s}$
Capillary number	$Ca = \frac{\mu_p U_{TP}}{\sigma}$
Reynolds number	$Re = \frac{\rho_p U_{TP} D}{\mu_p}$
Single phase Nusselt number	4.36 for constant heat flux wall
Viscosity of water	$\mu_p = 0.001002$ Pa.s
Kinematic viscosity of silicon oil	$\nu_s = 1.5$ cSt
Interfacial tension of water/silicon oil	$\sigma = 0.036$ N/m
Prandtl Number	$Pr = \frac{C_p \mu_p}{k}$
Slug length to diameter ratio	$L_s/D = 3$
Unit cell length to diameter ratio	$L_{UC}/D = 5$

3.2.4 Wall wettability and contact angle

The most important factor affecting the droplet's shape is its wall wettability. This occurs when the droplet moves as a sliding slug along the microchannel. The other variables that affect the shape of the droplet are the surface tension force, the contact angle, and the fluid viscous deformation force. Moreover, there are additional elements that influence wettability in addition to contact angle. When two immiscible liquids are combined on solid surfaces, the contact angle between them is precisely defined as the equipoise contact angle. Young's equation relates the angle to all of the different surface tension forces present at the three-phase interaction line [82].

$$\sigma_{l-g} \, cos(\theta_E) = \sigma_{s-g} - \sigma_{l-s} \qquad 3.14$$

where, σ_{l-g} is the difference in surface tension between a liquid and a gas, σ_{s-g} is between solid, gas and σ_{l-s} is between solid and liquid and θ_E is Young's equilibrium contact angle. When the equilibrium contact angle is tiny or when the wettability is high, it is known that the contact angle will be modest as well. When the equilibrium contact angle equals zero, the surface is completely wet, the liquid spreads spontaneously, and the surface has a high coefficient of attraction. It is called partial wetting if the equilibrium contact angle lies between 0 degrees and 90 degrees. If the equilibrium contact angle lies between 90 degrees and 180 degrees, it's called non-wetting, or liquid beads up formation [83]. This was used to determine the effect of the contact angle on heat transfer and droplet detachment during the setup stage.

3.3 Results and Summary

In Chapter 05, all results will be compared. The Level Set model was used to track the initial interface. because the computational power required for the simulations was relatively low in comparison to the other methods. Initially, triangle-based mesh elements were used; however, for improved computational performance, they were converted to quadrilateral mesh elements. This conversion significantly reduces the computational time.

4 NUMERICAL ANALYSIS OF FLOW IN CIRCULAR MICROCHANNEL WITH NANOPARTICLES

In this chapter details the methodology used in the current work, which includes the addition of nanoparticles to the fluid flow in order to perform numerical analysis in microchannels. This report discusses the problem formulation process and a few numerical methods for analysing heat transfer within a fluid flow.

According to Mudawar and Anderson [84] supercomputers are already exceeded 100 W/cm^2 heat flux in present. The term "nanofluid" refers to a fluid that contains nanoparticles. Nanofluid preparation can be accomplished in a single step or in two steps. Typically, a two-step process involves producing nanoparticles (even in the form of nanotubes or nanofibers) as a dry powder and then mixing them with a base fluid such as water, oil, or even organic liquid [85].

4.1 Problem Formulation and Solution procedure

As stated in chapter three, the problem formulation draws for the use of two-dimensional axisymmetric geometry to simulate the channel. Additionally, a three-phase flow has been introduced to model individual nanoparticles. This enables us to investigate the behaviour of the nanoparticles independently of the physical and chemical properties of the base or secondary fluid. Numerous studies have used a single-phase approach to simulate nanofluids by modifying their thermophysical properties in order to introduce the nanoparticle effect. This can significantly reduce the amount of time required for computation [86]. However, the disadvantage of this method is the difficulty of independently evaluating the effects of nanoparticles.

4.1.1 Conventional single-phase approach for analysis of nanofluid

When appropriate assumptions are made, nanofluids can be treated as a homogeneous liquid. The fundamental premise is that nanoparticles can be dispersed easily in the primary fluid (based fluid) [87]. The results of the conventional single-phase model are obtained by solving the standard mass, momentum, and energy equations. Chapter

3 section 3.1.2 discusses all conventional equations in detail. Apart from the conventional single-phase model, other types of single-phase models exist, such as the thermal dispersion model, the Crank-Nicolson FDM (Finite Deference Method) model, and so on.

However, using single-phase models to analyse nanofluids has a number of drawbacks. Examples include the fact that the findings produced using single-phase models are strongly dependent on the thermophysical parameters of the fluid and can have an impact on the Nusselt number [87], [88].

4.1.2 Multiphase analysis of nanofluid based liquid-liquid slug flow

Brownian force, Brownian diffusion, friction force, thermophoresis, and gravity all play a role in the synthesis of nanofluids as two-phase fluids. As a result, employing multiphase models may result in more realistic results. Lagrangian - Eulerian and Eulerian - Eulerian models are the two most often used two-phase techniques for modelling nanofluids.

- **Lagrangian-Eulerian model**

Both fluid and particle interactions are considered in the Lagrangian-Eulerian model, which includes momentum and energy equations. Solving Nervier–Stork (N-S) equations in time-averaged form and considering the fluid phase as a continuum yields the solutions.

- **Eulerian-Eulerian model**

Another sort of two-phase model is the Eulerian-Eulerian model. This model is well-suited for mixtures with a high number of particles. As a result, this model requires a high concentration of nanoparticles within the phase. The mixture model was chosen for this method due to its more economical approach compared to Lagrangian-Eulerian. The velocity of discrete phases is extracted from the algebraic formulations of the mixture momentum conservation equations using this method [89].

4.1.3 Governing Equations

Present study requires some additional sets of equations to model the behaviour of the phases based on the model itself. It solves the same fundamental equations as in Section 3.1.2, as well as the equations listed below.

- **Relative (Slip) Velocity** [74]

$$v_{pq} = v_p - v_q \qquad 4.1$$

where, v is fluid velocity while p & q are secondary phase and primary phase.

- **The mass fraction for any phase** [74]

$$c_k = \frac{\propto_k \rho_k}{\rho_m} \qquad 4.2$$

where $k, \propto, \rho,$ & c are phase, aspect ratio, density and heat capacity respectively.

- **Volume Fraction**

$$\varphi = \frac{\psi \rho_f}{\rho_s + \psi \rho_f - \psi \rho_s} \qquad [90] \quad 4.3$$

where, the volume, mass fractions and ρ from φ, ψ and density while subscript f and s denotes the fluid phase and nanoparticle phase.

4.2 Methodology

ANSYS Fluent was used to solve the general momentum, energy, and continuity equations, as well as other force interaction equations between the phases, in this study. The Eulerian model was used to study nanoparticles in a microchannel. This study is divided into two distinct sub-cases: nanoparticle injection into a base fluid and nanoparticle injection into a secondary fluid phase. The primary reason for switching from COMSOL Multiphysics to ANSYS Fluent is the advanced features available in the Lagrangian-Eulerian and Eulerian-Eulerian frameworks. Advantages in Eulerian-Eulerian framework can be found in these [91]–[97].

4.2.1 Nanoparticle injection in secondary fluid phase – ANSYS Fluent

As previously stated, the Eulerian mixture model was used to setup the study as a transient and axisymmetric model under the pressure-based solver. As with Chapter 03, this setup does not include a test for droplet detachment from the micro junction. This study concentrated exclusively on the behaviour of nanoparticles in a two-phase liquid-liquid slug flow. Cases are conducted with varying concentrations of nanoparticles in the secondary fluid. Figure 4-1 depicts the initial patched flow prior to the commencement of the numerical study.

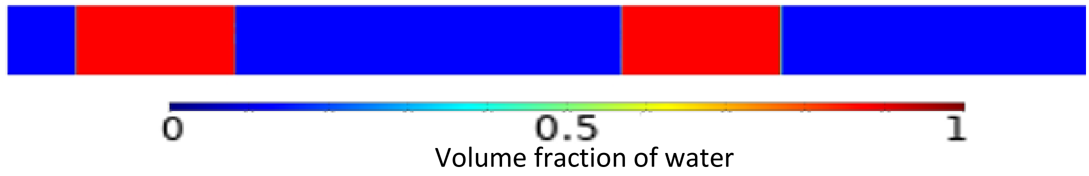

Figure 4-1: Initial Setup

4.2.2 Geometrical model with boundary conditions

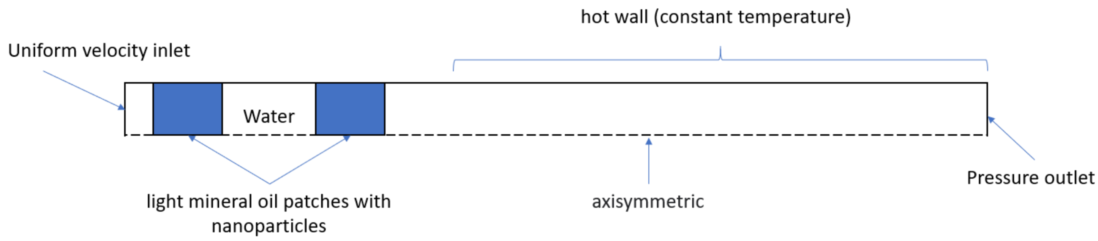

Figure 4-2: Schematic diagram of three-phase flow model

This geometrical model is divided into two sections: the region of flow development and the region of constant temperature wall. As a result, a 3000 μm long microchannel was chosen to allow for sufficient flow development. All fluid properties are identical to those listed in table 3.1. Additionally, nanoparticles were incorporated into the third phase. The reason for the use of aluminium oxide (Al_2O_3) is its wide availability, manufacturing cost, along with its high heat transfer capability. The most critical quality is chemical and physical stability over a broad temperature range and under a range of conditions. Vajjha and Das [98] have experimentally determined the conductive heat transfer coefficient of common oxide nanoparticles. Geng et al. [99] have compared the MWCNT (Multi–walled carbon nanotubes) with metal oxide ZnO to validate its thermal conductivity. Table 4-2 has the comparison of the properties with different non-metallic nanoparticles. Metal nanoparticles were avoided due to the instability (chemically and physically) with the based fluid in the present study.

Table 4-1: Material Properties including nanoparticles

Material	Density [kg/m^3]	Specific Heat [J/kg.K]	Thermal Conductivity [W/m.K]	Viscosity [Pa.s]
Water	998	4182	0.6	0.001002
Light Mineral Oil	838	1670	0.17	0.023
Aluminium	2690	917	239	N/A
Aluminium Oxide Nanoparticle [91]	3970 50nm spherical	765	40	N/A

Table 4-2: Different nanoparticle properties

Type of nanoparticle	Density [kg/m^3]	Thermal conductivity (W/m.K)	Particle size (nm)
Al_2O_3 [84]	**3600**	**36**	**53**
ZnO [84]	**5600**	**13**	**29 & 77**
CuO [84]	**6500**	**17.65**	**29**
MWCNT[90]	**2100**	**1500**	**30**
ZnO[90]	**5606**	**19**	**35**

4.2.3 Mesh Generation and study validation

The geometrical model is identical to the two–phase model except for the absence of the junction. The same mesh validation procedure was used in this study to demonstrate the mesh independence. The results of the validity study are depicted in Figure 4-3. According to Figure 4-3, the percentage variation in error between 0.5 µm and 1.0 µm meshes is 6%, while the error for 5 µm element size is 10%.

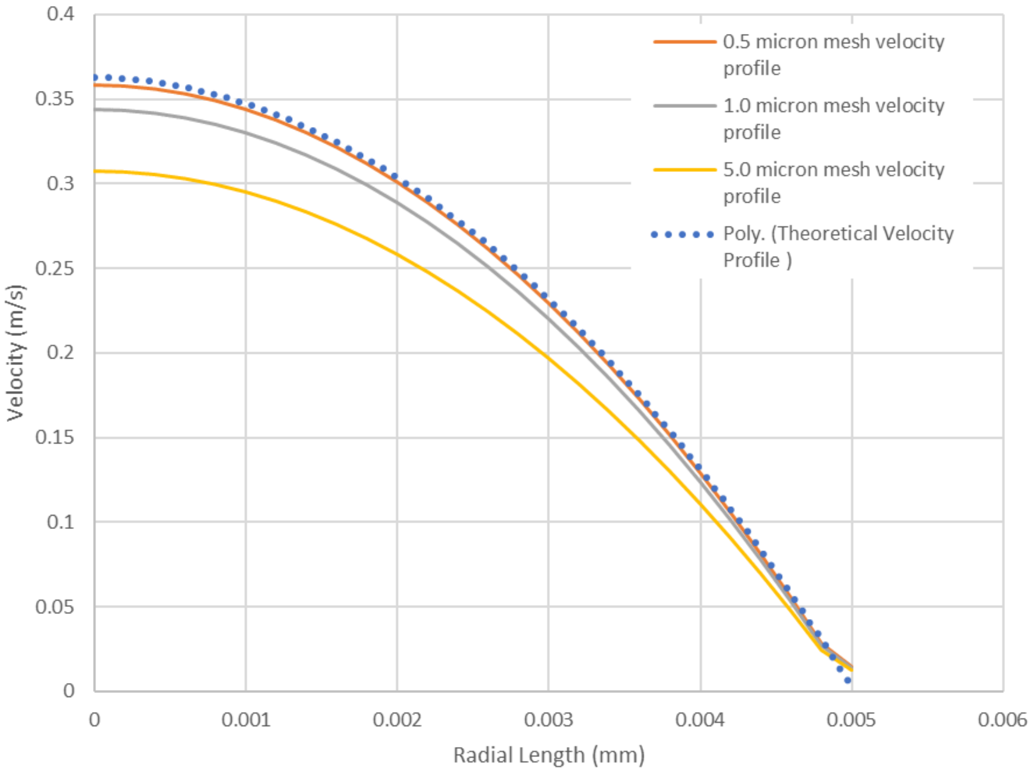

Figure 4-3: The distribution of velocity of a water slug along a line in the mid plane perpendicular to the axis

Throughout the simulations, the mesh elements at the two-fluid interface were automatically revised based on the gradient of volume fraction, with 0.15 and 0.1 serving as the refinement and coarsening threshold values, respectively, at the two-fluid interface.

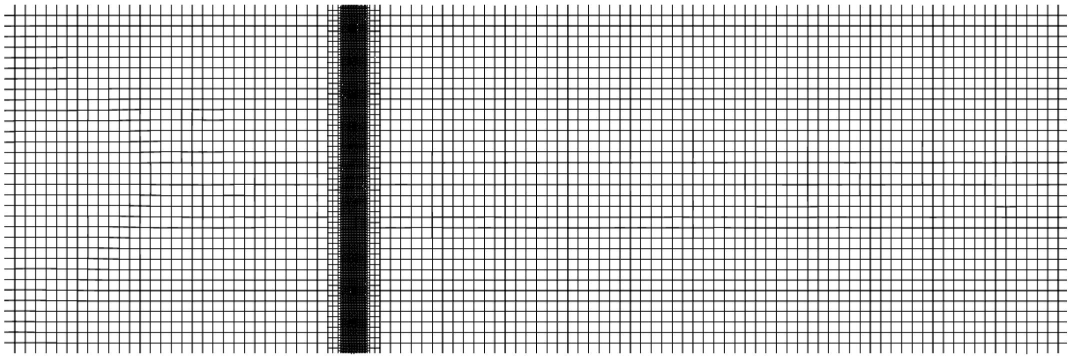

Figure 4-4: Computational mesh with refined gradient adaptation

The mesh with a 1 µm element size and refined gradient adaptation is shown in Figure 4-4. It is used to track the fine interface between the phases. This method generated the mesh using quadrants to conserve computational power. To aid comprehension, Figure 4-5 overlays the mesh with the phase contour.

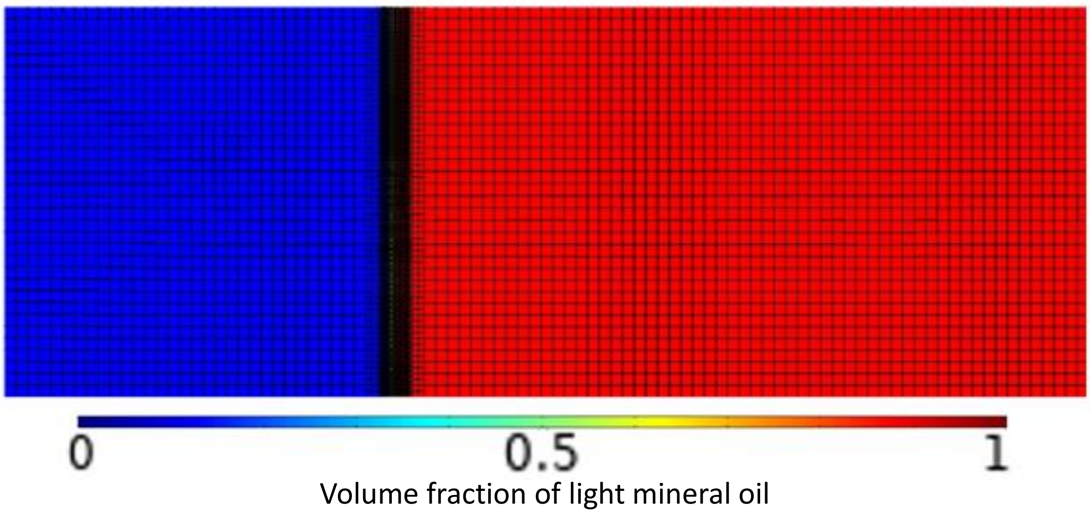

Figure 4-5: Mesh overlay with phase contour

The gradient adaptation algorithm adapts to the calculated interface in order to preserve the 0.1 and 0.15 refinement and coarsening threshold values. This method ensures greater accuracy while consuming the least amount of computational power possible. Overall mesh quality is approximately 0.8, while the minimum mesh quality is approximately 0.7. In the following table, 4-3, we summarize the mesh generation process.

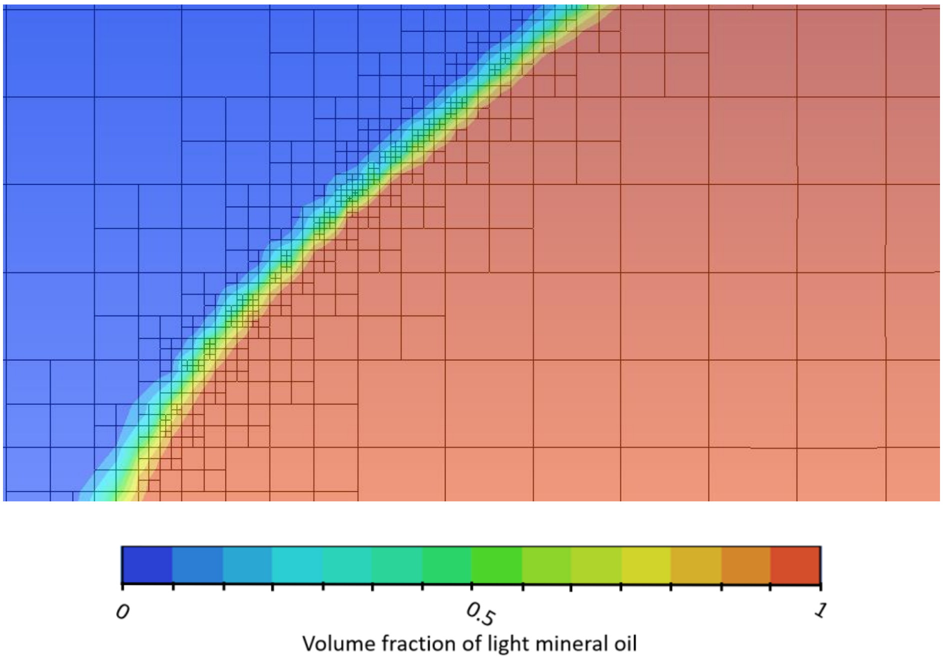

Figure 4-6: Adapted Mesh after t = 1s

Table 4-3: Mesh properties - Ansys Fluent

Quantity	Value	Unit
Physics Preference	CFD	1
Element Size	1	µm
Growth Rate	1	1
Target Quality	0.9	1
Pinch Tolerance	1.8	nm
Nodes	153051	1
Elements	150000	1

After completing the setup, several cases were numerically analysed. Table 4-4 summarizes the study's case details. The inlet velocity was maintained at 0.2 m/s in these studies to minimize the inlet velocity effect. Cases 01 and 02 were used to determine the effect of the nanoparticles on the light mineral oil phase, while cases 3 and 4 were used to determine the same effect on the water phase.

Table 4-4: Nanoparticle case details

Case No	Inlet Velocity	Nanoparticle Domain	Nanoparticle Concentration
01	0.2	Light mineral oil	0.02
02	0.2	Light mineral oil	0.05
03	0.2	Water	0.02
04	0.2	Water	0.05

4.3 Results and Summary

All results will be compared in Chapter 05. ANSYS In all of the studies, fluent mixture model simulations were used. The initial interface tracking was accomplished using VOF in conjunction with the granular effect of the nanoparticles. Initially, a quadrilateral-based mesh was used. Gradient adaptation was used to boost the computer's performance and improve the results. This conversion increased the computational load but improved the study's accuracy significantly. These studies examined the formation of droplets, pressure drop across the channel, film thickness, heat transfer through the wall to the fluid, and contact angle, among other things.

5 RESULTS AND DISCUSSION

The purpose of this chapter to describe and explain the findings of the numerical simulations that were carried out in Chapters three and four. The first set of cases (table 5-1) was used to examine how flow and droplet production occur under a variety of situations. Additionally, these cases prompt examination of the flow's general hydrodynamics, including velocity distribution, interface separation caused by surface tension, and pressure drop along the microchannel.

The cases in Table 5-2 were selected to demonstrate the effect of contact angle on the average Nusselt number. The cases mentioned in 5-4 and 5-5 were conducted to investigate heat transfer in liquid-liquid two-phase flow in microchannels, as well as the effect of nanoparticles. This chapter discusses the results in detail.

5.1 Flow development and droplet formation

A specially designed microchannel was used to simulate droplet detachment and formation in this study. Figure 5-1 illustrates the initial flow domains. Blue was used to indicate light mineral oil in this figure 5-1, while red was used to indicate water. This setup was capable of forming the desired droplets within the microchannel at a velocity of 0.1 m/s for both phases. Volume fraction contour mapping can be used to track refined interfaces, as illustrated in figure 5-2. The flow was able to reach its fully developed state after 1 millisecond. The velocity profile after one millisecond is depicted in Figure 5-3. The dimensionless flow parameters were obtained by solving the equations in Table 3-5. Reynolds number was 11.2 and capillary number was 0.0022, respectively.

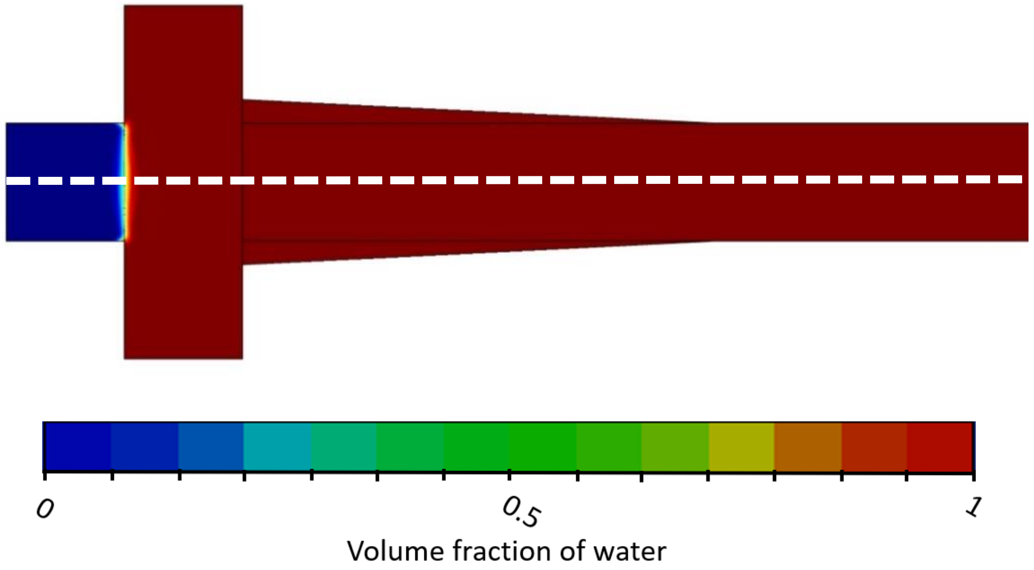

Figure 5-1: Initial flow domains at t = 0 s

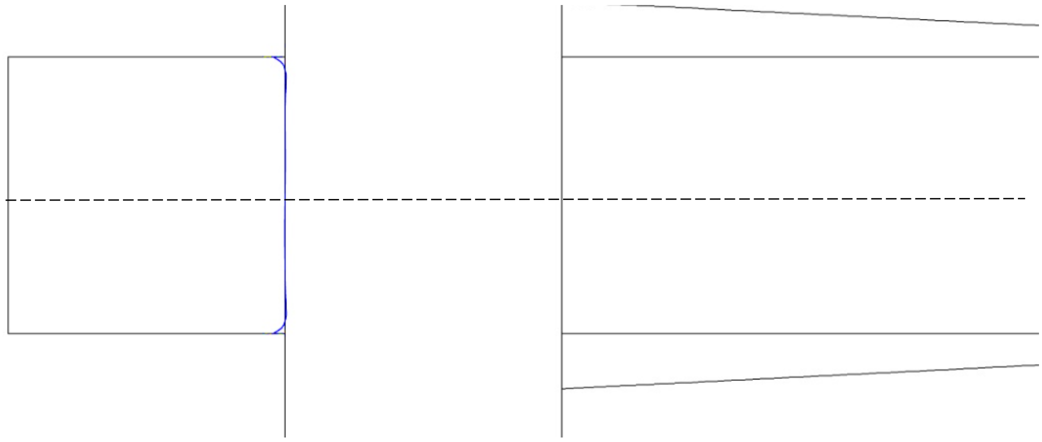

Figure 5-2: Initial interface contour at t = 0 s

This is the conventional velocity profile for a channel with fully developed fluid flow. After 1 millisecond, this plot was obtained at the outflow. This signifies that after 1 millisecond, the flow was fully developed. At 4.2 milliseconds, the first droplet separated from the main domain. The droplet separation at the junction is depicted in Figure 5-4. The droplet was decelerated before it separated from the parent domain due to interfacial surface tension. Figure 5-5 depicts the velocity profile in the above scenario.

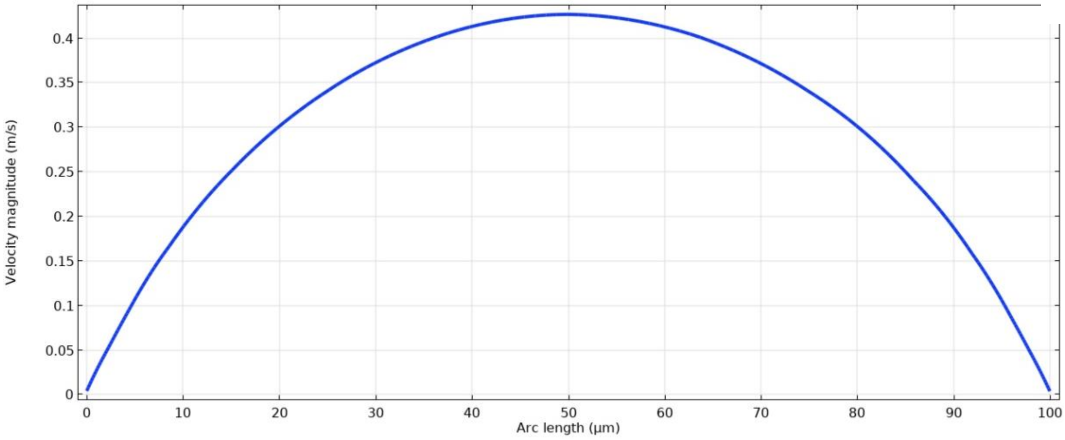

Figure 5-3: Outlet velocity magnitude at t = 1 ms

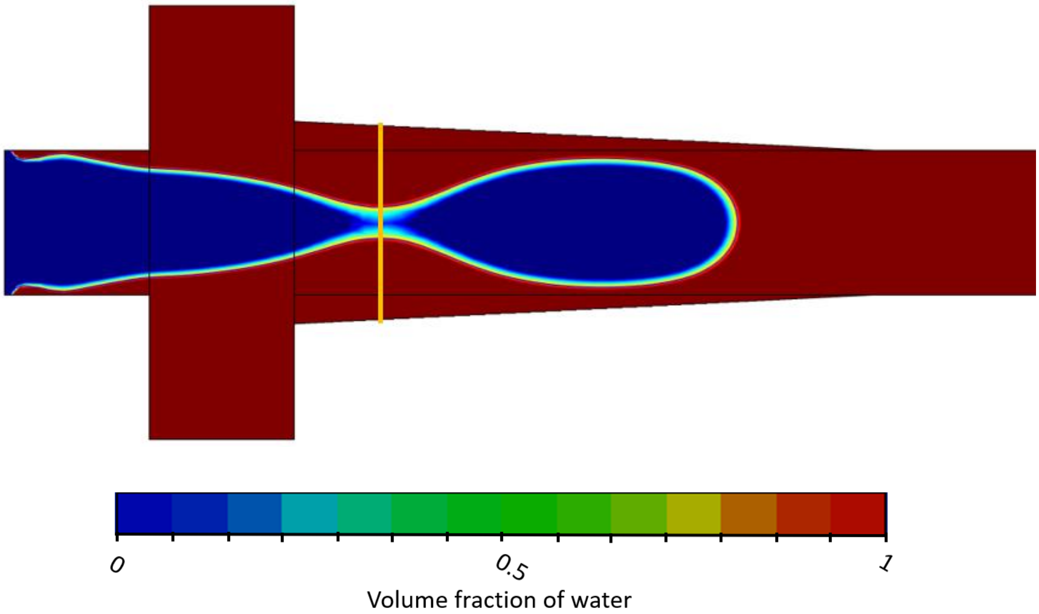

Figure 5-4: Droplet detachment from the main domain at t = 4.2 ms

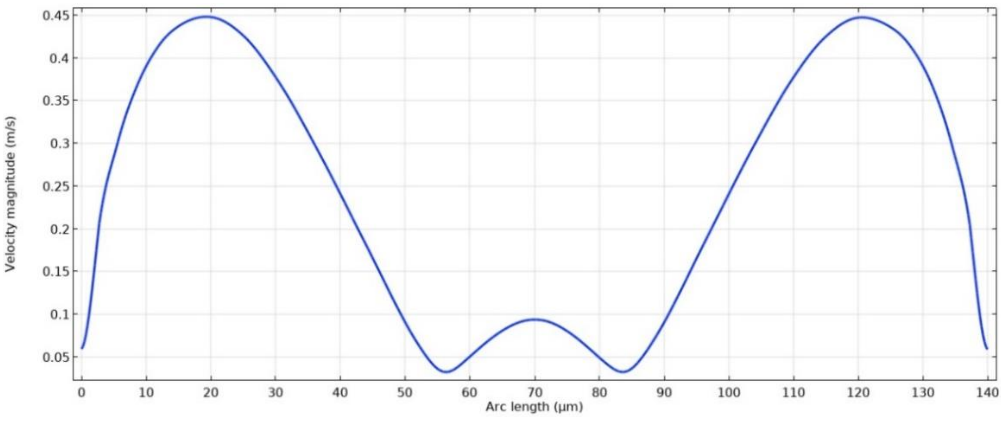

Figure 5-5: Velocity profile at the point of droplet detachment from the main domain at t = 4.2 ms

The separation occurs for a number of reasons, including the fast deceleration of the interface between the mineral oil and water domains, which causes the interface's shear stress to surpass the capillary number and interfacial pressure ratio, as shown in Figure 5-5. Hao Gu et al. [100] has validate this phenomena in 2011.

In this experiment, the spacing between two droplets is solely determined by the entrance velocities. Because all of the other factors were kept constant throughout the research. The effects of input velocities have been studied with several cases. The acquired results are shown in figures 5-6 to 5-9.

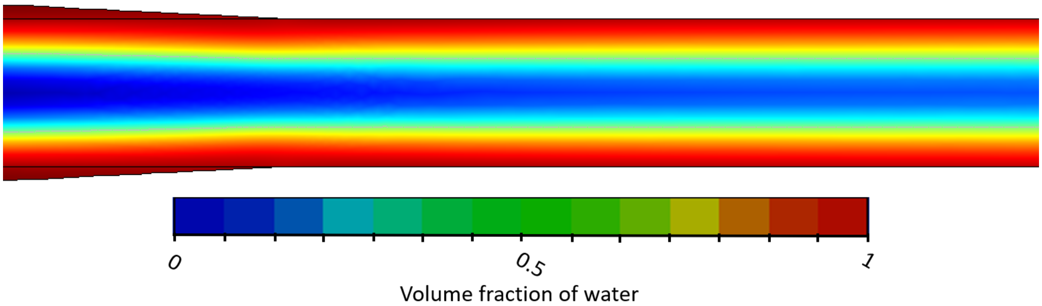

Figure 5-6: Flow formation with mineral oil inlet velocity at 0.5 m/s and water inlet velocity at 0.2 m/s

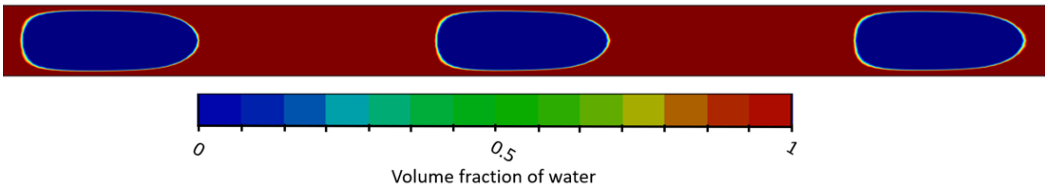

Figure 5-7: Flow formation with mineral oil inlet velocity at 0.2 m/s and water inlet velocity at 0.2 m/s

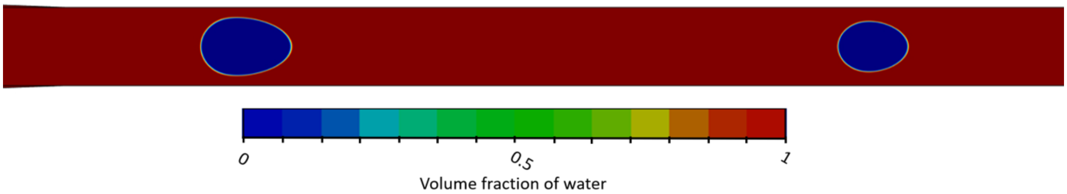

Figure 5-8: Flow formation with mineral oil inlet velocity at 0.1 m/s and water inlet velocity at 0.5 m/s

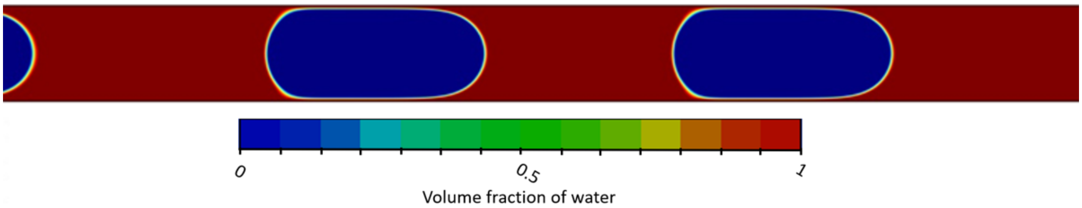

Figure 5-9: Flow formation with mineral oil inlet velocity at 0.1 m/s and water inlet velocity at 0.1 m/s

According to the findings, velocity ratios play a significant effect in droplet formation. As illustrated in figure 5-6, velocities of 0.5 m/s and 0.2 m/s at the oil domain inlet and water domain inlet, respectively, result in an annular flow rather than a slug flow or a Taylor flow. When two velocities differ, the distance between two adjacent drops changes as well. The summary and distance between two neighbouring drops based on their entrance velocities are shown in Table 5-1.

Table 5-1: Distance between two adjacent droplets

Case Number	***Mineral Oil Inlet Velocity (m/s)***	***Water Inlet Velocity (m/s)***	***Type of the flow***	***Distance between two adjacent droplets (μm)***
Case 01	0.5	0.2	Annular Flow	N/A
Case 02	0.2	0.2	Slug Flow	290
Case 03	0.1	0.5	Slug Flow	500
Case 04	0.1	0.1	Slug Flow	210

5.2 Pressure and velocity distribution across the channel with two phase liquid – liquid Flow

Following the development of the flow, multiple investigations were done to determine the velocity and pressure distribution over the microchannel. As previously stated, the flow develops fully after a flow distance of 200 μm (1 millisecond of simulation time) (Figure 5-3). As demonstrated in Figure 5-10, two phase flows typically result in large pressure declines.

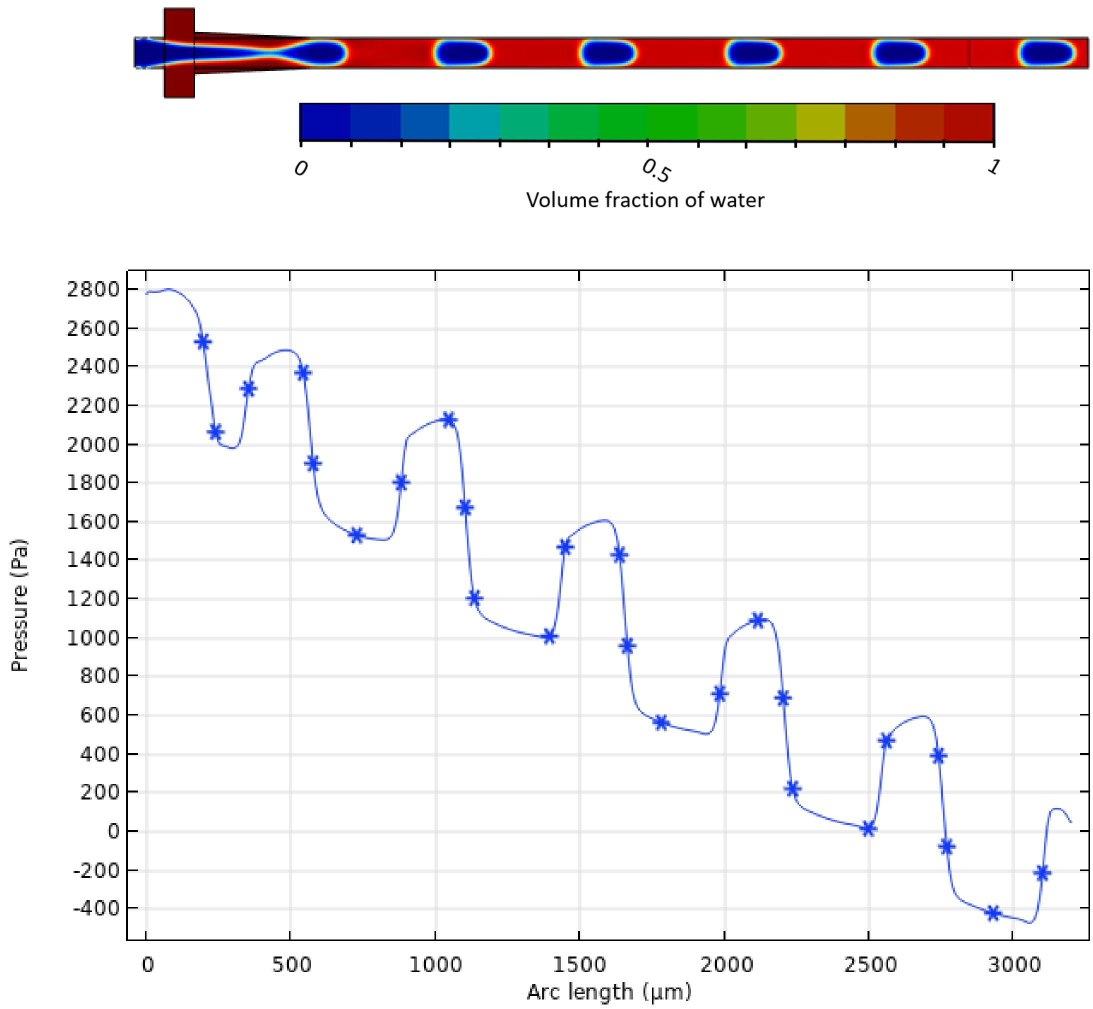

Figure 5-10: Axial Pressure Drop

As illustrated in Figure 5-10, this high-pressure drop is classified into two distinct subcategories: frictional and interfacial pressure drops. This occurs for a variety of reasons, including film leakage around the slug, the slug's low velocity, and phase viscosity [58], [101], [102]. This is the most difficult scenario for a two-phase slug flow. This necessitated the use of additional micro pumping power to deliver the required flow. The axial velocity distribution of the slug clearly demonstrates the slug's low velocity in figures 5-11 and 5-12.

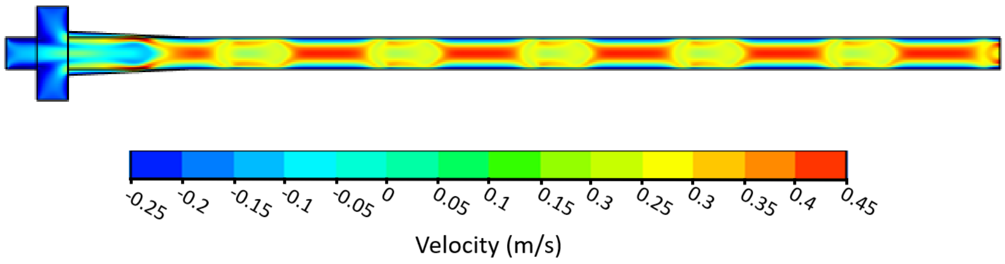

Figure 5-11: Velocity Contour Map

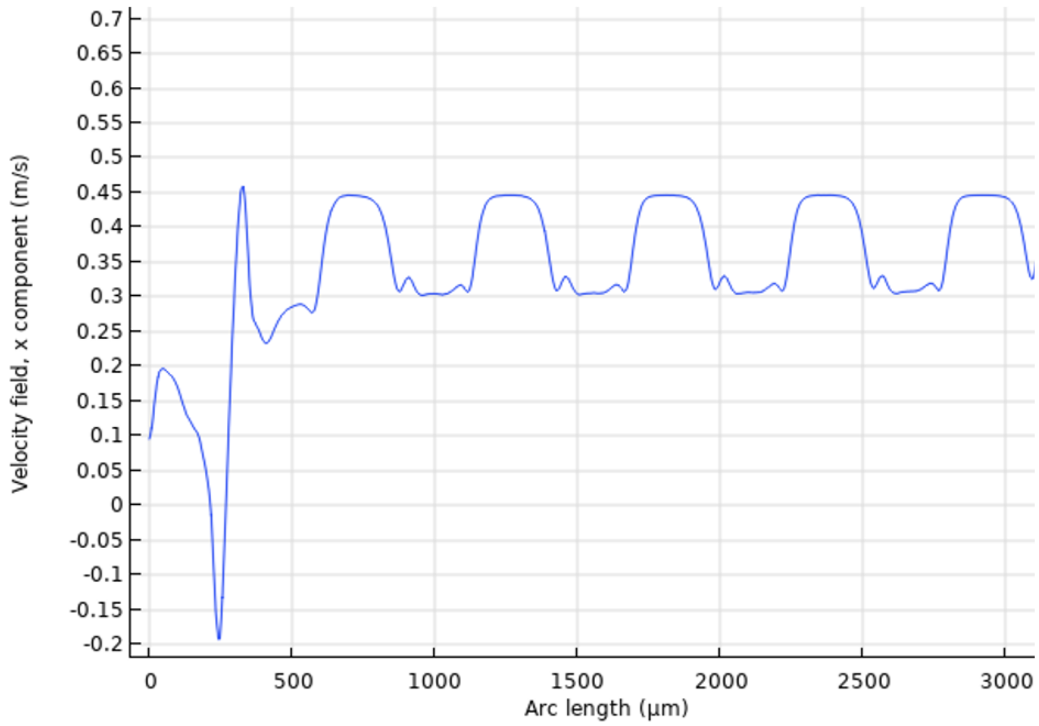

Figure 5-12: Axial Velocity Distribution Plot

The velocity distribution in Figure 5-12 shows how fluids circulate between two phases. These findings prompted the researchers to analyse the two phases' relative velocity distributions. Section 5.3 will explain this investigation.

When the film thickness is present, the slug's slip velocity can be determined. This clearly indicates that the primary and secondary fluid phases have unique velocities. Figure 5-13 shows the fully formed fluid flow at a channel length of 2800 µm, whereas Figure 5-14 represents the secondary slug's slip effect. The channel is illustrated in Figure 5-14 utilizing the x component velocity across the channel when one bubble passes at a length of 2800 µm where the slip velocity can be measured.

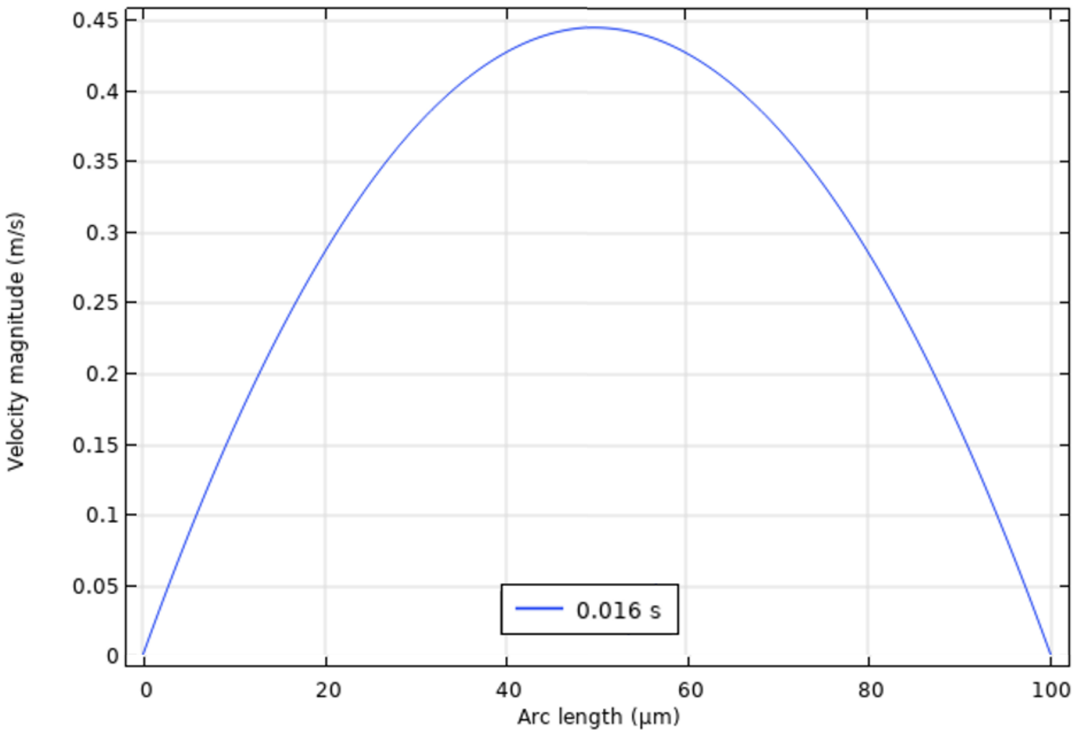

Figure 5-13: Velocity distribution at 2800 µm where t = 0.016 s

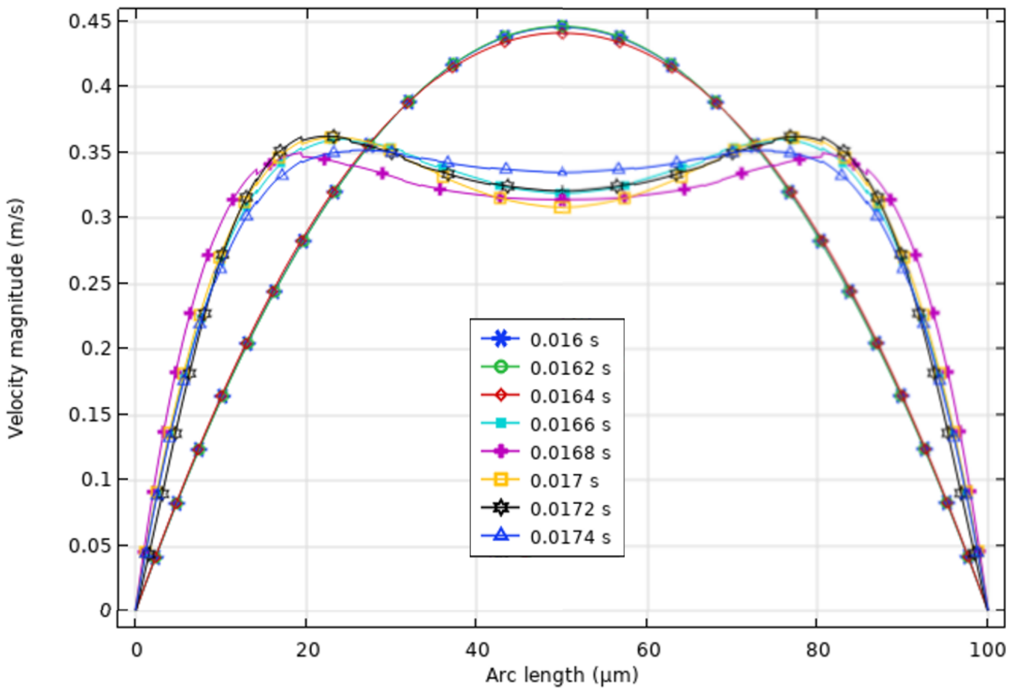

Figure 5-14: Velocity distribution at 2800 µm when one bubble passes.

5.3 Relative velocity distribution within the droplet of a two-phase liquid–liquid flow

At various contact angles, the relative velocity distribution within a droplet in a two-phase liquid–liquid flow was examined. Six cases were chosen to investigate possible fluid inter-circulation and possible nanoparticle circulation paths. Table 5-2 summarizes the cases. When a slug is present, an average Nusselt number has been determined along the axis at 2800 µm. To verify the local Nusselt number, it was compared to published data [5]. Table 5-3 compares the CFD local Nusselt number to the literature. In this analysis, the local Nusselt number of two-phase liquid-liquid slug flows is calculated using equation 5.1, and the average thermal conductivity of the liquid-liquid slug flow is calculated using equation 5.2.

$$Nu_x = \frac{qD_h}{k(T_w - T_m)} = \frac{hD_h}{k} \tag{5.1}$$

$$k_{avg} = \varphi k_s + (1 - \varphi)k_p \tag{5.2}$$

Table 5-2: Average Nusselt numbers for different test cases.

Case No	Fluid bulk velocity (m/s)	Contact angle (degree)	Film thickness (µm)	Nu $_{avg}$
01	0.2	90	N/A	6.9
02	0.2	100	N/A	8.9
03	0.2	120	N/A	10.2
04	0.2	150	N/A	10.4
05	0.2	160	1.5	10.6
06	0.2	170	1.8	10.5

Table 5-3:Nusselt number comparison

Case No	Average Nusselt number using CFD results	Average Nusselt number using literature [5]
01	6.9	6.3
02	8.9	N/A
03	10.2	10.1
04	10.4	10.5
05	10.6	N/A
06	10.5	10.4

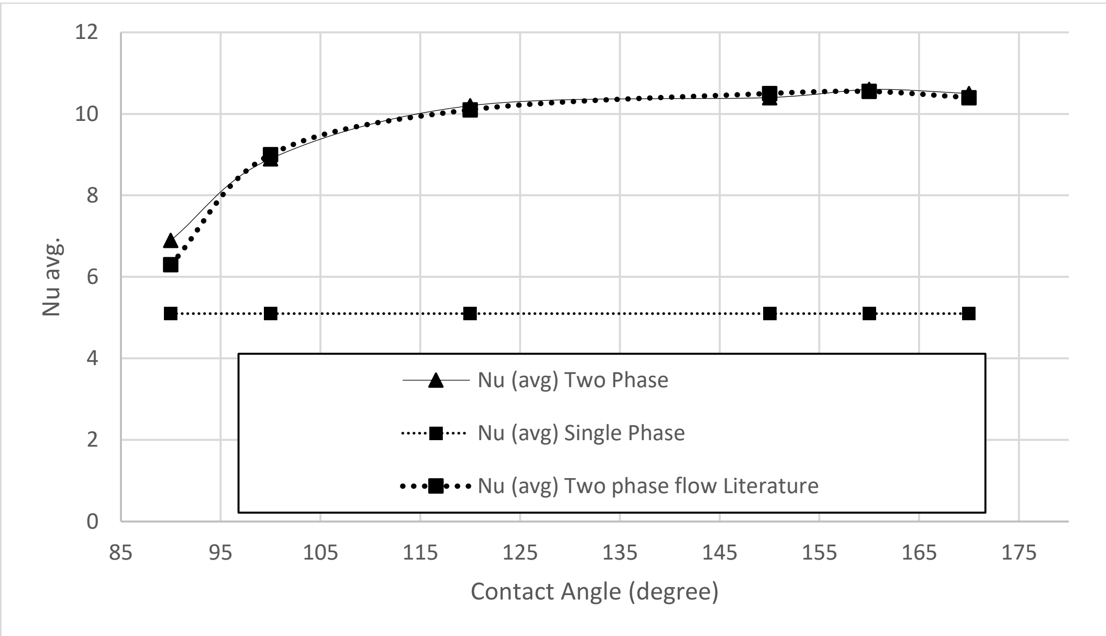

Figure 5-15: Average Nusselt number vs contact angle

After plotting the velocity and volume fraction contours, promising results were obtained. Figure 5-16 depicts the volume fraction and velocity contours at various contact angles.

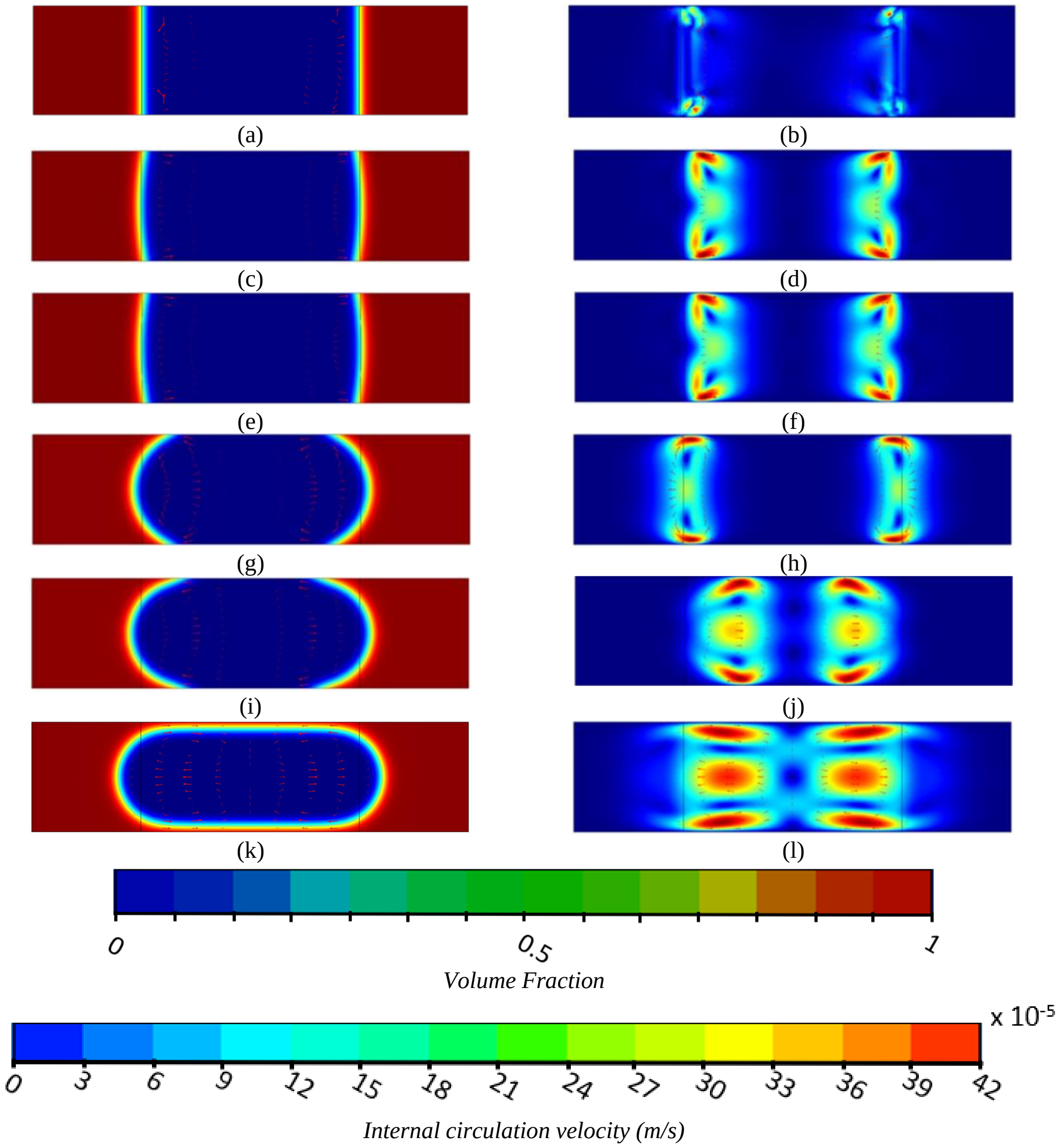

Figure 5-16: Volume fraction (a): at 90-degree contact angle, (c): at 100-degree contact angle, (e): at 120-degree contact angle, (g): at 150-degree contact angle, (i): at 160-degree contact angle, (k): at 170-degree contact angle, internal circulation velocity (b): at 90-degree contact angle, (d): at 100-degree contact angle, (f): at 120-degree contact angle, (h): at 150-degree contact angle, (k): at 160-degree contact angle, (l): at 170-degree contact angle,

In these flow conditions, the inter-circulation of the secondary fluid has increased with respect to the contact angle (Figure 5-16: (b), (d), (f), (h), (j), (l)). Flows with 160 and 170 degrees have sliding slug flow, which creates a thin primary film around the slug [103], [104]. hen nanoparticles are added, the circulation of the particles will make it easier for heat to move through, which will make the overall heat transfer better.

5.4 Effect of nanoparticles in two phase liquid – liquid slug flow

Cases involving nanoparticles in the base fluid and those involving nanoparticles in the secondary fluid have been classified in Chapter 4. A range of experiments on nanoparticles in a two-phase liquid-liquid slug flow yielded the following outcomes. A discussion of secondary phase nanoparticles will set the stage for the research, which will conclude with a look at the role of base fluid nanoparticles in heat transfer.

5.4.1 Effect of nanoparticles in secondary fluid on heat transfer

Al_2O_3 nanoparticles were examined in Chapter 04 to determine their impact. For the purposes of this investigation, two case studies were developed and examined. A two-phase flow containing Al_2O_3 nanoparticles is depicted in Figure 5-17. Temperature differences can be quantified by looking at the Nusselt Number.

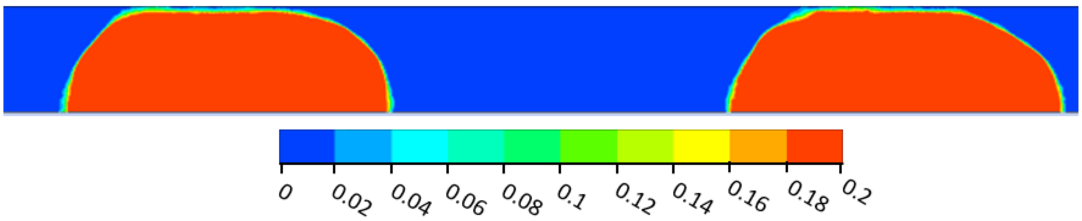

Figure 5-17: Volume fraction of Nanophase Al2O3

Azmi et al. [105] validated equation 5.3 experimentally to determine the Nusselt number of a nanofluid. This was within a maximum of 15% of the experimental values at high Nusselt numbers, with an average deviation of 4.6 percent and a standard deviation of 5.7 percent. Due to the inclusion of the twisted tape effect, this cannot be utilized in a straight microchannel. The following equation can be used to compute the Nusselt number:

$$Nu_{nf} = \frac{h_{nf} D}{k_{nf}} = 0.073 Re^{0.702} Pr_{nf}^{0.4} \left(1 + \frac{D}{H}\right)^{1.3} \quad 5.3$$

where, Nu_{nf}, $h_{nf}, k_{nf}, D, Re, Pr_{nf}, and\ H$ are Nusselt number of the nanofluid, convection heat transfer coefficient, thermal conductivity, diameter of the channel, Reynolds number, Prandtl number and helical pitch of the twisted tape for 180 degrees rotation respectively.

As a result, the Ramirez Tijerina et al. [106] correlation was applied. In a straight tube, he conducted the experiment and postulated a link between the Nusselt number of a nanofluid and the temperature of the surrounding wall.

$$Nu_{nf} = \frac{h_{nf}D}{k_{nf}} = 0.073Re^{0.702}Pr_{nf}^{0.4} \tag{5.4}$$

The correlations discovered by Sharma et al. in 2012 [2] are used to compute the parameters of the nanofluid, such as its viscosity and thermal conductivity. The viscosity and thermal conductivity of a liquid can be calculated using equations 5.5 and 5.6, respectively.

$$\frac{\mu_{nf}}{\mu_w} = \mu_{eff} = C_1\left(1+\frac{\varphi}{100}\right)^{11.3}\left(1+\frac{T_{nf}}{70}\right)^{-0.038}\left(1+\frac{d_p}{170}\right)^{-0.061} \tag{5.5}$$

$$k_{eff} = \frac{k_{nf}}{k_w} = \left[0.8938\left(1+\frac{\varphi}{100}\right)^{1.37}\left(1+\frac{T_{nf}}{70}\right)^{0.2777}\left(1+\frac{d_p}{150}\right)^{-0.0366}\left(\frac{\alpha_p}{\alpha_w}\right)^{0.01737}\right] \tag{5.6}$$

μ_{nf}, μ_w, μ_{eff}, φ, T_{nf}, C_1, α_p, α_w and d_p denotes absolute viscosity of nanofluid, absolute viscosity of water, ratio of nanofluid to water viscosity (effective viscosity) values, volume fraction of nanoparticles, temperature, a constant (where 1.4 for SiC and 1.0 for water based nanofluid), thermal diffusivity of nano material, thermal diffusivity water and diameter of a nanoparticle respectively.

The dynamic viscosities were calculated by averaging line values in the CFD results. Equation 5.5 yields the values in Table 5-4 for dynamic viscosity and viscosity based on CFD calculations.

The CFD numerical analysis results were in line with the previously stated correlation as well as the experimentally measured effective thermal conductivity values (k_{eff}) of 1.130 and 1.274 in cases one and two, respectively. Hemmat Esfe et al. [1] conducted a study in 2014 that yielded the experimental values. Fig. 5-19 compares the effective thermal conductivity in the different cases shown. All CFD results are within 3% to 4% of the literature and experimental data.

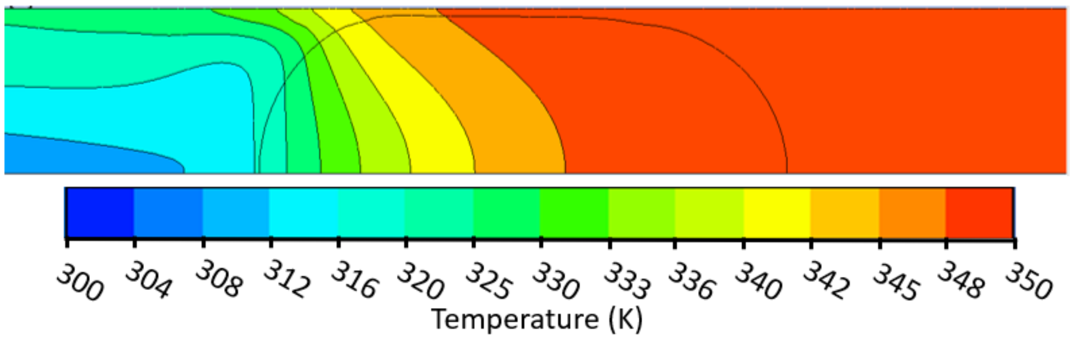

Figure 5-18: Temperature Distribution inside a one bubble

Figure 5-18 depicts the dispersion of temperature within a single bubble. Mineral oil with nanoparticles plugs has a higher temperature at the front, but a lower temperature at the back. This causes an internal circulation because of the large temperature difference in the single plug. This could lead to an increase in heat transfer by creating an inter-fluid circulation inside the droplet.

Table 5-4: Effect of nanoparticles in secondary fluid on heat transfer case parameters

Case No	**Al_2O_3 Volume Fraction**	**Properties of bulk fluid**	**CFD Result (Nanodomain)**	**Sharma et al. Model**	**Nanofluid**
01	2.00% (v/v)	Dynamic viscosity	0.02254124 [Pa.s]	0.02202796 [Pa.s]	Light mineral oil/Al_2O_3
		Thermal conductivity	0.1997 [W/m.K]	0.1974 [W/m.K]	
		Average Nusselt Number	17.1245 *Using Equation 5.1*		
02	5.00% (v/v)	Dynamic viscosity	0.0228117 [Pa.s]	0.0221027 [Pa.s]	
		Thermal conductivity	0.2236 [W/m.K]	0.2057 [W/m.K]	
		Average Nusselt Number	20.524 *Using Equation 5.1*		

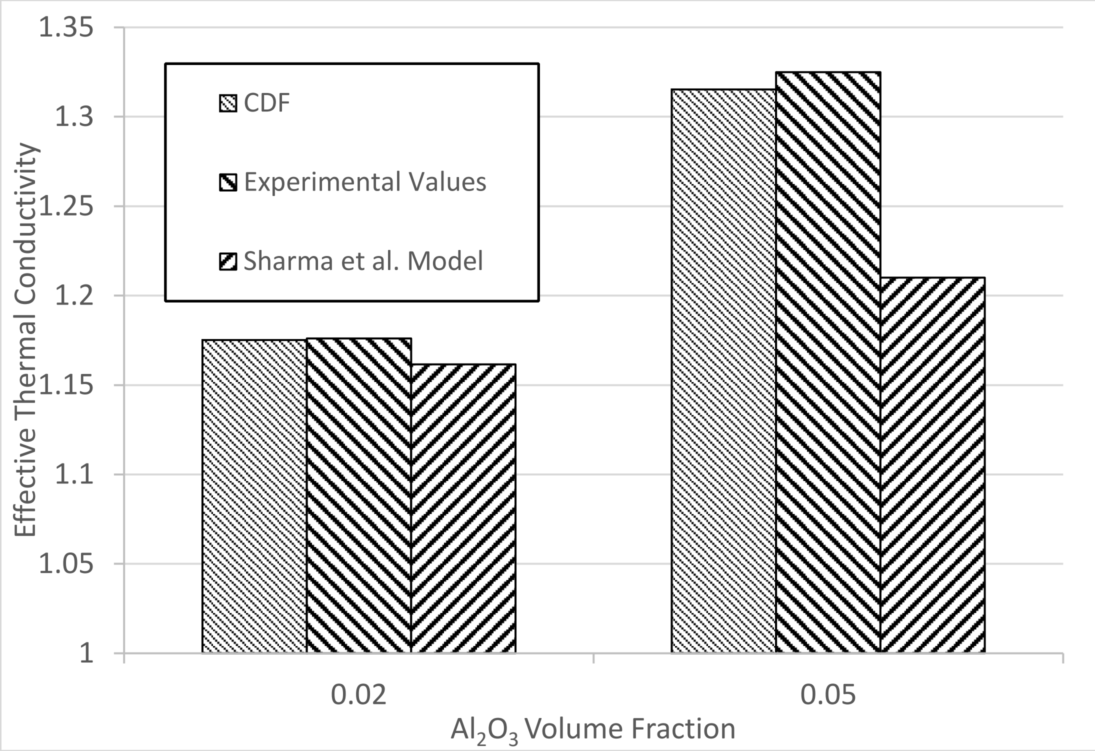

Figure 5-19: Effective Thermal Conductivity Comparison

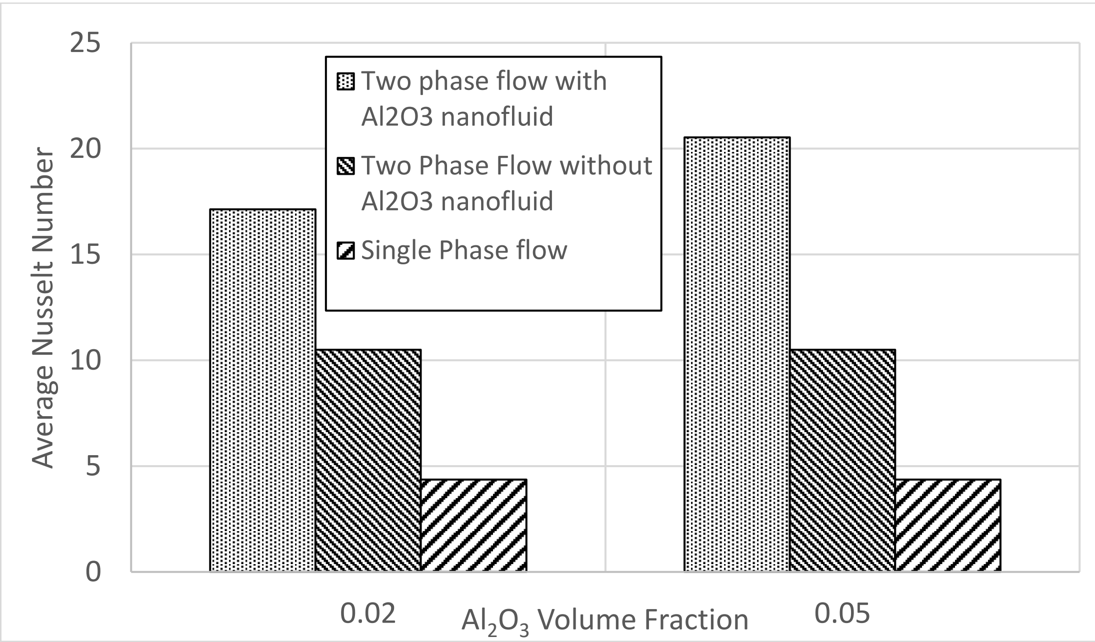

Figure 5-20: Nusselt number comparison of the nanofluid-based liquid-liquid two-phase slug flow) nanofluid as the droplet) with respect to single phase and liquid-liquid two-phase slug flow without nanoparticles

The Nusselt number of the nanofluid-based liquid-liquid two-phase slug flow is compared to that of the single phase and nanoparticle-free liquid-liquid two-phase slug flow in Figure 5-20. The Nusselt number has increased in comparison to the two-phase liquid-liquid slug flow, as indicated by the findings. This occurs as a result of the base fluid's thermal conductivity remaining constant. As a result, the proportion of heat transfer via convection to heat transfer via conduction is increased. Here as outcome, the average Nusselt number has risen. Figure 5-20 illustrates the Nusselt number comparison between a nanofluid-based liquid-liquid two-phase slug flow and a single-phase and two-phase slug flow without nanoparticles. The Nusselt number has risen in comparison to the two-phase liquid-liquid slug flow, according to the results. As a result, the base fluid's thermal conductivity has not changed. Consequently, the convection/conduction heat transfer ratio improves. As a result, the average Nusselt number has increased.

Figure 5-21 represents the relationship between the Nusselt number and axial length as a series of two consecutive bubbles. There is a local Nusselt number of 40.84, and this number drops as the mean temperature rises because of the decreasing thermal gradient. The Nusselt number variation with the axial length is shown in figure 5-21 to illustrate the change in the Nusselt number along with two consecutive bubbles. This shows the maximum of 40.84 as the local Nusselt number, and when the mean temperature increases, it drops because of the reducing thermal gradient.

The increased convective heat transfer due to the nanoparticle circulation is the reason for the higher Nusselt number. A single bubble of aluminium oxide nanoparticles is shown in Figure 5-22 with its relative velocity magnitude to the host fluid. The increased convective heat transfer in a two-phase flow is a result of the nanoparticles' relative velocity, which induces a convective heat current inside the bubble. With the addition of aluminium oxide nanoparticles, the overall thermal conductivity of the fluid flow will increase. As a result, the fluid flow experiences a higher overall heat transfer. 2.09 times more than a two-phase liquid-liquid slug flow without nanofluid and 5.09 times more than a single-phase laminar flow in terms of Nusselt number have been achieved by using this approach.

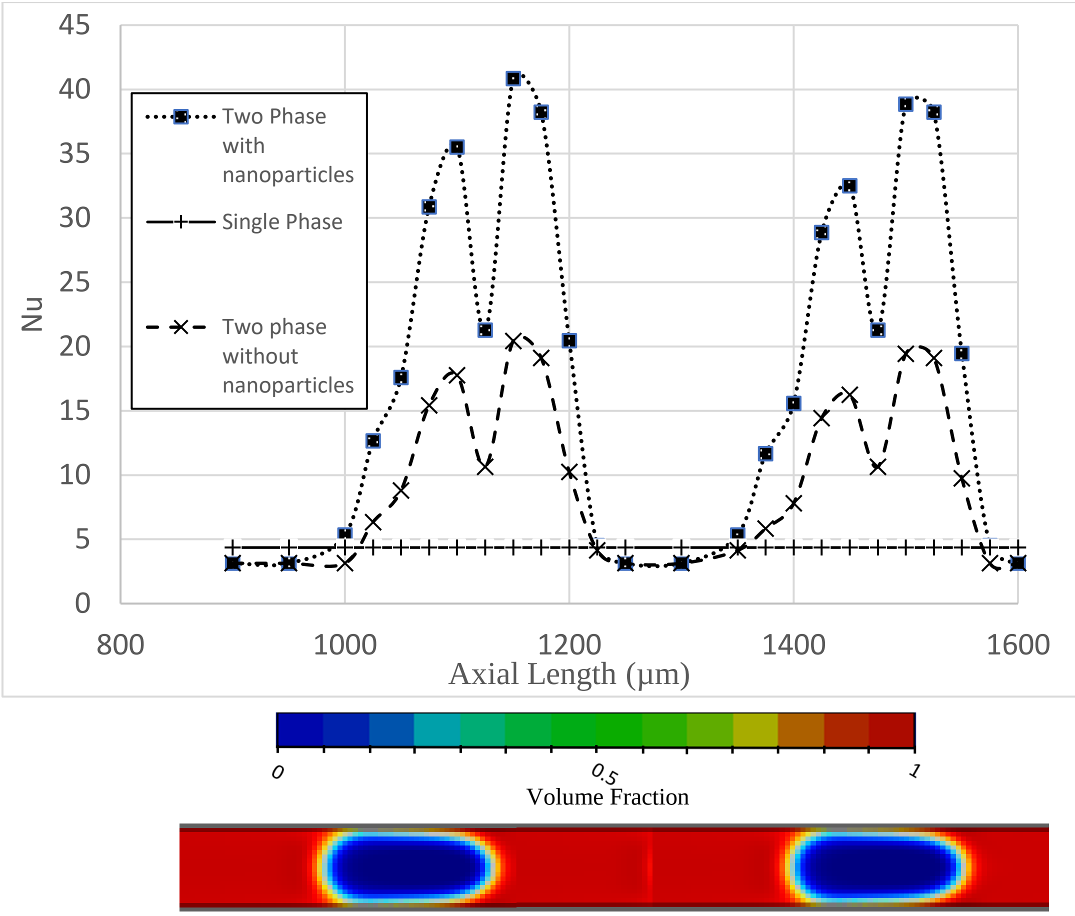

Figure 5-21:The Nusselt number variation with the axial length

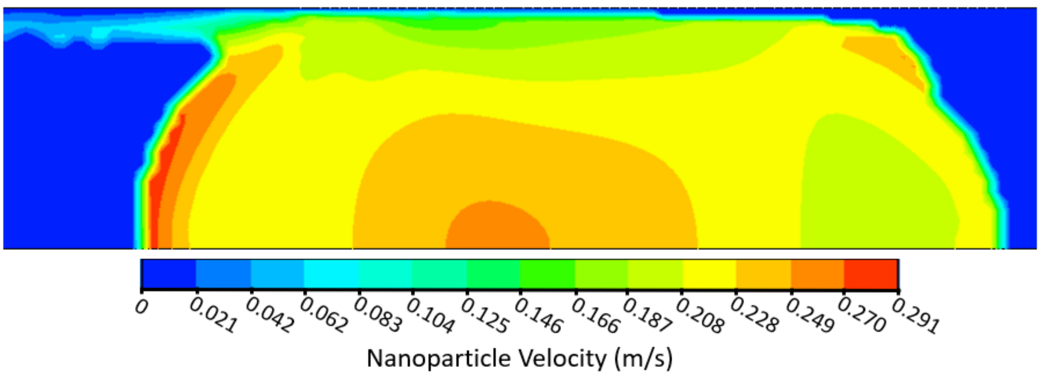

Figure 5-22: The relative velocity magnitude of the Al_2O_3 nanoparticles with respect to the host fluid in a single bubble

5.4.2 Effect of nanoparticles in based fluid on heat transfer

As described in Section 5.4, an additional set of cases was numerically solved to investigate the effect of nanoparticles in the based fluid. The effect of nanoparticles in the base fluid on heat transfer was studied using the same approach as in Section 5.4.1. This section investigates the effect of nanoparticles on heat transfer by introducing them into the primary fluid (water). The first two cases involved varying the volume fraction of Al_2O_3 nanoparticles in the based fluid. The following table details the study's case parameters.

Table 5-5: Effect of nanoparticles in based fluid on heat transfer case parameters

Case No	Al_2O_3 Volume Fraction	Property of the bulk fluid	CFD Result (Nanodomain)	Sharma et al. Model	Nanofluid
01	2.00% (v/v)	Dynamic viscosity	0.00098294 [Pa.s]	0.000959652 [Pa.s]	Water /Al_2O_3
		Thermal conductivity	0.7051 [W/m.K]	0.6969 [W/m.K]	
		Average Nusselt Number	20.874* 16.6769** *Using Equation 5.1*		
02	5.00% (v/v)	Dynamic viscosity	0.00952851 [Pa.s]	0.00962910 [Pa.s]	
		Thermal conductivity	0.7891 [W/m.K]	0.7251 [W/m.K]	
		Average Nusselt Number	22.231* 16.903** *Using Equation 5.1*		

*** Using 0.6 as thermal conductivity of based fluid**

**** Using respective thermal conductivity of based fluid**

When considering the nominal thermal conductivity of water, the Nusselt number has increased in the flow, as shown in table 5-5 with respect to the two-phase liquid-liquid slug flow without nanoparticles. Since the nanoparticles were introduced into the primary fluid during the study, it has been regarded as a separate phase rather than a component of the primary fluid [15], [107], [108]. But once the temperature contour is considered and the updated thermal conductivity is based on the literature, the Nusselt number can be calculated in a two-phase liquid-liquid slug flow.

Figure 5-23 illustrates the temperature gradients within a single bubble. In the absence of nanoparticles, the temperature distribution of the droplet is equal to that of the two-phase liquid-liquid slug flow [109]. Without nanoparticles, the average Nusselt number was found to be lower in two-phase liquid-liquid slug flow. Nonetheless, global heat transfer has risen. This can be demonstrated using figures 5-24 and 5-25, which depict the axial temperature distribution without and with nanofluid, respectively.

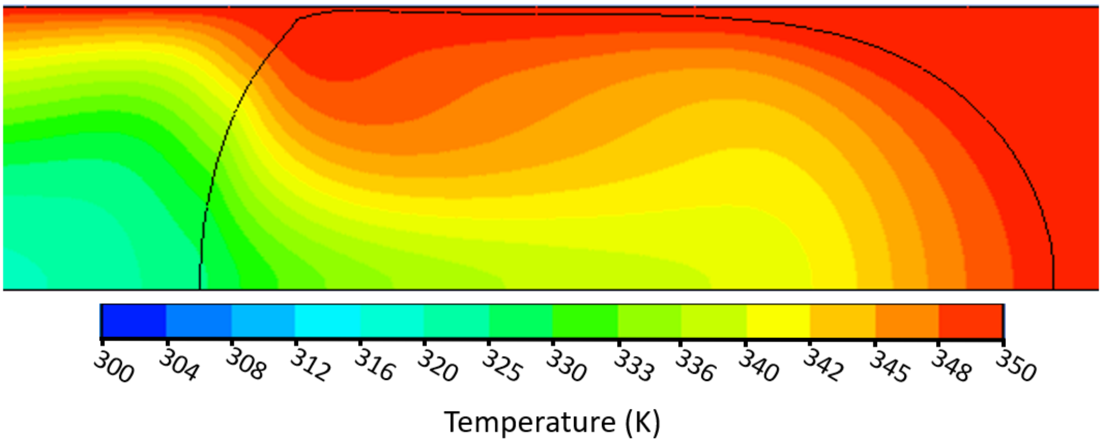

Figure 5-23: Temperature variation inside a bubble (Case 01)

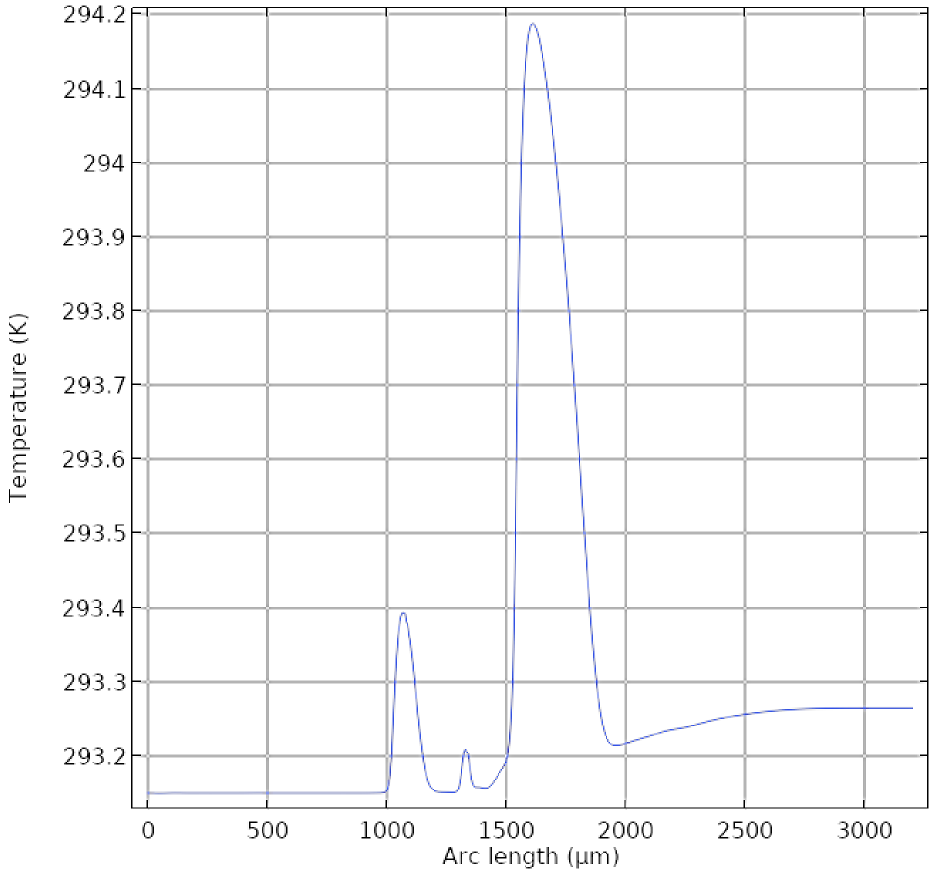

Figure 5-24: Axial Temperature distribution in two-phase liquid-liquid slug flow without nanoparticles

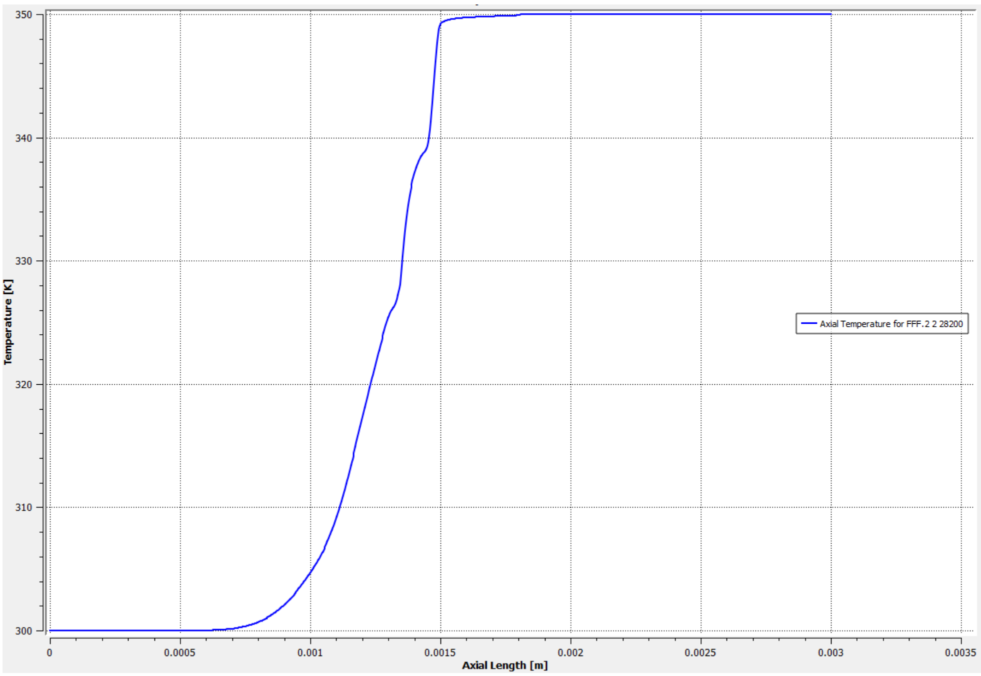

Figure 5-25:Axial Temperature distribution in two-phase liquid-liquid slug flow with nanoparticles

This demonstrates unequivocally that when nanofluid is used as the primary fluid, the maximum temperature is reached more quickly than when water alone is used as the primary fluid.

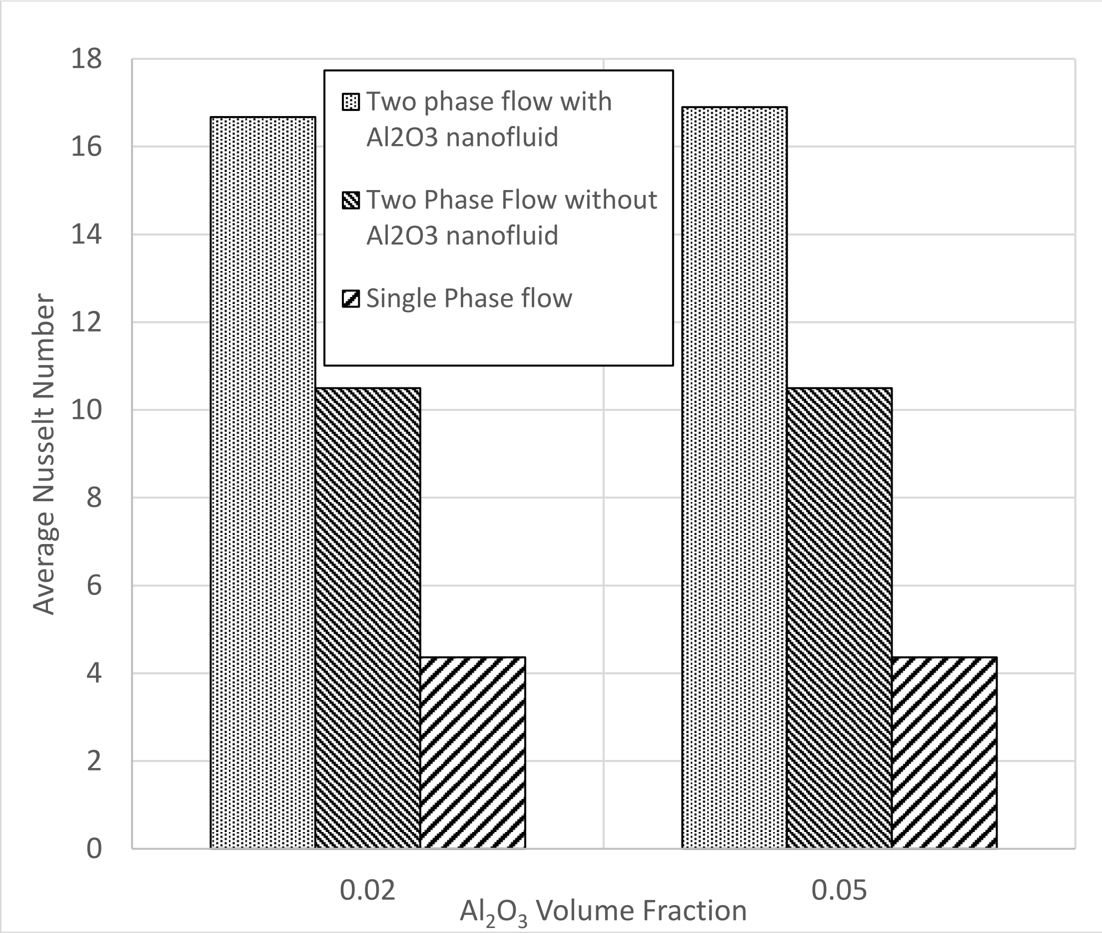

Figure 5-26: Nusselt number comparison of the nanofluid-based liquid-liquid two-phase slug flow (nanofluid as the slug) with respect to single phase and liquid-liquid two-phase slug flow without nanoparticles

Figure 5-26 illustrates the variance in the Nusselt number for the different scenarios. Figure 5-27 depicts the fluctuation in the local Nusselt number along the two neighbouring drops. Even with a low Nusselt number due to the high thermal conductivity, the two-phase flow containing nanoparticles reached the maximum temperature faster than the two-phase flow excluding the nanoparticles. This may be further supported by examining the average Nusselt number. Results have shown that the thermal conductivity of the fluid flow has been increased. But compared to nanoparticles in the secondary fluid, the average Nusselt number has decreased.

However, a slight increase in the Nusselt number is critical in indicating that convective heat transfer increased during these tests [110].

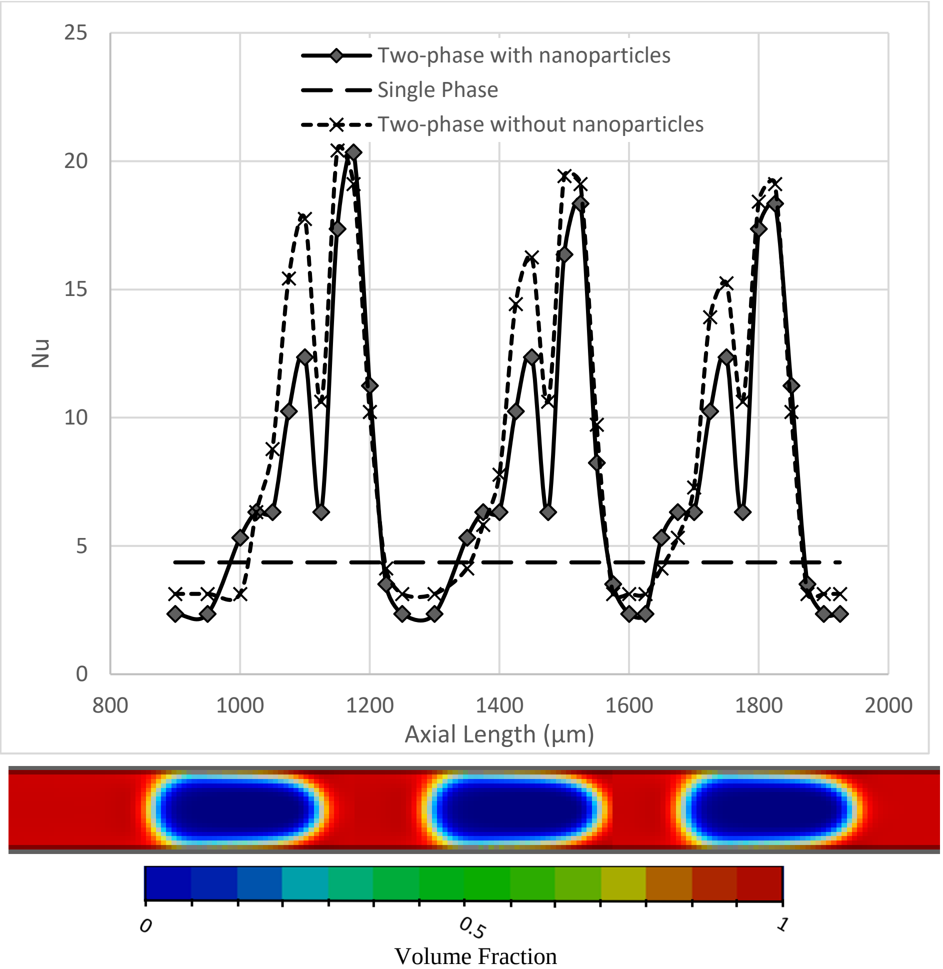

Figure 5-27: Nusselt number variation with respect to different cases.

5.4.3 Pressure drop associate with nanoparticles

It is usual to see considerable pressure loss across the microchannel when dealing with two-phase liquid-liquid slug flows. The fluctuation in axial pressure across the microchannel is presented in figure 5-28. It clearly indicates that the total pressure drop rises when nanoparticles are added to a fluid in the primary phase. This occurs as a result of the high viscosity of the primary fluid as a result of the nanoparticles present. But the differential pressure between the droplet and the base fluid is much higher when nanoparticles are present in the secondary fluid. Nanoparticles in light mineral oil make the fluid more viscous, which makes it more difficult to move.

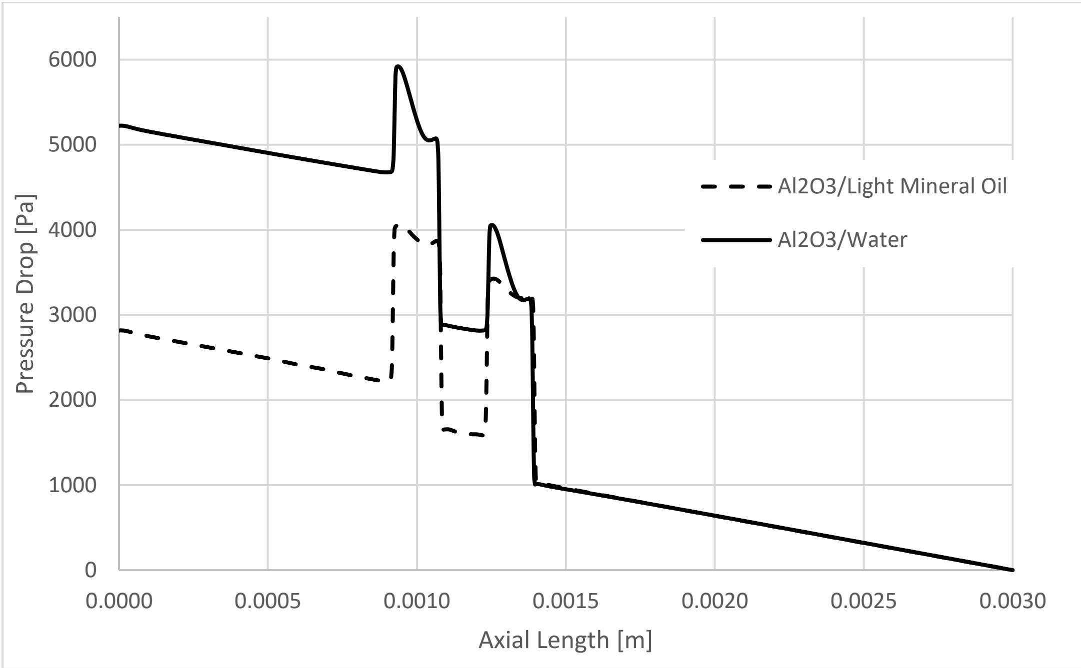

Figure 5-28: Axial pressure drop across the channel with nanoparticles

5.5 Summary

All analyses were classified into three categories: two-phase slug flow without nanoparticles; two-phase flow with nanoparticles in the secondary fluid; and two-phase flow with nanoparticles in the primary fluid. Additionally, all experiments were conducted in a microchannel with a diameter of 100 microns. To begin, hydrodynamic parameters such as velocity ratios and velocity profiles in a two-phase system were investigated, as well as their effect on heat transfer. The formation of droplets was discovered to be caused by the interfacial tension and velocity difference between the two phases. Then, the effect of the contact angle between the two phases on heat transfer was investigated. The study examined various contact angles ranging from 90 to 175 degrees. The maximum Nusselt number was 10.6 at the 160-degree contact angle. Additional contact angle increases resulted in a slight decrease in the Nusselt number. This occurred as a result of the thin film leakage at the wall caused by the primary fluid phase. After completing the contact angle study, the relative velocity distribution within the secondary phase was examined to determine the possibility of nanoparticle circulation. Following that, the effect of nanoparticles on heat transfer was investigated by introducing them into each primary and secondary phase. The nanoparticle size was kept constant throughout the studies at 50 nm. The nanoparticles were considered a separate phase and were treated as solids. When nanoparticles are introduced into the secondary fluid, the Nusselt number increases even more than in two-phase liquid-liquid slug flow. The results indicated a maximum of 40 while maintaining an average of 20, with a volume fraction of aluminium oxide nanoparticles of 5%. This occurred primarily as a result of nanoparticle circulation within the droplet. This fluid circulation enables nanoparticles to be heated more efficiently. Finally, the same set of studies was conducted using nanoparticles suspended in primary fluid. According to the results, the maximum Nusselt number was 16 when aluminium oxide nanoparticles were added at a concentration of 2% v/v to the primary fluid's modified thermal conductivity. When the nanophase was treated as a separate solid phase, the maximum Nusselt number was 22, which corresponded to a volume fraction of 5% v/v.

All of the examples demonstrated an increase in total effective heat transfer via fluid flow. The conclusion and recommendations are discussed in Chapter 6.

6 CONCLUSIONS AND RECOMMENDATIONS

In this part, the significant results, observations, and conclusions of this research are summarized, along with suggestions for further study. This study aimed to determine the effect of nanoparticles on the overall quantity of heat transmitted to the surroundings in microchannels undergoing two-phase liquid-liquid slug flow. Consequently, a series of numerical studies were conducted to examine the impacts of liquid-liquid slug flow hydrodynamics and efficient heat transfer. The primary results, which are presented below, are as follows:

6.1 Conclusions

- Due to the shear stress at the interface surpassing the capillary number and interfacial pressure ratio, the interfacial velocity of a two-phase liquid-liquid slug is diminished
- Fluid circulation within the droplet is caused by slip velocity
- 400% heat transfer enhancement can be obtained by using liquid-liquid slug flow
- Due to the disruption of the thermal boundary layer, heat transfer has been increased in two-phase flow
- Thermal conductivity is only slightly increased with nanoparticle volume fraction
- Addition of nanoparticles to either phase has increased the overall heat transfer by two-fold.
- Adding 5% of nanoparticles to the based fluid, has increased its thermal conductivity by 1.31 times
- Introduction of nanoparticles to the secondary fluid has increased the heat transfer efficiency by 2.09 times
- Further investigations are required to understand the motion of nanoparticles in a two-phase slug flow

6.2 Recommendation for future work

There have been few studies on two-phase flows. Numerous approaches can be taken to increase overall heat transfer. The following suggestion can further improve the heat transfer efficiency of traditional liquid-liquid Taylor flow systems.

- Detailed investigation of the effect of velocity on slug flow with and without nanoparticles.
- More research on the effect of nanoparticles with experiments is needed, as is validation of CFD results with experimental data.
- comprehensive study on nanoparticle behaviour with flow visualization in a microchannel. As an example, consider the clogging effect and nanoparticle aggregation within the fluid.
- Further studies are required to study nanofluid stability in a microchannel.
- Utilizing liquid metal in a liquid-liquid Taylor flow system might boost the heat transmission. Therefore, this can be the subject of future research

REFERENCE LIST

[1] M. Hemmat Esfe, S. Saedodin, O. Mahian, and S. Wongwises, ‘Thermal conductivity of Al2O3/water nanofluids: Measurement, correlation, sensitivity analysis, and comparisons with literature reports’, *J Therm Anal Calorim*, vol. 117, no. 2, pp. 675–681, Aug. 2014, doi: 10.1007/s10973-014-3771-x.

[2] K. V. Sharma, P. K. Sarma, W. H. Azmi, R. Mamat, and K. Kadirgama, ‘Correlations to predict friction and forced convection heat transfer coefficients of water based nanofluids for turbulent flow in a tube’, p. 25, 2012.

[3] D. Juncker, A. R. Wheeler, and D. Sinton, ‘Lab on a chip Canada – rapid diffusion over large length scales’, *Lab Chip*, vol. 13, no. 13, p. 2438, 2013, doi: 10.1039/c3lc90052e.

[4] A. Olanrewaju, M. Beaugrand, M. Yafia, and D. Juncker, ‘Capillary microfluidics in microchannels: From microfluidic networks to capillaric circuits’, *Lab on a Chip*, vol. 18, no. 16, pp. 2323–2347, 2018, doi: 10.1039/c8lc00458g.

[5] P. M. T. Bandara, ‘Heat Transfer Enhancement in Microchannels With Liquid-Liquid Slug Flow’, Dissertation, RMIT University, 2015.

[6] D. B. Tuckerman and R. F. W. Pease, ‘High-Performance Heat Sinking for VLSI’, no. 5, pp. 126–129, 1981.

[7] A. Asthana, I. Zinovik, C. Weinmueller, and D. Poulikakos, ‘International Journal of Heat and Mass Transfer Significant Nusselt number increase in microchannels with a segmented flow of two immiscible liquids : An experimental study’, *International Journal of Heat and Mass Transfer*, vol. 54, no. 7–8, pp. 1456–1464, 2011, doi: 10.1016/j.ijheatmasstransfer.2010.11.048.

[8] C. Y. Zhao and T. J. Lu, ‘Analysis of microchannel heat sinks for electronics cooling’, *International Journal of Heat and Mass Transfer*, vol. 45, no. 24, pp. 4857–4869, Nov. 2002, doi: 10.1016/S0017-9310(02)00180-1.

[9] N. Ramesh Korasikha, T. Karthikeya Sharma, G. Amba Prasad Rao, and K. Madhu Murthy, ‘Recent Advancements in Thermal Performance Enhancement

in Microchannel Heatsinks for Electronic Cooling Application', in *Heat Transfer - Design, Experimentation and Applications*, M. Araiz Vega, Ed. IntechOpen, 2021. doi: 10.5772/intechopen.97087.

[10] R. van Erp, R. Soleimanzadeh, L. Nela, G. Kampitsis, and E. Matioli, 'Co-designing electronics with microfluidics for more sustainable cooling', *Nature*, vol. 585, no. 7824, pp. 211–216, Sep. 2020, doi: 10.1038/s41586-020-2666-1.

[11] L. D. Stevanovic, R. A. Beaupre, A. V. Gowda, A. G. Pautsch, and S. A. Solovitz, 'Integral micro-channel liquid cooling for power electronics', in *2010 Twenty-Fifth Annual IEEE Applied Power Electronics Conference and Exposition (APEC)*, Palm Springs, CA, USA, Feb. 2010, pp. 1591–1597. doi: 10.1109/APEC.2010.5433444.

[12] A. Bar-Cohen, M. Arik, and M. Ohadi, 'Direct liquid cooling of high flux micro and nano electronic components', *Proceedings of the IEEE*, vol. 94, no. 8, pp. 1549–1570, 2006, doi: 10.1109/JPROC.2006.879791.

[13] J. Albadr, S. Tayal, and M. Alasadi, 'Case Studies in Thermal Engineering Heat transfer through heat exchanger using Al 2 O 3 nanofluid', *Case Studies in Thermal Engineering*, vol. 1, no. 1, pp. 38–44, 2013, doi: 10.1016/j.csite.2013.08.004.

[14] L. Liu, V. Stetsyuk, K. J. Kubiak, Y. F. Yap, and J. C. Chai, 'Nanoparticles for convective heat transfer enhancement : heat transfer coefficient and the effects of particle size and zeta potential', *Chemical Engineering Communications*, vol. 0, no. 0, pp. 1–11, 2018, doi: 10.1080/00986445.2018.1525364.

[15] X.-Q. Wang and A. S. Mujumdar, 'A review on nanofluids - part I: theoretical and numerical investigations', *Braz. J. Chem. Eng.*, vol. 25, no. 4, pp. 613–630, Dec. 2008, doi: 10.1590/S0104-66322008000400001.

[16] X. B. Nie, S. Y. Chen, W. N. E, and M. O. Robbins, 'A continuum and molecular dynamics hybrid method for micro- and nano-fluid flow', *J. Fluid Mech.*, vol. 500, pp. 55–64, Jan. 2004, doi: 10.1017/S0022112003007225.

[17] A. Mohebbi, 'Prediction of specific heat and thermal conductivity of nanofluids by a combined equilibrium and non-equilibrium molecular dynamics

simulation', *Journal of Molecular Liquids*, vol. 175, pp. 51–58, Nov. 2012, doi: 10.1016/j.molliq.2012.08.010.

[18] D. Xu, Y. Hu, and D. Li, 'A lattice Boltzmann investigation of two-phase natural convection of Cu-water nanofluid in a square cavity', *Case Studies in Thermal Engineering*, vol. 13, p. 100358, Mar. 2019, doi: 10.1016/j.csite.2018.11.009.

[19] S. Chen and G. D. Doolen, 'Lattice Boltzmann method for fluid flows', *Annual Review of Fluid Mechanics*, vol. 30, no. 1, pp. 329–364, 1998.

[20] Y. Xuan and Z. Yao, 'Lattice Boltzmann model for nanofluids', *Heat Mass Transfer*, Jul. 2004, doi: 10.1007/s00231-004-0539-z.

[21] S. Witharana, C. Hodges, D. Xu, X. Lai, and Y. Ding, 'Aggregation and settling in aqueous polydisperse alumina nanoparticle suspensions', *J Nanopart Res*, vol. 14, no. 5, p. 851, May 2012, doi: 10.1007/s11051-012-0851-3.

[22] S. T. W. Nam-Trung Nguyen, *Fundamentals and Applications of Microfluidics*.

[23] L. Brigo, 'Water slippage over micro and nano structured surfaces', p. 147.

[24] N.-T. Nguyen, S. T. Wereley, and A. House, *Fundamentals and Applications of Microfluidics - Second Edition*. 2002.

[25] W. Yu and H. Xie, 'A Review on Nanofluids : Preparation , Stability Mechanisms , and Applications', vol. 2012, 2012, doi: 10.1155/2012/435873.

[26] S. K. Das, S. U. S. Choi, and H. E. Patel, 'Heat transfer in nanofluids - A review', *Heat Transfer Engineering*, vol. 27, no. 10, pp. 3–19, 2006, doi: 10.1080/01457630600904593.

[27] R. Davarnejad, S. Barati, and M. Kooshki, 'CFD simulation of the effect of particle size on the nanofluids convective heat transfer in the developed region in a circular tube', pp. 1–6, 2013.

[28] Z. Jia-Fei, 'Dependence of Nanofluid Viscosity on Particle Size and pH Value Dependence of Nanofluid Viscosity on Particle Size and pH Value', vol. 066202, pp. 10–13.

[29] Cengel Dr., Yunus A. and Afshin J. Ghajar, *Heat and Mass Transfer: Fundamentals and Applications*, 5th ed. McGraw-Hill Education, 2014. [Online]. Available: https://www.amazon.com/Heat-Mass-Transfer-Fundamentals-Applications/dp/0073398187

[30] T. Bandara, N. T. Nguyen, and G. Rosengarten, 'Slug flow heat transfer without phase change in microchannels: A review', *Chemical Engineering Science*, vol. 126, pp. 283–295, 2015, doi: 10.1016/j.ces.2014.12.007.

[31] A. K. Coker, 'Physical Properties of Liquids and Gases', *Ludwig's Applied Process Design for Chemical and Petrochemical Plants*, pp. 103–132, 2007, doi: 10.1016/b978-075067766-0/50010-5.

[32] B. E. Rapp, 'Fluids: Prandtl Numbers', in *Microfluidics: Modelling, Mechanics and Mathematics*, 2017, pp. 243–263. doi: 10.1016/B978-1-4557-3141-1.50009-5.

[33] G. Hetsroni, A. Mosyak, E. Pogrebnyak, and L. P. Yarin, 'Heat transfer in micro-channels: Comparison of experiments with theory and numerical results', *International Journal of Heat and Mass Transfer*, vol. 48, no. 25–26, pp. 5580–5601, 2005, doi: 10.1016/j.ijheatmasstransfer.2005.05.041.

[34] M. A. Ebadian and C. X. Lin, 'A Review of High-Heat-Flux Heat Removal Technologies', *Journal of Heat Transfer*, vol. 133, no. 11, p. 110801, 2011, doi: 10.1115/1.4004340.

[35] Peter A. Kew, 'Correlation For the prediction of boiling heat trasfer in small-diameter channels', *Applied Thermal Engineering*, vol. 17, no. 8–10, pp. 705–715, Oct. 1997.

[36] A. J. Karabelas, 'Scale formation in tubular heat exchangers—research priorities', *International Journal of Thermal Sciences*, vol. 41, no. 7, pp. 682–692, Jun. 2002, doi: 10.1016/S1290-0729(02)01363-7.

[37] G. L. Morini, 'Scaling Effects for Liquid Flows in Microchannels', *Heat Transfer Engineering*, vol. 27, no. 4, pp. 64–73, May 2006, doi: 10.1080/01457630500523865.

[38] Y. A. Çengel and M. A. Boles, *Thermodynamics An Engineering Approach*, 6th Edition. McGraw-Hill Education.

[39] T. Al-Shemmeri, *Engineering Thermodynamics*, vol. 181. 1958. doi: 10.1038/1811028b0.

[40] G. P. Celata, M. Cumo, V. Marconi, S. J. McPhail, and G. Zummo, 'Microtube liquid single-phase heat transfer in laminar flow', *International Journal of Heat and Mass Transfer*, vol. 49, no. 19–20, pp. 3538–3546, Sep. 2006, doi: 10.1016/j.ijheatmasstransfer.2006.03.004.

[41] P. Rosa, T. G. Karayiannis, and M. W. Collins, 'Single-phase heat transfer in microchannels : The importance of scaling effects', *Applied Thermal Engineering*, vol. 29, no. 17–18, pp. 3447–3468, 2009, doi: 10.1016/j.applthermaleng.2009.05.015.

[42] Y. Zhai, G. Xia, Z. Li, and H. Wang, 'Experimental investigation and empirical correlations of single and laminar convective heat transfer in microchannel heat sinks', *Experimental Thermal and Fluid Science*, vol. 83, pp. 207–214, May 2017, doi: 10.1016/j.expthermflusci.2017.01.005.

[43] J. Bowers *et al.*, 'Flow and heat transfer behaviour of nanofluids in microchannels', *Progress in Natural Science: Materials International*, vol. 28, no. 2, pp. 225–234, Apr. 2018, doi: 10.1016/j.pnsc.2018.03.005.

[44] J.-Y. Jung, H.-S. Oh, and H.-Y. Kwak, 'Forced convective heat transfer of nanofluids in microchannels', *International Journal of Heat and Mass Transfer*, vol. 52, no. 1–2, pp. 466–472, Jan. 2009, doi: 10.1016/j.ijheatmasstransfer.2008.03.033.

[45] E. Manay and B. Sahin, 'Heat Transfer and Pressure Drop of Nanofluids in a Microchannel Heat Sink', *Heat Transfer Engineering*, vol. 38, no. 5, pp. 510–522, Mar. 2017, doi: 10.1080/10407782.2016.1195162.

[46] S. Tahir and M. Mital, 'Numerical investigation of laminar nanofluid developing flow and heat transfer in a circular channel', *Applied Thermal Engineering*, vol. 39, pp. 8–14, Jun. 2012, doi: 10.1016/j.applthermaleng.2012.01.035.

[47] Md. J. A. Khan, Md. R. Hasan, and Md. A. H. Mamun, ‘Flow Behavior and Temperature Distribution in Micro-Channels for Constant Wall Heat Flux’, *Procedia Engineering*, vol. 56, pp. 350–356, 2013, doi: 10.1016/j.proeng.2013.03.130.

[48] M. Renksizbulut, H. Niazmand, and G. Tercan, ‘Slip-flow and heat transfer in rectangular microchannels with constant wall temperature’, *International Journal of Thermal Sciences*, vol. 45, no. 9, pp. 870–881, Sep. 2006, doi: 10.1016/j.ijthermalsci.2005.12.008.

[49] S. Chen and Z. Tian, ‘Simulation of thermal micro-flow using lattice Boltzmann method with Langmuir slip model’, *International Journal of Heat and Fluid Flow*, vol. 31, no. 2, pp. 227–235, Apr. 2010, doi: 10.1016/j.ijheatfluidflow.2009.12.006.

[50] L. S. Tong and Y. S. Tang, *Boiling heat transfer and two-phase flow*, 2nd ed. Washington, D.C: Taylor & Francis, 1997.

[51] A. J. Ghajar and C. C. Tang, ‘Importance of Non-Boiling Two-Phase Flow Heat Transfer in Pipes for Industrial Applications’, *Heat Transfer Engineering*, vol. 31, no. 9, pp. 711–732, Aug. 2010, doi: 10.1080/01457630903500833.

[52] A. J. Ghajar, ‘Non-boiling heat transfer in gas-liquid flow in pipes: a tutorial’, *J. Braz. Soc. Mech. Sci. & Eng.*, vol. 27, no. 1, pp. 46–73, Mar. 2005, doi: 10.1590/S1678-58782005000100004.

[53] N. Janes, Y. S. Muzychka, B. Guy, E. J. Walsh, and P. Walsh, ‘Heat transfer in gas-liquid and liquid-liquid two phase plug flow systems’, in *2010 12th IEEE Intersociety Conference on Thermal and Thermomechanical Phenomena in Electronic Systems*, Las Vegas, NV, USA, Jun. 2010, pp. 1–11. doi: 10.1109/ITHERM.2010.5501409.

[54] Y. S. Lim, S. C. M. Yu, and N. T. Nguyen, ‘Flow visualization and heat transfer characteristics of gas–liquid two-phase flow in microtube under constant heat flux at wall’, *International Journal of Heat and Mass Transfer*, vol. 56, no. 1–2, pp. 350–359, Jan. 2013, doi: 10.1016/j.ijheatmasstransfer.2012.08.063.

[55] A. Ładosz and P. Rudolf von Rohr, 'Pressure drop of two-phase liquid-liquid slug flow in square microchannels', *Chemical Engineering Science*, vol. 191, pp. 398–409, Dec. 2018, doi: 10.1016/j.ces.2018.06.057.

[56] R. W. Lockhart and R. C. Martinelli, 'Proposed correlation of data for isothermal two-phase, two-component flow in pipes', *Chemical Engineering Progress*, vol. 45, no. 1, pp. 39–48, 1949.

[57] Y. Taitel and A. E. Dukler, 'A theoretical approach to the Lockhart-Martinelli correlation for stratified flow', *International Journal of Multiphase Flow*, vol. 2, no. 5–6, pp. 591–595, Apr. 1976, doi: 10.1016/0301-9322(76)90019-7.

[58] E. Walsh, Y. Muzychka, P. Walsh, V. Egan, and J. Punch, 'Pressure drop in two phase slug/bubble flows in mini scale capillaries', *International Journal of Multiphase Flow*, vol. 35, no. 10, pp. 879–884, Oct. 2009, doi: 10.1016/j.ijmultiphaseflow.2009.06.007.

[59] J. Jovanović, W. Zhou, E. V. Rebrov, T. A. Nijhuis, V. Hessel, and J. C. Schouten, 'Liquid–liquid slug flow: Hydrodynamics and pressure drop', *Chemical Engineering Science*, vol. 66, no. 1, pp. 42–54, Jan. 2011, doi: 10.1016/j.ces.2010.09.040.

[60] M. N. Kashid, Y. M. Harshe, and D. W. Agar, 'Liquid−Liquid Slug Flow in a Capillary: An Alternative to Suspended Drop or Film Contactors', *Ind. Eng. Chem. Res.*, vol. 46, no. 25, pp. 8420–8430, Dec. 2007, doi: 10.1021/ie070077x.

[61] A. Salim, M. Fourar, J. Pironon, and J. Sausse, 'Oil-water two-phase flow in microchannels: Flow patterns and pressure drop measurements', *Can. J. Chem. Eng.*, vol. 86, no. 6, pp. 978–988, Dec. 2008, doi: 10.1002/cjce.20108.

[62] Q. He, Y. Hasegawa, and N. Kasagi, 'Heat transfer modelling of gas–liquid slug flow without phase change in a micro tube', *International Journal of Heat and Fluid Flow*, vol. 31, no. 1, pp. 126–136, Feb. 2010, doi: 10.1016/j.ijheatfluidflow.2009.11.004.

[63] P. Urbant, A. Leshansky, and Y. Halupovich, 'On the forced convective heat transport in a droplet-laden flow in microchannels', *Microfluid Nanofluid*, vol. 4, no. 6, pp. 533–542, Jun. 2008, doi: 10.1007/s10404-007-0211-2.

[64] A. Mohammed Adham, N. Mohd-Ghazali, and R. Ahmad, ‘Thermal and hydrodynamic analysis of microchannel heat sinks: A review’, *Renewable and Sustainable Energy Reviews*, vol. 21, pp. 614–622, May 2013, doi: 10.1016/j.rser.2013.01.022.

[65] L. Cheng and G. Xia, ‘Two Phase Flow and Thermal Physics of Nanofluids: Understanding the Fundamentals, Mechanisms and Challenges’, presented at the The 3rd World Congress on Momentum, Heat and Mass Transfer, Apr. 2018. doi: 10.11159/icmfht18.2.

[66] A. Sabaghan, M. Edalatpour, M. C. Moghadam, E. Roohi, and H. Niazmand, ‘Nanofluid flow and heat transfer in a microchannel with longitudinal vortex generators: Two-phase numerical simulation’, *Applied Thermal Engineering*, vol. 100, pp. 179–189, May 2016, doi: 10.1016/j.applthermaleng.2016.02.020.

[67] M. S. Kamel, F. Lezsovits, and A. K. Hussein, ‘Experimental studies of flow boiling heat transfer by using nanofluids: A critical recent review’, *J Therm Anal Calorim*, May 2019, doi: 10.1007/s10973-019-08333-2.

[68] X. Fang, Y. Chen, H. Zhang, W. Chen, A. Dong, and R. Wang, ‘Heat transfer and critical heat flux of nanofluid boiling: A comprehensive review’, *Renewable and Sustainable Energy Reviews*, vol. 62, pp. 924–940, Sep. 2016, doi: 10.1016/j.rser.2016.05.047.

[69] C. W. Hirt and B. D. Nichols, ‘Volume of fluid (VOF) method for the dynamics of free boundaries’, *Journal of Computational Physics*, vol. 39, no. 1, pp. 201–225, Jan. 1981, doi: 10.1016/0021-9991(81)90145-5.

[70] S. Osher and J. A. Sethian, ‘Fronts propagating with curvature-dependent speed: Algorithms based on Hamilton-Jacobi formulations’, *Journal of Computational Physics*, vol. 79, no. 1, pp. 12–49, Nov. 1988, doi: 10.1016/0021-9991(88)90002-2.

[71] A. Bertei, A. Lamorgese, R. Mauri, and B. Tellini, ‘Phase Field Modeling of Phase Separation and Dendrite Growth’, p. 1.

[72] A. Bamshad, A. Nikfarjam, M. H. Sabour, and H. Raji, ‘Theoretical and Numerical Investigation of Liquid-Gas Interface Location of Capillary Driven

Flow During the Time Throughout Circular Microchannels', in *2017 5th RSI International Conference on Robotics and Mechatronics (ICRoM)*, Tehran, Oct. 2017, pp. 432–438. doi: 10.1109/ICRoM.2017.8466144.

[73] S. Zhou, X. Zhuang, and T. Rabczuk, 'A phase-field modeling approach of fracture propagation in poroelastic media', *Engineering Geology*, vol. 240, pp. 189–203, Jun. 2018, doi: 10.1016/j.enggeo.2018.04.008.

[74] ANSYS, Inc, 'ANSYS FLUENT 12.0/12.1 Documentation'. ANSYS, Inc. [Online]. Available: https://www.afs.enea.it/project/neptunius/docs/fluent/

[75] A. Bar-Cohen, M. Arik, and M. Ohadi, 'Direct liquid cooling of high flux micro and nano electronic components', *Proceedings of the IEEE*, vol. 94, no. 8, pp. 1549–1570, 2006, doi: 10.1109/JPROC.2006.879791.

[76] K. A. Triplett, S. M. Ghiaasiaan, S. I. Abdel-Khalik, and D. L. Sadowski, 'Gas liquid two-phase Flow in microchannels Part I: two-phase Flow patterns', *International Journal of Multiphase Flow*, p. 18, 1999.

[77] R. Gupta, D. F. Fletcher, and B. S. Haynes, 'CFD modelling of flow and heat transfer in the Taylor flow regime', *Chemical Engineering Science*, vol. 65, no. 6, pp. 2094–2107, Mar. 2010, doi: 10.1016/j.ces.2009.12.008.

[78] H. Ganapathy, E. Al-Hajri, and M. M. Ohadi, 'Phase Field Method for Simulation of Multiphase Flow', in *Volume 6: Fluids and Thermal Systems; Advances for Process Industries, Parts A and B*, Denver, Colorado, USA, Jan. 2011, pp. 1309–1319. doi: 10.1115/IMECE2011-66279.

[79] B. Wang, B. Ke, B. Chen, R. Li, and R. Tian, 'A technical review of research progress on thin liquid film thickness measurement', *Exp. Comput. Multiph. Flow*, vol. 2, no. 4, pp. 199–211, Dec. 2020, doi: 10.1007/s42757-019-0051-9.

[80] P. Aussillous and D. Quéré, 'Quick deposition of a fluid on the wall of a tube', *Phys. Fluids*, vol. 12, no. 10, p. 2367, 2000, doi: 10.1063/1.1289396.

[81] Y. Han and N. Shikazono, 'Measurement of liquid film thickness in micro square channel', *International Journal of Multiphase Flow*, vol. 35, no. 10, pp. 896–903, Oct. 2009, doi: 10.1016/j.ijmultiphaseflow.2009.06.006.

[82] J. Göhl, A. Mark, S. Sasic, and F. Edelvik, ‘An immersed boundary based dynamic contact angle framework for handling complex surfaces of mixed wettabilities’, *International Journal of Multiphase Flow*, vol. 109, pp. 164–177, Dec. 2018, doi: 10.1016/j.ijmultiphaseflow.2018.08.001.

[83] J. J. Licari and D. W. Swanson, ‘Functions and theory of adhesives’, in *Adhesives Technology for Electronic Applications*, Elsevier, 2011, pp. 35–74. doi: 10.1016/B978-1-4377-7889-2.10002-6.

[84] I. Mudawar and T. M. Anderson, ‘Parametric Investigation Into the Effects of Pressure, Subcooling, Surface Augmentation and Choice of Coolant on Pool Boiling in the Design of Cooling Systems for High-Power-Density Electronic Chips’, *Journal of Electronic Packaging*, vol. 112, no. 4, pp. 375–382, Dec. 1990, doi: 10.1115/1.2904392.

[85] S. U. S. Choi, ‘Nanofluids: From Vision to Reality Through Research’, *Journal of Heat Transfer*, vol. 131, no. 3, p. 033106, Mar. 2009, doi: 10.1115/1.3056479.

[86] M. Nazififard, M. Nematollahi, K. Jafarpur, and K. Y. Suh, ‘Numerical Simulation of Water-Based Alumina Nanofluid in Subchannel Geometry’, *Science and Technology of Nuclear Installations*, vol. 2012, pp. 1–12, 2012, doi: 10.1155/2012/928406.

[87] M. R. Safaei *et al.*, ‘Mathematical Modeling for Nanofluids Simulation: A Review of the Latest Works’, in *Modeling and Simulation in Engineering Sciences*, N. S. Akbar and O. A. Beg, Eds. InTech, 2016. doi: 10.5772/64154.

[88] Y. Karimi, A. R. Solaimany Nazar, and M. Motevasel, ‘CFD simulation of nanofluid heat transfer considering the aggregation of nanoparticles in population balance model’, *J Therm Anal Calorim*, vol. 143, no. 1, pp. 671–684, Jan. 2021, doi: 10.1007/s10973-019-09218-0.

[89] H. M. El-Batsh, M. A. Doheim, and A. F. Hassan, ‘On the application of mixture model for two-phase flow induced corrosion in a complex pipeline configuration’, *Applied Mathematical Modelling*, vol. 36, no. 11, pp. 5686–5699, Nov. 2012, doi: 10.1016/j.apm.2012.01.017.

[90] T. Ambreen, A. Saleem, and C. W. Park, ‘Homogeneous and Multiphase Analysis of Nanofluids Containing Nonspherical MWCNT and GNP Nanoparticles Considering the Influence of Interfacial Layering’, *Nanomaterials*, vol. 11, no. 2, p. 277, Jan. 2021, doi: 10.3390/nano11020277.

[91] D. Araújo dos Santos, S. Baluni, and A. Bück, ‘Eulerian Multiphase Simulation of the Particle Dynamics in a Fluidized Bed Opposed Gas Jet Mill’, *Processes*, vol. 8, no. 12, p. 1621, Dec. 2020, doi: 10.3390/pr8121621.

[92] M. Azarpira, A. Zarrati, and P. Farrokhzad, ‘Comparison between the Lagrangian and Eulerian Approach in Simulation of Free Surface Air-Core Vortices’, *Water*, vol. 13, no. 5, p. 726, Mar. 2021, doi: 10.3390/w13050726.

[93] H. Enwald’ and E. Peirano, ‘Eulerian two-phase flow theory applied to fluidization’, p. 46.

[94] T. Maric and T. U. Darmstadt, ‘Lagrangian / Eulerian numerical methods for fluid interface advection on unstructured meshes’, p. 238.

[95] C. Pena-Monferrer, J. L. Munoz-Cobo, G. Monros-Andreu, R. Martinez-Cuenca, and S. Chiva, ‘An Eulerian-Lagrangian open source solver for bubbly flow in vertical pipes’, p. 8.

[96] M. Mahdavi, M. Sharifpur, and J. P. Meyer, ‘CFD modelling of heat transfer and pressure drops for nanofluids through vertical tubes in laminar flow by Lagrangian and Eulerian approaches’, *International Journal of Heat and Mass Transfer*, vol. 88, pp. 803–813, Sep. 2015, doi: 10.1016/j.ijheatmasstransfer.2015.04.112.

[97] Z. Zhang and Q. Chen, ‘Comparison of the Eulerian and Lagrangian methods for predicting particle transport in enclosed spaces’, *Atmospheric Environment*, vol. 41, no. 25, pp. 5236–5248, Aug. 2007, doi: 10.1016/j.atmosenv.2006.05.086.

[98] R. S. Vajjha and D. K. Das, ‘Experimental determination of thermal conductivity of three nanofluids and development of new correlations’, *International Journal of Heat and Mass Transfer*, vol. 52, no. 21–22, pp. 4675–4682, Oct. 2009, doi: 10.1016/j.ijheatmasstransfer.2009.06.027.

[99] Y. Geng, A. A. A. A. Al-Rashed, B. Mahmoudi, A. S. Alsagri, A. Shahsavar, and P. Talebizadehsardari, 'Characterization of the nanoparticles, the stability analysis and the evaluation of a new hybrid nano-oil thermal conductivity', *J Therm Anal Calorim*, vol. 139, no. 2, pp. 1553–1564, Jan. 2020, doi: 10.1007/s10973-019-08434-y.

[100] H. Gu, M. H. G. Duits, and F. Mugele, 'Droplets Formation and Merging in Two-Phase Flow Microfluidics', *IJMS*, vol. 12, no. 4, pp. 2572–2597, Apr. 2011, doi: 10.3390/ijms12042572.

[101] H. Liu, C. O. Vandu, and R. Krishna, 'Hydrodynamics of Taylor Flow in Vertical Capillaries: Flow Regimes, Bubble Rise Velocity, Liquid Slug Length, and Pressure Drop', *Ind. Eng. Chem. Res.*, vol. 44, no. 14, pp. 4884–4897, Jul. 2005, doi: 10.1021/ie049307n.

[102] D. Kim, 'Improved convective heat transfer correlations for two-phase two-component pipe flow', *KSME International Journal*, vol. 16, no. 3, pp. 403–422, Mar. 2002, doi: 10.1007/BF03185238.

[103] S. C. M. Yu, C. P. Tso, and R. Liew, 'Analysis of thin film thickness determination in two-phase flow using a multifiber optical sensor', p. 9.

[104] Y. A. Al-Aufi, B. N. Hewakandamby, G. Dimitrakis, M. Holmes, A. Hasan, and N. J. Watson, 'Thin film thickness measurements in two phase annular flows using ultrasonic pulse echo techniques', *Flow Measurement and Instrumentation*, vol. 66, pp. 67–78, Apr. 2019, doi: 10.1016/j.flowmeasinst.2019.02.008.

[105] W. H. Azmi, K. V. Sharma, P. K. Sarma, R. Mamat, S. Anuar, and L. Syam Sundar, 'Numerical validation of experimental heat transfer coefficient with SiO 2 nanofluid flowing in a tube with twisted tape inserts', *Applied Thermal Engineering*, vol. 73, no. 1, pp. 296–306, Dec. 2014, doi: 10.1016/j.applthermaleng.2014.07.060.

[106] R. Ramirez-Tijerina, C. Rivera-Solorio, J. Singh, and K. Nigam, 'Numerical Study of Heat Transfer Enhancement for Laminar Nanofluids Flow', *Applied Sciences*, vol. 8, no. 12, p. 2661, Dec. 2018, doi: 10.3390/app8122661.

[107] M. Jama *et al.*, 'Critical Review on Nanofluids: Preparation, Characterization, and Applications', *Journal of Nanomaterials*, vol. 2016, pp. 1–22, 2016, doi: 10.1155/2016/6717624.

[108] W. Yu and H. Xie, 'A Review on Nanofluids: Preparation, Stability Mechanisms, and Applications', *Journal of Nanomaterials*, vol. 2012, pp. 1–17, 2012, doi: 10.1155/2012/435873.

[109] T. Bandara, M. Chandrashekar, and G. Rosengarten, 'CFD Modelling of Liquid-Liquid Slug Flow Heat Transfer in Microchannels', *The 28th International Symposium on Transport Phenomena University of Peradeniya*, p. 8, Sep. 2017.

[110] Sh. M. Vanaki, P. Ganesan, and H. A. Mohammed, 'Numerical study of convective heat transfer of nanofluids: A review', *Renewable and Sustainable Energy Reviews*, vol. 54, pp. 1212–1239, Feb. 2016, doi: 10.1016/j.rser.2015.10.042.